

For Reference

NOT TO BE TAKEN FROM THIS ROOM

For Reference

NOT TO BE TAKEN FROM THIS ROOM

Ex LIBRIS
UNIVERSITATIS
ALBERTAENSIS





Digitized by the Internet Archive
in 2018 with funding from
University of Alberta Libraries

<https://archive.org/details/Barter1964>

Thesis
1964
#4

THE UNIVERSITY OF ALBERTA
ECCENTRICALLY LOADED CONCRETE COLUMNS

by

SANDFORD LANE BARTER

A THESIS

SUBMITTED TO THE FACULTY OF GRADUATE STUDIES
IN PARTIAL FULFILMENT OF THE REQUIREMENTS FOR THE DEGREE
OF MASTER OF SCIENCE

DEPARTMENT OF CIVIL ENGINEERING

EDMONTON, ALBERTA

MAY, 1964

ABSTRACT

The results of an investigation of the behavior of long restrained reinforced concrete columns bent in double curvature are presented in this thesis. A short review of previous column research is given and theoretical aspects of behavior of long columns, including buckling and material failures, are discussed.

Eight reinforced concrete columns with one slenderness ratio $h/t = 27.3$ were tested under short time loading conditions. Buckling out of the plane of the applied eccentricities, and sidesway, were prevented. Four columns were hinged and four were restrained, and two eccentricity ratios, corresponding to tension and compression failures, were used. Loads were applied to the column ends with equal and opposite end eccentricities.

The columns deflected laterally under the applied loads, and in some cases the deflections reduced the ultimate load capacity. The restrained columns had higher load capacities than the hinged columns. The test results were compared with a theoretical long column analysis with varying degrees of agreement.

The hinged columns showed long column strength reductions of from zero to two percent. For the restrained columns, the combined effects of slenderness and restraints resulted in long column strengths from seven to 38 percent greater than short column strengths based on initial unrestrained eccentricities. The test results were compared with the ultimate strength design provisions of the American Concrete Institute Building Code (ACI 318-63). The test columns showed load capacities from one to 37 percent greater than given by the Code.

ACKNOWLEDGEMENTS

This investigation was carried out under the sponsorship of the Department of Civil Engineering of the University of Alberta. Funds for the purchase of materials and equipment were provided by a University of Alberta General Research Grant.

The author wishes to express his grateful appreciation to Associate Professor J.G. MacGregor for his assistance during the course of the investigation and for his constructive criticism during preparation of the manuscript.

The author also wishes to acknowledge the assistance of his employer, Associated Engineering Services Ltd., in printing the thesis.

TABLE OF CONTENTS

	Page
Title Page	i
Approval Sheet	ii
Abstract	iii
Acknowledgements	v
Table of Contents	vi
List of Tables	ix
List of Figures	xi
CHAPTER I INTRODUCTION	1
1.1 Long Columns Bent In Double Curvature	1
1.2 Review Of Column Research	6
1.3 Scope	12
1.4 Outline Of Testing Program	13
1.5 Notation	16
CHAPTER II THEORETICAL COLUMN STRENGTH	21
2.1 Ultimate Strength Of Columns Bent In Double Curvature	21
2.2 Computation Of Interaction Curves	27
CHAPTER III DETAILS OF TESTS	37
3.1 Details Of Test Specimens	37
3.2 Hinged Column Tests	46

3.3	Restrained Column Tests	50
3.4	Presentation Of Test Results	54
CHAPTER IV RESULTS OF TESTS OF COLUMNS WITH LARGE ECCENTRICITY		58
4.1	Introduction	58
4.2	Test Series B	58
4.3	Test Series D	68
CHAPTER V RESULTS OF TESTS OF COLUMNS WITH SMALL ECCENTRICITY		91
5.1	Introduction	91
5.2	Test Series A	91
5.3	Test Series C	103
CHAPTER VI THEORETICAL ANALYSIS OF LONG COLUMNS		129
6.1	Theoretical Analysis	129
6.2	Comparison Of Test Results With Theoretical Analysis	142
CHAPTER VII DISCUSSION		152
7.1	Effect Of Slenderness On Column Strength	152
7.2	American Concrete Institute Building Code (ACI 318-63)	163

CHAPTER VIII SUMMARY AND CONCLUSIONS	173
8.1 Summary	173
8.2 Conclusions	173
List Of References	178
Appendix A	A1
Appendix B	B1
Appendix C	C1
C.1 Hinged Column Tests	C1
C.2 Restrained Column Tests	C4
C.3 Thrust Line Computations For Analysis Of Restrained Columns in Chapter VI.	C13

LIST OF TABLES

TABLE		Page
3 - 1	Reinforcement Properties	42
3 - 2	Concrete Mix Proportions	44
3 - 3	Concrete Strengths	46
7 - 1	Effect of Column Slenderness	154
7 - 2	Ultimate Strength Design.....	167
B - 1	Observed Test Data, Specimen A1	B3
B - 2	Observed Test Data, Specimen A2	B3
B - 3	Observed Test Data, Specimen B1	B4
B - 4	Observed Test Data, Specimen B2	B4
B - 5	Observed Test Data, Specimen C1	B5
B - 6	Observed Test Data, Specimen C2	B6
B - 7	Observed Test Data, Specimen D1	B7
B - 8	Observed Test Data, Specimen D2	B8
C - 1	Reduced Test Data, Specimen A1	C2
C - 2	Reduced Test Data, Specimen A2	C2
C - 3	Reduced Test Data, Specimen B1	C3
C - 4	Reduced Test Data, Specimen B2	C3
C - 5	Reduced Test Data, Specimen C1	C5

TABLE	Page
C - 6 Reduced Test Data, Specimen C2	C6
C - 7 Reduced Test Data, Specimen D1	C7
C - 8 Reduced Test Data, Specimen D2	C8

FIGURE		Page
3 - 8	Hinged Column Measuring Points	52
3 - 9	Restrained Column Measuring Points	52
4 - 1	Key Diagram, Test Series B	60
4 - 2	Deflection Profile Diagram, Specimen B1	60
4 - 3	Deflection Profile Diagram, Specimen B2	60
4 - 4	Load-Deflection Graph, Specimen B1	61
4 - 5	Load-Deflection Graph, Specimen B2	61
4 - 6	Load-Moment Diagram, Specimen B1	62
4 - 7	Load-Moment Diagram, Specimen B2	63
4 - 8	Key Diagram, Test Series D	69
4 - 9	Deflection Profile Diagram, Specimen D1	70
4 - 10	Deflection Profile Diagram, Specimen D2	71
4 - 11	Load-Deflection Graph, Specimen D1	72
4 - 12	Load-Deflection Graph, Specimen D2	73
4 - 13	Beam Reaction Graph, Specimen D1	74
4 - 14	Beam Reaction Graph, Specimen D2	74
4 - 15	Moment Distribution Diagram, Specimen D1	75
4 - 16	Moment Distribution Diagram, Specimen D2	76
4 - 17	Load-Moment Diagram, Specimen D1	77
4 - 18	Load-Moment Diagram, Specimen D2	78

FIGURE	Page
4 - 19 Specimen B1, Failure Zone	79
4 - 20 Specimen B2, After Failure	79
4 - 21 Specimen D1 At 7.50 Kips Load	79
5 - 1 Key Diagram, Test Series A	93
5 - 2 Deflection Profile Diagram, Specimen A1	93
5 - 3 Deflection Profile Diagram, Specimen A2	93
5 - 4 Load-Deflection Graph, Specimen A1	94
5 - 5 Load-Deflection Graph, Specimen A2	94
5 - 6 Load-Moment Diagram, Specimen A1	95
5 - 7 Load-Moment Diagram, Specimen A2	96
5 - 8 Key Diagram, Test Series C	105
5 - 9 Deflection Profile Diagram, Specimen C1	106
5 - 10 Deflection Profile Diagram, Specimen C2	107
5 - 11 Load-Deflection Graph, Specimen C1	108
5 - 12 Load-Deflection Graph, Specimen C2	109
5 - 13 Beam Reaction Graph, Specimen C1	110
5 - 14 Beam Reaction Graph, Specimen C2	110
5 - 15 Moment Distribution Diagram, Specimen C1	111
5 - 16 Moment Distribution Diagram, Specimen C2	112
5 - 17 Load-Moment Diagram, Specimen C1	113

FIGURE	Page
5 - 18	Load-Moment Diagram, Specimen C2 114
5 - 19	Specimen A2, Failure Zone 115
5 - 20	Specimen D2 At 7.50 Kips Load..... 115
5 - 21	Specimen C2 At 35.00 Kips Load..... 115
6 - 1	Typical Moment-Curvature Curves 131
6 - 2	Typical Load-Moment-Curvature Curves 131
6 - 3	Column Model For Analysis 137
6 - 4	Beam Model For Analysis 137
6 - 5	Restraining Moment-Joint Rotation Curve 137
6 - 6	Beam Moment-Deflection Data..... 143
A - 1	Details Of Testing Frame A2
C - 1	External Forces On Restrained Column Specimen C10

1891
1892
1893
1894
1895
1896
1897
1898
1899
1900
1901
1902
1903
1904
1905
1906
1907
1908
1909
1910
1911
1912
1913
1914
1915
1916
1917
1918
1919
1920
1921
1922
1923
1924
1925
1926
1927
1928
1929
1930
1931
1932
1933
1934
1935
1936
1937
1938
1939
1940
1941
1942
1943
1944
1945
1946
1947
1948
1949
1950
1951
1952
1953
1954
1955
1956
1957
1958
1959
1960
1961
1962
1963
1964
1965
1966
1967
1968
1969
1970
1971
1972
1973
1974
1975
1976
1977
1978
1979
1980
1981
1982
1983
1984
1985
1986
1987
1988
1989
1990
1991
1992
1993
1994
1995
1996
1997
1998
1999
2000
2001
2002
2003
2004
2005
2006
2007
2008
2009
2010
2011
2012
2013
2014
2015
2016
2017
2018
2019
2020
2021
2022
2023
2024
2025
2026
2027
2028
2029
2030
2031
2032
2033
2034
2035
2036
2037
2038
2039
2040
2041
2042
2043
2044
2045
2046
2047
2048
2049
2050
2051
2052
2053
2054
2055
2056
2057
2058
2059
2060
2061
2062
2063
2064
2065
2066
2067
2068
2069
2070
2071
2072
2073
2074
2075
2076
2077
2078
2079
2080
2081
2082
2083
2084
2085
2086
2087
2088
2089
2090
2091
2092
2093
2094
2095
2096
2097
2098
2099
2100

CHAPTER I

INTRODUCTION

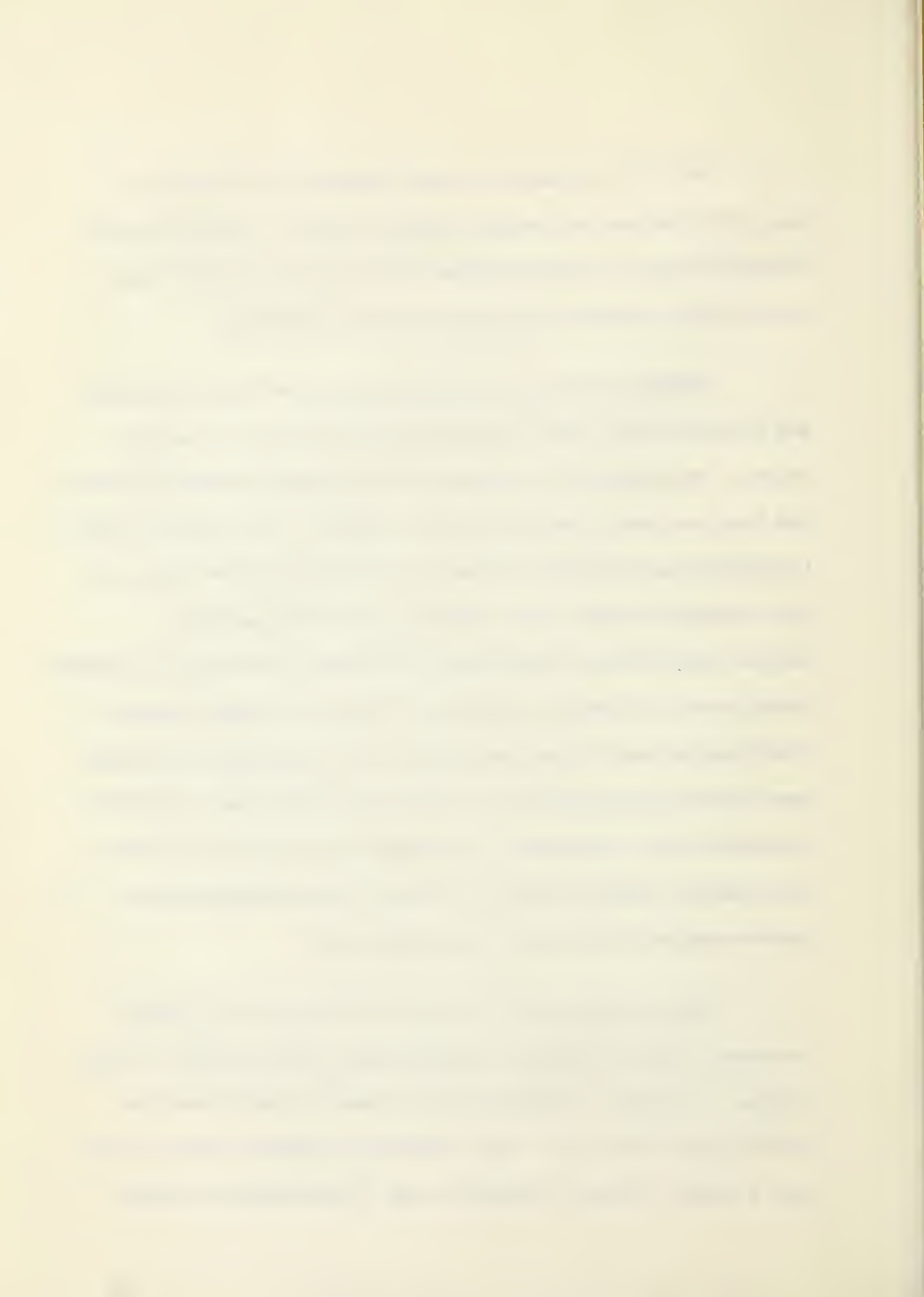
1.1 Long Columns Bent In Double Curvature

Recent trends in reinforced concrete design have increased the importance of slender columns. The use of higher strength concrete and reinforcing steel in columns has resulted in smaller cross-sectional area requirements and larger slenderness ratios. The most recent building codes contain liberalized slenderness limitations. The Canadian National Building Code of 1953 limited the column slenderness ratio, h/t , to 20. The 1960 edition permits values of h/t as large as 30, on the condition that a stability analysis be carried out where h/t exceeds 20. The 1956 American Concrete Institute Building Code (ACI 318-56) limited h/t to 20 for columns with definite bending stresses, which includes most columns in monolithic frames. The 1963 edition (ACI 318-63) permits values of h/t up to 25 for circular columns, and 30 for rectangular columns, with the use of a specified long column strength reduction factor. No limitation is placed on h/t if a special analysis is made.

ACI 318-63 contains the most comprehensive treatment, to date, of the analysis and design of slender columns. The long column strength reduction coefficients given in Section 916 of the Code were based on work carried out by Broms and Viest (1958-(3)).

Although theoretical analyses by Broms and Viest showed that end restraints always have a beneficial effect on the load capacity of columns, the conservative assumption of hinged ends proposed by Broms and Viest was used in deriving the Code equations. This was due in part to questions as to the effectiveness of restraints at ultimate load, when plastic hinges may form in the column or restraining members. Another reason for not considering end restraints was the lack of reported results of tests of slender, restrained, eccentrically loaded columns which could be used to check the validity of the simplifying assumptions used in the theoretical analysis. Subsequent investigations, discussed in Section 1.2(b), used a more rigorous analysis, but test results were still needed to verify the theoretical behavior before these analyses could be used as the basis for code requirements.

This investigation is concerned with the behavior of slender restrained columns subjected to combined axial load and double curvature bending. A column is considered bent in double curvature when the initial eccentricities cause a point of inflection within the column length. Such a column is shown in FIGURE 1-1(a). This condition is usually



the result of end moments or eccentricities applied as shown in FIGURE 1-1(b). For convenience in denoting the relationship between end eccentricities, the larger of the two eccentricities for a given column will be called e_2 , and the smaller e_1 . Thus the algebraic ratio e_1/e_2 indicates the loading condition. Since e_1 is always smaller than e_2 , the ratio has a range of values from 1 to -1, as shown in FIGURE 1 - 2. It is seen that single curvature bending results when e_1/e_2 is equal to or greater than zero, and double curvature bending results when e_1/e_2 is less than zero.

Structural members of all materials may be found bent in double curvature in rigid frames, trusses and conventional building frames. In reinforced concrete the most common occurrence of this loading condition is in monolithic building frames. Exterior columns and interior columns with unequal bay widths or unbalanced floor loading may fall into the double curvature range.

Where the building frame provides resistance to lateral loads, double curvature bending may be induced in otherwise symmetrically loaded columns. This condition and that of sidesway buckling, both of which involve lateral displacement of the column ends, will not be considered in this investigation. In addition, only buckling in the plane of the applied eccentricities is considered.

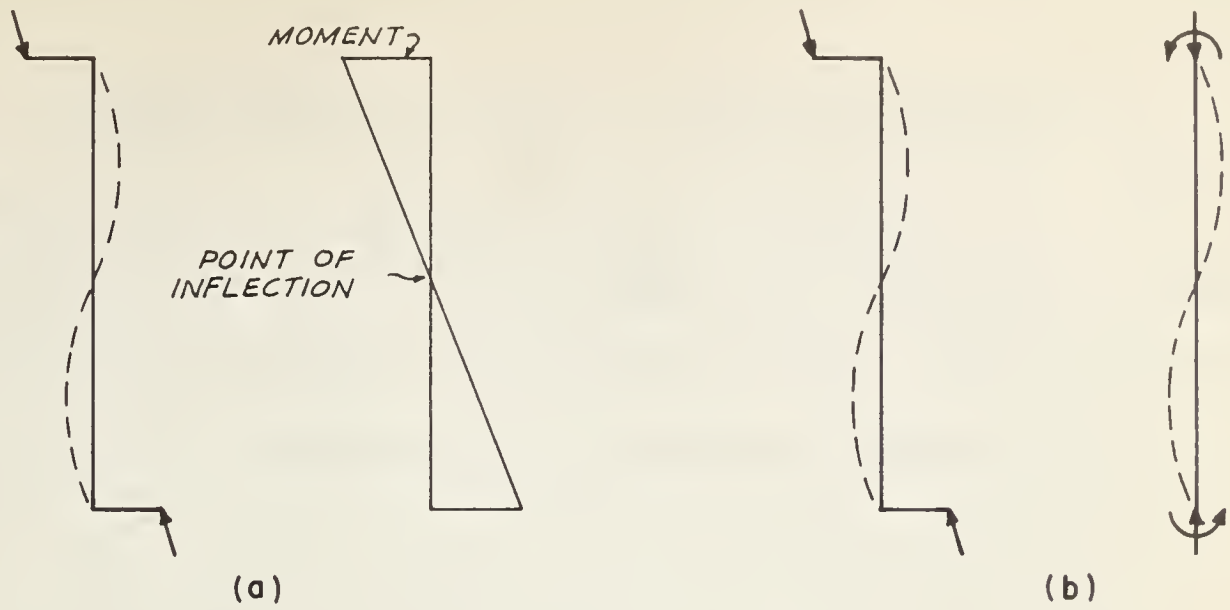


FIGURE 1-1 DOUBLE CURVATURE BENDING

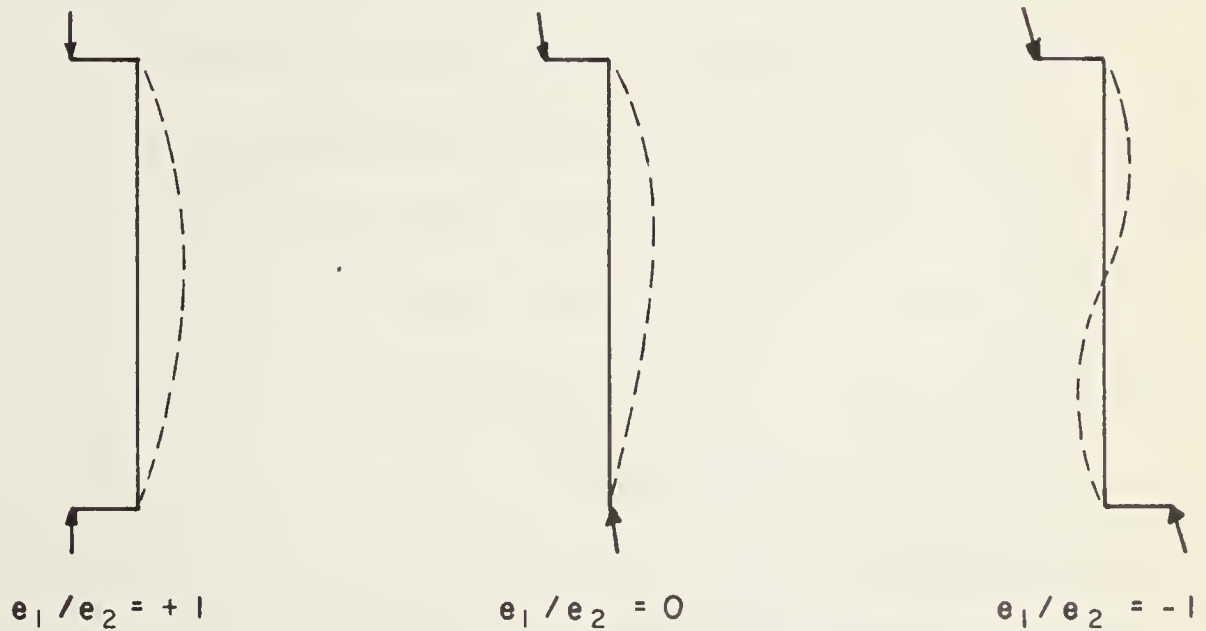
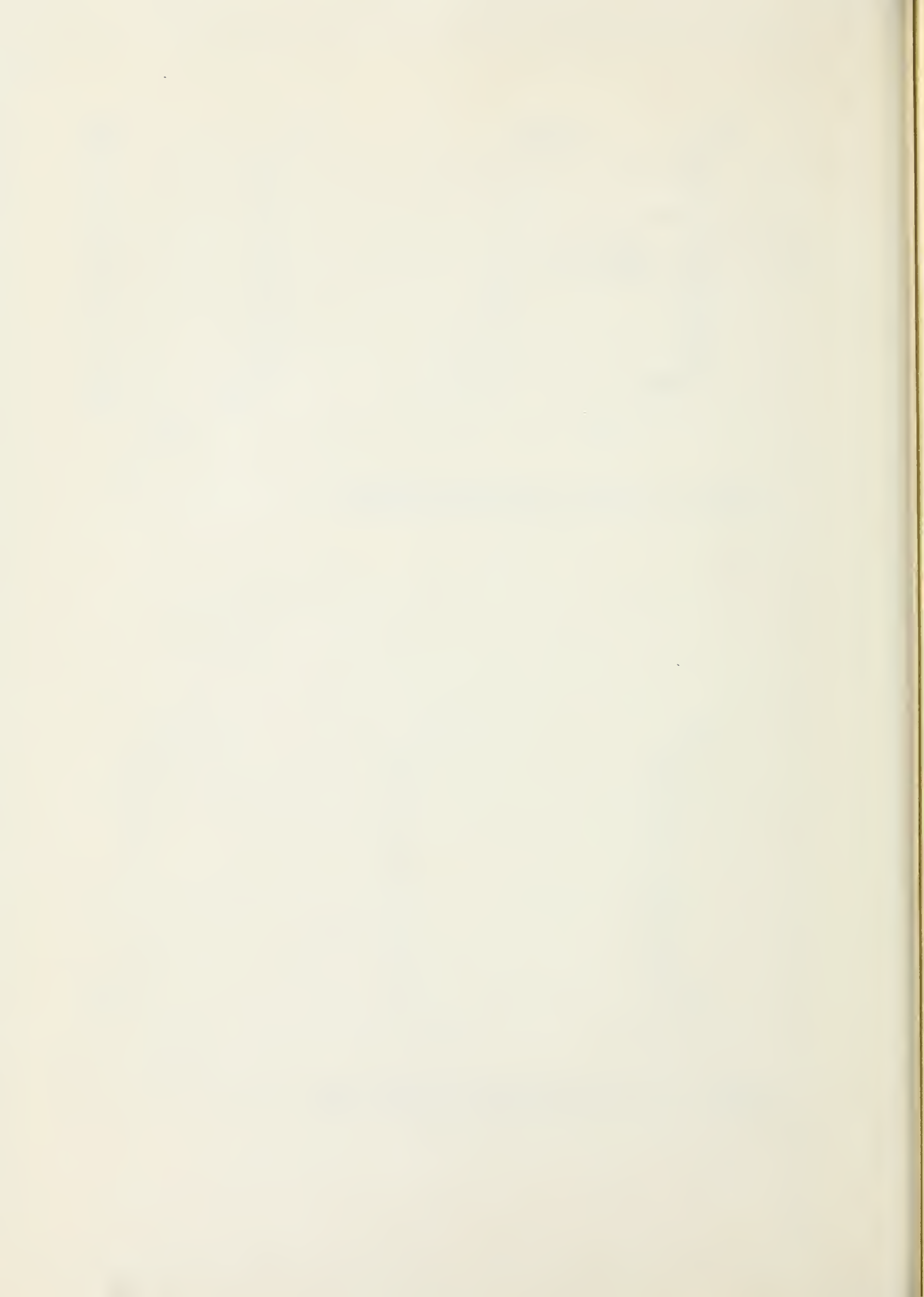


FIGURE 1-2 RATIO OF END ECCENTRICITIES



Bending moments in columns are generally caused by unbalanced moments in the beams framing into the column ends. These beams also provide most of the restraining effect, resulting in a complex interaction between applied and restraining moments. This is complicated by the variation in column and beam stiffnesses at different load levels.

The situation is further complicated in the case of double curvature bending with $e_1/e_2 = -1$. This loading condition is antisymmetrical and the point of inflection lies initially at mid-height of the column. Although the column would have an antisymmetrical configuration at all load levels under ideal conditions, slight imperfections present in an actual column will cause a departure from the idealized shape before the ultimate load is reached. Depending on the particular conditions of slenderness, eccentricity, and restraint, the actual strength may be considerably less than the ideal case would indicate. Various methods have been used in theoretical analyses to compensate for this effect (Broms and Viest, 1958-(1); Pfrang and Siess, 1961). However, because of the large number of factors involved, it appears that testing is necessary to obtain complete understanding of the unsymmetrical behavior of actual columns. The present investigation was limited to the case of $e_1/e_2 = -1$, and was designed to provide information on the effect of restraints on column strength.

1.2 Review Of Column Research

(a) Buckling Of Eccentrically Loaded Columns

The review presented in this section is based on Sections 9, 10 and 11 of Chapter I of "Buckling Strength Of Metal Structures" (Bleich, 1952). References to the individual works discussed in Bleich are included in the List of References.

VonKármán (1910) was the first to treat the buckling of an eccentrically loaded column as a stability problem. He presented the exact solution for a hinged steel column stressed beyond the elastic limit. His work showed that failure is not the result of the maximum stress reaching a certain value, but that at the critical load, stable equilibrium is not possible between the internal moment resistance and the externally applied moment.

Although vonKármán considered the stability of a mild steel column, the principle of the solution is applicable to any material for which the stress-strain relationship is known. The solution has formed the basis of all work on the buckling of eccentrically loaded reinforced concrete columns to the present time.

THE ANTHROPOLOGY OF THE
FUTURE

BY
H. H. HALL, F.R.S.

RECEIVED BY THE EDITOR, 1901.

THE JOURNAL OF THE
ROYAL ANTHROPOLOGICAL INSTITUTE

FOR 1901.

THE JOURNAL OF THE
ROYAL ANTHROPOLOGICAL INSTITUTE

FOR 1901.

THE JOURNAL OF THE
ROYAL ANTHROPOLOGICAL INSTITUTE

FOR 1901.

THE JOURNAL OF THE
ROYAL ANTHROPOLOGICAL INSTITUTE

FOR 1901.

THE JOURNAL OF THE
ROYAL ANTHROPOLOGICAL INSTITUTE

FOR 1901.

THE JOURNAL OF THE
ROYAL ANTHROPOLOGICAL INSTITUTE

FOR 1901.

THE JOURNAL OF THE
ROYAL ANTHROPOLOGICAL INSTITUTE

FOR 1901.

In a paper on the stability of eccentrically loaded steel columns Westergaard and Osgood (1928) presented a simplification of von Kármán's method. Using von Kármán's theory of buckling, the analysis was modified by assuming a shape for the deflected column axis instead of determining the true shape by integration. In this case a cosine wave was used, with the length and amplitude based on the curvature of the most highly stressed section.

(b) Eccentrically Loaded Reinforced Concrete Columns

The first major research on the buckling of eccentrically loaded reinforced concrete columns was carried out by Baumann (1934). Von Kármán's exact theory was used to compute the theoretical buckling loads. The stress-strain relation for concrete was determined from separate tests. Good agreement was found between measured and computed buckling loads in a series of tests of hinged columns.

Hognestad (1951) reported the results of a comprehensive study of the properties of reinforced concrete cross-sections under combined axial load and bending. The stress-strain curve for concrete proposed by Hognestad has been used in most investigations since that time. This study provided a basis for computing ultimate load capacities and load-moment-curvature relationships for reinforced concrete sections.

Accurate knowledge of these relationships was essential to studies of column buckling using vonKármán's theory. Further work on the stress-strain properties of concrete gave additional data for ultimate strength computations (Hognestad, Hanson and McHenry, 1955).

Ernst, Hromadik and Riveland published a study of hinged reinforced concrete columns in 1953. VonKármán's theory, as simplified by Westergaard and Osgood, was used to compute theoretical buckling loads. Hognestad's stress-strain curve was used to derive the load-moment-curvature relationships. The deflected column shape was assumed to be a portion of a cosine wave with the length and amplitude based on the curvature of the most highly stressed cross-section. This assumption takes into consideration the reduced stiffness of the cracked section at the most highly stressed section, but not the variation in cracking and stiffness over the remainder of the column length. Since the deflections are based on the cross-section with the least stiffness they are generally over-estimated by this method.

Broms and Viest (1958-(1)) presented the results of a theoretical investigation of the ultimate strength of hinged reinforced concrete columns. Both concentrically and eccentrically loaded columns were considered. The theoretical analysis of the eccentrically loaded columns was similar to the method of Ernst, Hromadik and Riveland, but was

extended to include a larger range of variables. Hognestad's stress-strain curve for concrete was used, and the deflected column shape was again taken as a cosine wave. Among the ratios of end eccentricities considered was $e_1/e_2 = -1$. This was the first published analysis of reinforced concrete columns bent in double curvature. The computed ultimate loads for single curvature columns were compared with the results of a number of previously published tests with reasonable agreement. No test results for the double curvature case were available. The effect of sustained loading was taken into account in some analyses by doubling the strains corresponding to a given stress level on the concrete stress-strain curve.

Later in 1958, Broms and Viest (1958-(2)) presented the results of a theoretical investigation of the ultimate strength of restrained reinforced concrete columns. Both concentrically and eccentrically loaded columns were considered. The theoretical analysis of the eccentrically loaded columns was similar to that of the earlier paper except that the effects of end restraints were included. The end restraints were assumed to behave elastically and to have no yield point. The effect of sustained loading was considered briefly, based on the assumption that the restraints were not affected by time. No test results for eccentrically loaded restrained columns were available for comparison with the theoretical ultimate loads.

Based on the results of their earlier analyses of hinged and restrained long columns, Broms and Viest (1958-(3)) proposed a design procedure for working strength and ultimate strength methods. The design procedure for long eccentrically loaded columns required that the short column strength first be determined, using the appropriate eccentricity. For restrained columns the eccentricity was determined from an elastic frame analysis. The short column strength was then modified by a reduction coefficient reflecting the effect of column slenderness. The reduction coefficient was given as a function of the slenderness ratio h/t and the ratio of end eccentricities e_1/e_2 . The proposed design procedure was checked against available test results and found to give safe designs.

Pfrang and Siess (1961) presented the results of a theoretical investigation of factors affecting the behavior of long restrained reinforced concrete columns. Among the variables investigated were: the ratio of end eccentricities, the slenderness ratio, and the degree of end restraint. Only one concrete strength, reinforcement yield point, and cross-section was considered. About 300 individual columns were solved using an electronic computer. VonKármán's exact theory was used and the true deflected column shape was found by integrating curvatures. Hognestad's stress-strain curve for concrete was used. The end restraints were assumed to behave elastically at all load levels.

The double curvature case, with $e_1/e_2 = -0.98$, was solved for hinged and restrained columns similar to those of the present investigation. Pfrang and Siess presented a number of curves showing theoretical strength relationships, and they proved useful in discussing the results of the tests reported herein. This discussion is presented in Chapter VII.

Chang and Ferguson (1963) published the results of an experimental investigation of long hinged reinforced concrete columns carried out in 1961. The theoretical analysis was based on vonKármán's theory with the deflected column shape determined by integrating curvatures. The load-moment-curvature relationships were based on Hognestad's stress-strain curve for concrete. Measured and computed unit curvatures were compared and good agreement was found at all load levels. The effect of neglecting concrete tensile stresses was noticeable in the comparison of maximum deflections. Reasonably good agreement was found between measured and computed lateral deflection profiles.

Breen (1962) presented the results of tests of long reinforced concrete columns which formed an integral part of rectangular frames. The test specimens simulated conditions found in a real structure, with axial loads applied to the column ends and bending moments applied through the beams. The columns were bent in double curvature.

The test specimens were statically indeterminate and moments were found by means of measured curvatures and theoretical moment-curvature relationships. Test results showed that the effective column eccentricities were considerably reduced by the restraining beams. Long column strength reductions were small, ranging in value from zero to 8 percent for h/t as large as 30.

1.3 Scope

A theoretical solution of eccentrically loaded reinforced concrete columns has been established, as outlined in the review of previous investigations in Section 1.2. A large number of tests of slender hinged columns bent in single curvature have been reported and used for comparison with theoretical solutions. However, there is a definite lack of reported tests of columns bent in double curvature, both hinged and restrained. The present investigation is an attempt to provide some information concerning the behavior of columns of this type.

The main aims of the investigation were:

- (1) To provide data illustrating the behavior of hinged and restrained columns with equal and opposite end eccentricities ($e_1/e_2 = -1$).
- (2) To determine the effect of end restraints on the behavior of the columns.

The first part of the paper discusses the importance of the study of the history of the United States. It is a study of the past which helps us to understand the present and to prepare for the future. The study of history is not only a study of the past, but also a study of the human mind and of the human condition. It is a study of the things which have made the world what it is today, and of the things which will make the world what it will be tomorrow.

The second part of the paper discusses the importance of the study of the history of the United States. It is a study of the past which helps us to understand the present and to prepare for the future. The study of history is not only a study of the past, but also a study of the human mind and of the human condition. It is a study of the things which have made the world what it is today, and of the things which will make the world what it will be tomorrow.

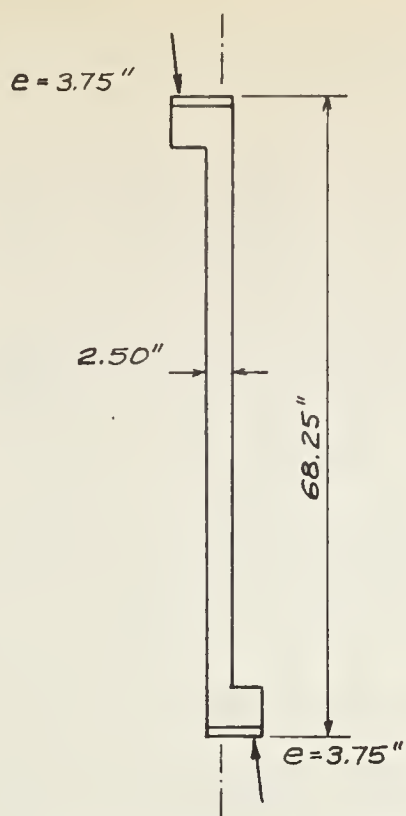
The third part of the paper discusses the importance of the study of the history of the United States. It is a study of the past which helps us to understand the present and to prepare for the future. The study of history is not only a study of the past, but also a study of the human mind and of the human condition. It is a study of the things which have made the world what it is today, and of the things which will make the world what it will be tomorrow.

- (3) Where possible, to compare the test observations with the results of theoretical analyses.
- (4) To compare the ultimate load capacity of the test columns with that permitted by current design codes.

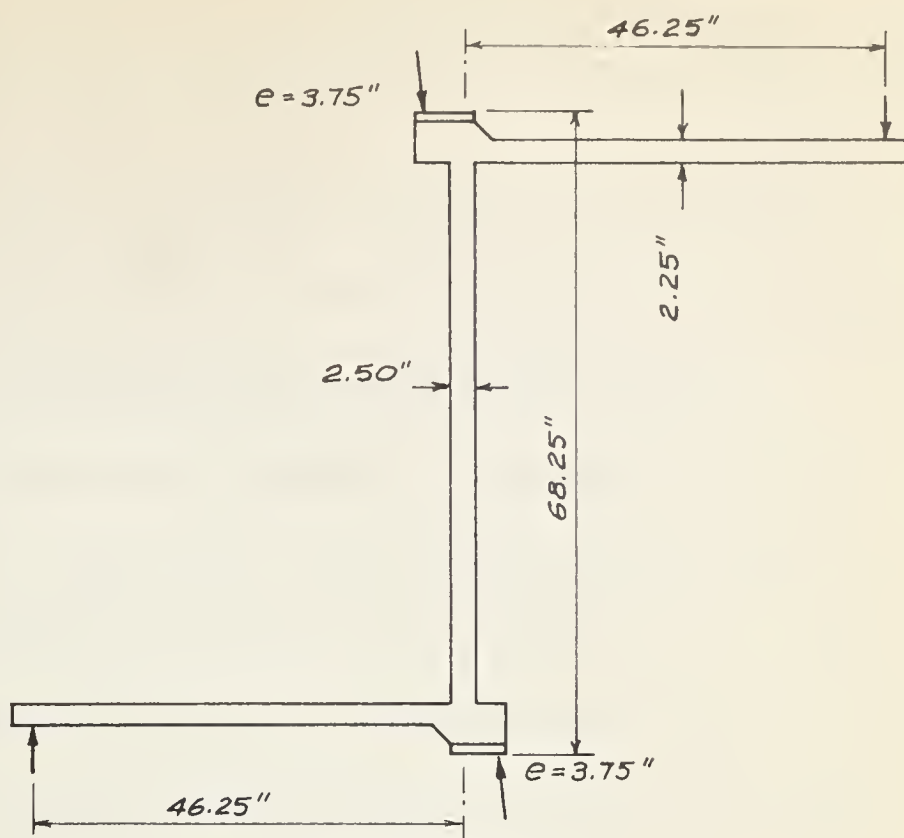
1.4 Outline Of Testing Program

Eight individual specimens were tested in four series. Each series consisted of two specimens which were identical except for random variations in concrete strength. Duplication was considered necessary in view of the lack of previous test results for columns of this type. The main variable in the program was the condition of restraint at the column ends. Four columns were cast with restraining beams at both ends, and four were hinged at the ends. In addition, two different end eccentricities were investigated. Complete details of the test specimens, instrumentation and experimental procedure are given in Chapter III.

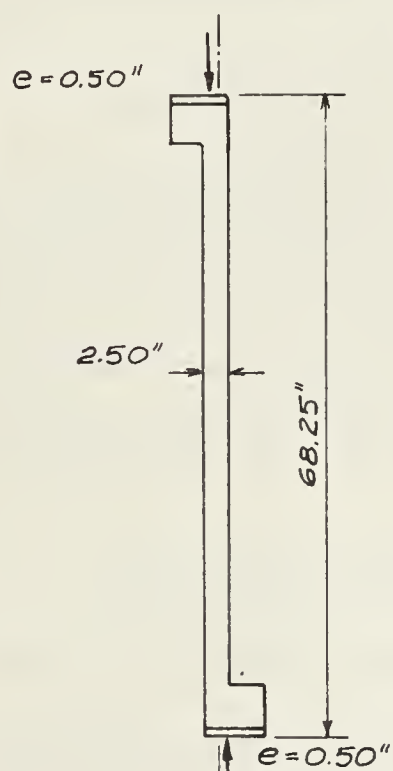
The main dimensions of the test specimens are given in FIGURE 1 - 3. The dimensions and reinforcement of the columns were the same for all series. The dimensions and reinforcement of the beams were the same for all the restrained specimens. The column thickness, 2.50 inches, was chosen to provide the desired slenderness ratio in conjunction with the height limitation of the testing machine.



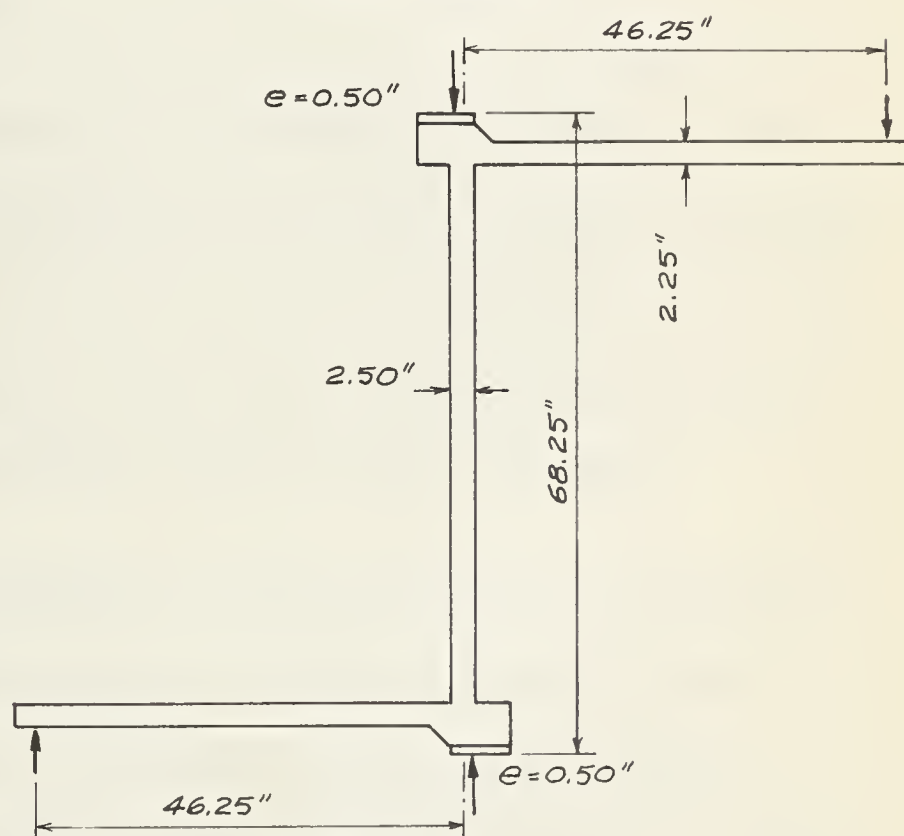
TEST SERIES B



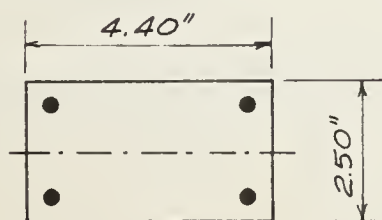
TEST SERIES D



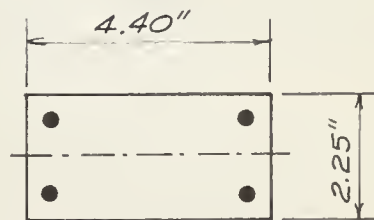
TEST SERIES A



TEST SERIES C



COLUMN CROSS - SECTION



BEAM CROSS - SECTION

FIGURE 1-3 TEST SPECIMENS

The column width, 4.40 inches, was chosen to provide lateral stability and ensure bending about the desired axis. With the longitudinal reinforcement of 4 - #3 bars these dimensions gave a steel ratio of exactly 4 percent. The effective column length was taken as the distance between load pivot axes (FIGURE 3 - 3) giving $h/t = 27.3$ about the axis of bending. Taking $r = 0.3t$, as specified in ACI 318-63, gives $h/r = 91$. This slenderness ratio places the test columns in the long column range according to most design codes, and long column strength reduction coefficients would be required in design.

End eccentricities were chosen to obtain test results in both the tension failure and compression failure regions. Series A and C had nominal end eccentricities of 0.50 inches ($e/t = 0.2$) and were expected to fail in compression. Series B and D had nominal end eccentricities of 3.75 inches ($e/t = 1.5$) and were expected to fail in tension.

Because of the slenderness of the test columns, the beam and column proportions cannot be directly related to the range of sizes commonly found in practice. The restraining beams were sized to provide approximately the same degree of restraint assumed by Pfrang and Siess (1961) in a portion of their computations. This was desired in order that a comparison could be made.

1.5 Notation

- a = depth of concrete compression block (FIGURE 2 - 5).
- A_{st} = total area of longitudinal reinforcement .
- b = overall width of a rectangular cross-section measured parallel to the axis of bending .
- C = concrete compressive force (FIGURE 2 - 7).
- C_1 = concrete compressive force (FIGURE 2 - 8).
- C_2 = fictitious concrete compressive force (FIGURE 2 - 8)
- d = distance from the extreme compression fibre to the centroid of the tension reinforcement.
- d'' = distance from the centroid of cross-section to the centroid of the tension or compression reinforcement (FIGURE 2 - 6)
- D = load applied to the column by the testing machine, given by the load dial reading.
- dh = axial shortening of the column.
- e_i = initial eccentricity of applied load in a column.
- e_1, e_2 = end eccentricities of the applied load; e_2 is taken as the larger value and is always positive.
- E_c = modulus of elasticity of concrete.
- E_s = modulus of elasticity of steel.
- f_c = concrete stress

- f'_C = compressive strength of concrete determined from standard 28 day cylinder tests.
- f''_C = maximum compressive stress in concrete, in structural members.
- f_s = steel stress.
- f_y = yield strength of steel.
- F_2, F_3 = steel tension forces (FIGURES 2 - 7 and 2 - 8).
- h = unsupported length of a column.
- k_1, k_2 = coefficients which define the magnitude and location of the resultant compressive force in a concrete compression block (See Section 2.2(b)(ii)).
- k_3 = the ratio of the maximum compressive stress in concrete, in structural members, f''_C to the compressive strength of concrete determined from standard 28 day cylinder tests, f'_C .
- f''_C/f'_C .
- M = moment in a column, including the effects of initial eccentricity, restraint and deflection.
- M_A = applied moment = the externally applied moment at a beam-column joint, in a restrained column specimen.
- M_b = moment capacity of a column cross-section at simultaneous crushing of concrete and yielding of tension steel (balanced conditions).

M_C = column moment = the portion of the moment applied at a beam-column joint, in a restrained column specimen, that is resisted by the column.

M_r = theoretical restraining moment at the end of a column.
= $\propto \theta$.

M_R = restraining moment = the portion of the moment applied at a beam-column joint, in a restrained column specimen, that is resisted by the restraining beam.

p = ratio of reinforcement.
= $\frac{A_{st}}{bt}$

P = axial column load.

P_b = axial load capacity of a column cross-section at simultaneous crushing of concrete and yielding of tension steel (balanced conditions).

P_{Long} = ultimate load capacity of a long column (See Section 7.1(a)).

P_{Short} = ultimate load capacity of a short column (See Section 7.1(a)).

P'_{Short} = ultimate load capacity of a short column based on an eccentricity determined as specified in ACI 318-63 (ACI Section 914).

Py-moment = moment produced in a column as a result of deflection from the initial straight position. (See Section 2.1(a)(i)).

...
...
...

...
...
...

...
...
...

...
...
...

...
...
...

...
...
...

...
...
...

...
...
...

- r = radius of gyration perpendicular to the axis of bending
(taken as $0.3t$ for rectangular sections).
- R = reduction factor for long columns as defined in Section 916
of ACI 318-63.
- R_L, R_U = lower and upper restraining beam reactions, respectively,
in the restrained column test specimens.
- s = a concrete compression block dimension shown in FIGURE
2 - 8.
- t = overall thickness of a rectangular cross-section measured
perpendicular to the axis of bending.
- x, x_1, x_2 = moment arms of concrete compression forces shown in
FIGURES 2 - 7 and 2 - 8.
- y = lateral deflection of column from its unloaded straight
position.
- α = coefficient of end restraint.
= M_r / Θ .
- Δ = lateral displacement of a beam-column joint in a restrained
column specimen.
- ϵ_o = strain corresponding to the maximum stress in the Hognestad
stress-strain curve for concrete, (FIGURE 2 - 4).
- ϵ_u = ultimate compressive concrete strain.

ϵ_y = yield point strain for steel.

$$= f_y / E_s .$$

ϵ_1, ϵ_4 = concrete strains (See FIGURE 2 - 7).

ϵ_2, ϵ_3 = steel strains (See FIGURE 2 - 7).

ϕ = unit curvature, or angle change per unit length.

$$= (\epsilon_4 - \epsilon_1) / t .$$

θ = angular rotation of beam-column joint in a restrained column test specimen.

CHAPTER II

THEORETICAL COLUMN STRENGTH

2.1 Ultimate Strength Of Columns Bent In Double Curvature

The introduction to theoretical column strength and behavior presented in this chapter is intended as a background for interpretation of the test results. The discussion includes the significance of the interaction of the effect of load and moment on column strength, and the conditions of buckling and material failure.

(a) Interaction Of Load And Moment

Three identical columns are shown in FIGURE 2 - 1. All the columns have equal and opposite end eccentricities, but the magnitude of the maximum end eccentricity is different in each case. As a result of this difference each column will exhibit a different type of behavior at ultimate load. The behavior may be illustrated by tracing the load-moment curve for the failure section in each case. The failure section is the point at which crushing of the concrete first occurs, and will be located at the end of the column as in Case (c) or at some point away

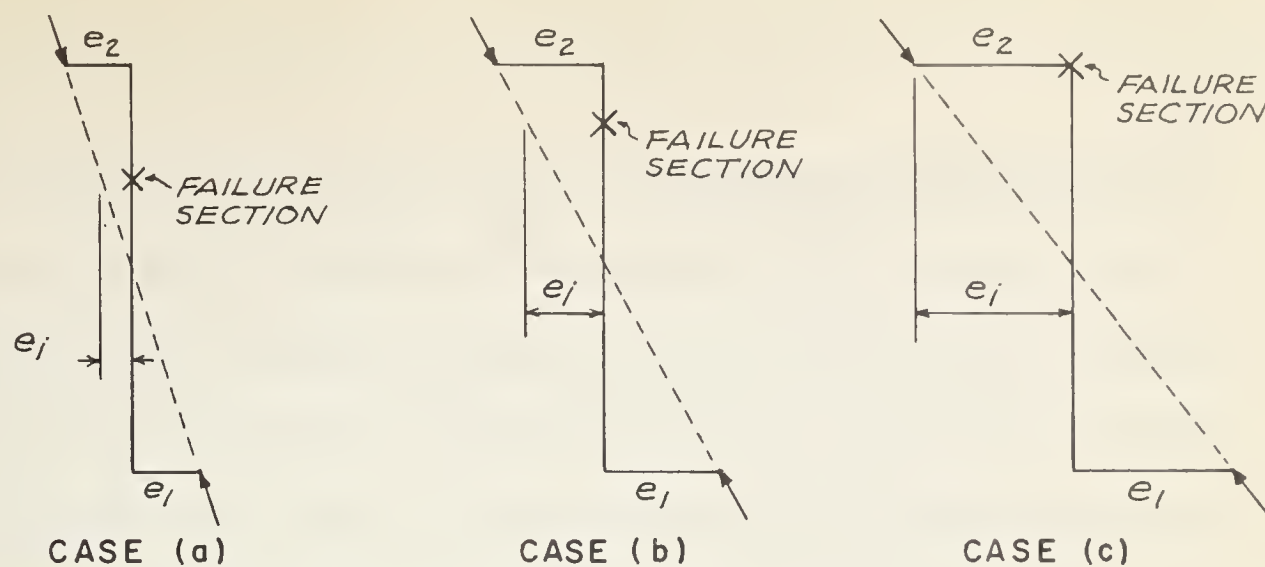


FIGURE 2-1 LOCATION OF FAILURE SECTIONS

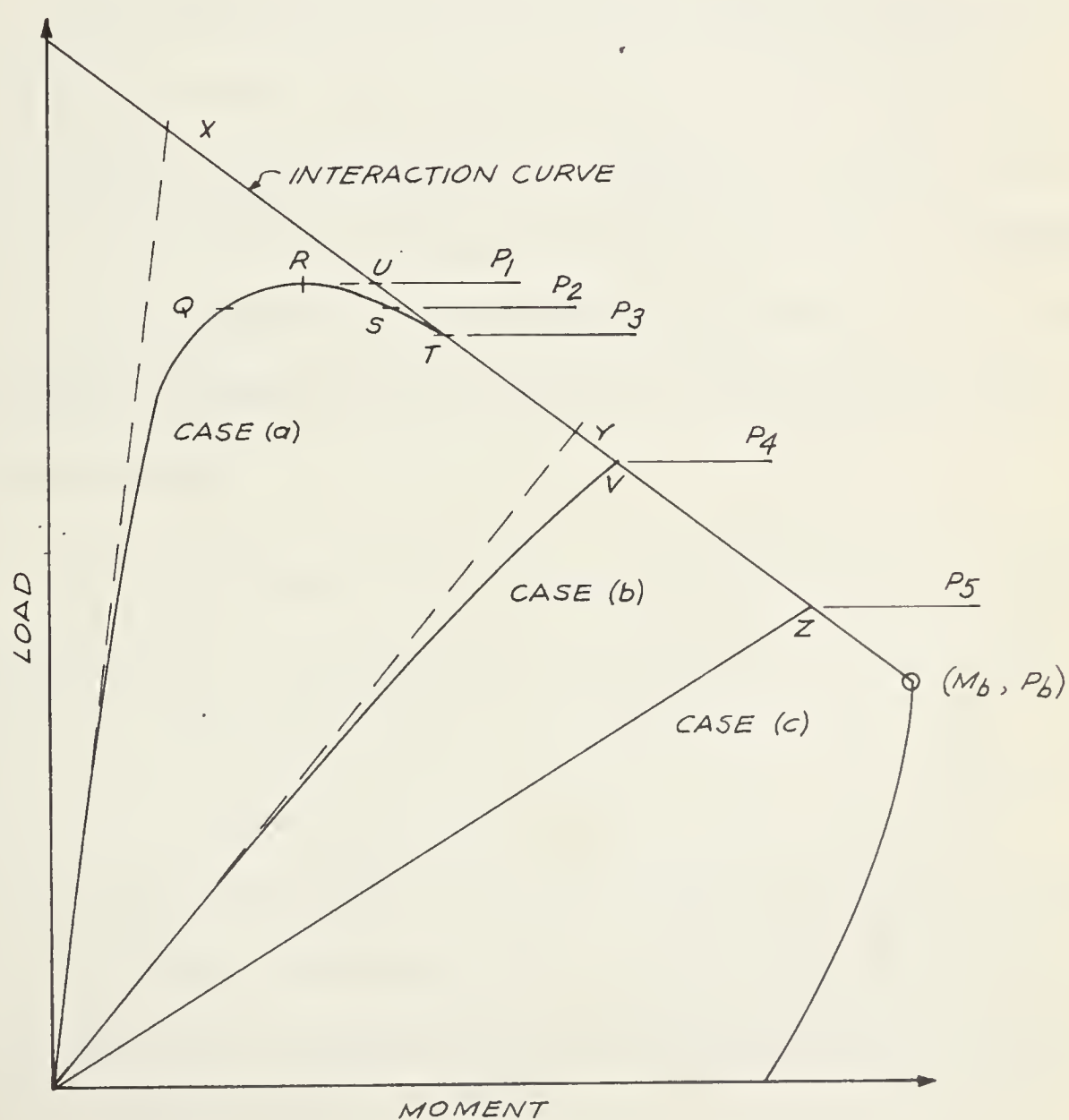


FIGURE 2-2 LOAD-MOMENT CURVES FOR FAILURE SECTIONS

from the end, as in Cases (a) and (b). With perfectly antisymmetrical conditions there are theoretically two equally critical sections, one in each half length. However, because of imperfections which are always present in a real member, failure will occur near one end or the other. In FIGURE 2 - 1 the failure sections were arbitrarily shown in the upper half of the column.

The relationship between the applied loads and moments and the strength of a short column are expressed on a load-moment interaction diagram, such as FIGURE 2 - 2. Typical load-moment curves for the failure sections of Cases (a), (b), and (c) are shown in FIGURE 2 - 2, and are marked Case (a), (b) and (c), respectively. Each curve corresponds to a particular type of behavior, and is discussed in the following sections.

Each load-moment curve mentioned above terminates at the interaction curve. The interaction curve forms the envelope of all load-moment combinations which are possible for a given cross-section without failure of the column material. Any combination of load and moment which falls on the curve produces crushing of the concrete at the extreme compression fibre. Details of the assumptions and methods used in obtaining interaction curves for the test columns are given in Section 2.2.

(i) Buckling Failure. One possible mode of failure of an eccentrically loaded column is by buckling in the plane of the applied eccentricity. Von Karman's theory of the buckling of an eccentrically loaded column (Bleich, 1952) may be described using the load-moment curve for the failure section. In a buckling failure, the failure section will generally be located away from the column end, as shown in Case (a) of FIGURE 2 - 1. The curve marked Case (a) in FIGURE 2 - 2 represents a typical load-moment curve for this section during a buckling failure. The initial eccentricity at the section, e_i , is represented by Line O-X which has the slope $P/M = 1/e_i$.

Because of the moments resulting from the end eccentricities the column will deflect laterally as soon as load is applied, and the total eccentricity at the failure section will be larger than e_i by the amount of the lateral deflection. The load-moment curve is therefore shown to the right of Line O-X. The additional moment caused by the deflection is equal to P_y , where y is the lateral deflection at the section. This additional moment is often termed "Py-moment". For simplicity it will be referred to in this way in the balance of this thesis. As loading is continued, the rate of deflection will increase at an increasing rate, due to the Py-moment effect, and the load-moment curve will depart from Line O-X at an increasing rate.

At load P_2 , two values of moment and hence deflection are possible if the failure section behaves according to Line O-Q-R-S-T. The first configuration, corresponding to Point Q, is stable because an increase in load would be required to increase the deflection. The second configuration, corresponding to Point S, is unstable since an increase in deflection would require a decrease in load.

As loading is continued the maximum possible load will be reached, which is the value P_1 corresponding to Point R. At this load there is a transition from stable to unstable equilibrium, so that Load P_1 is the critical or buckling load.

The post-buckling behavior will depend on the type of loading. With a reaction-type loading, as in the tests reported herein, crushing of the concrete will not occur at the buckling load, but at some reduced load, P_3 , corresponding to Point T. With a gravity-type loading, as found in most real structures, no equilibrium is possible after Point R is passed, and the deflections will increase rapidly until crushing occurs under the applied load.

(ii) Material Failure. Another possible mode of failure of an eccentrically loaded column is by material failure with the failure section located away from the column end, as in Case (b), FIGURE 2 - 1.

The curve marked Case (b) in FIGURE 2 - 2 represents a typical load-moment curve for this section. The initial eccentricity at the section, e_i , is represented by Line O-Y which has the slope $P/M = 1/e_i$. Normally e_2 and e_i for this case will be greater than for Case (a).

As in the case of buckling failure, the column will deflect laterally as soon as load is applied, and the total eccentricity at the failure section will become larger than e_i by the amount of the lateral deflection. As loading is continued, deflections will increase at an increasing rate due to the P_y -moment effect. The total eccentricity will become larger than the maximum end eccentricity, e_2 . Finally, if the failure section behaves according to Line O-V, crushing of the concrete will occur at load P_4 corresponding to Point V, while the column is still in stable equilibrium. Therefore, in Case (b) material failure will have occurred before the buckling behavior described previously could develop.

Material failure may also take place with the failure section located at the column end, as in Case (c), FIGURE 2 - 1. The curve marked Case (c) in FIGURE 2 - 2 represents the load-moment curve for this section. The initial eccentricity at the section, e_i , is equal to e_2 and is represented by the line O-Z which has the slope $P/M = 1/e_2$. Normally e_2 for Case (c) will be greater than e_2 for Cases (a) and (b).

As in the previous cases, the column will deflect laterally as soon as load is applied. However, the total eccentricity at points away from the column end will not exceed e_2 . Crushing of the concrete will occur at the end of the column, at load P_5 , corresponding to Point Z in FIGURE 2-2, while the column is still in stable equilibrium. In Case (c), as in Case (b), material failure will have preceded buckling. Unlike Case (b), the ultimate load in Case (c) is not affected by the magnitude of lateral column deflections.

It is possible to determine whether instability preceded material failure by interpretation of the load-moment curve for the failure section. If the curve has attained zero slope before intersecting the interaction curve then instability has preceded material failure. On the other hand, if the curve has maintained a positive slope throughout, instability has not preceded material failure.

2.2 Computation Of Interaction Curves

(a) Introduction

As explained in Section 2.1, the behavior of a column subjected to combined bending and axial load may be interpreted with the aid of a short column failure interaction curve, or simply interaction curve. A

typical interaction curve is shown in FIGURE 2 - 2. The curve forms the envelope of all load-moment combinations, for a given cross-section, which are possible without material failure. Any combination of load and moment which falls on the curve will produce crushing of the concrete at the extreme compression fibre. At the "balance point", ($M = M_b$, $P = P_b$), the tension steel reaches the yield point simultaneously with crushing of the concrete at the compression face. At failure loads less than P_b , yielding of the tension steel precedes crushing of the concrete. Failure is therefore initiated by tension yielding, and is termed a tension failure. At failure loads greater than P_b , failure is initiated as a result of compression crushing prior to yielding of the tension steel, and is termed a compression failure.

Details of the assumptions and computations used in obtaining interaction curves for the test columns are presented in this section.

(b) Assumptions

The assumptions made in computing the interaction curves were similar to those originally proposed by Hognestad (1951). These assumptions have been used, with slight variations in the numerical constants, in all the investigations carried out since 1951, reviewed in Section 1.2.

(i) Steel Stress-Strain Relationship. The simplified elasto-plastic stress-strain curve shown in FIGURE 2 - 3 was assumed for the reinforcing steel in tension and compression. The modulus of elasticity, E_s , was taken as 30,000,000 psi. As indicated in Chapter III, the median yield point stress, f_y , for all the reinforcing steel was 46,400 psi and this value was used in all the computations.

(ii) Concrete Stress-Strain Relationship. The assumed stress-strain curve for concrete in compression is shown in FIGURE 2 - 4. The initial elastic modulus, E_c , was taken as:

$$E_c = 1,800,000 + 460 f'_c \text{ psi} \quad (\text{EQ. 2-1})$$

The ultimate concrete strain, ϵ_u , was taken as 0.0038 inches per inch for all concrete strengths. Concrete was assumed to have no tensile strength. These assumptions are identical with those proposed by Hognestad (1951).

The properties of the compressive stress block obtained from the assumed stress-strain curve may be represented by the coefficients k_1 and k_2 . The coefficient k_1 is the ratio of the average stress to the maximum concrete compressive stress in a structural member, f'_c . The coefficient k_2 is the ratio of the distance between the compression face and the compression centroid to the depth of the stress block, a , as shown in FIGURE 2 - 5. The coefficients are a function of the maximum

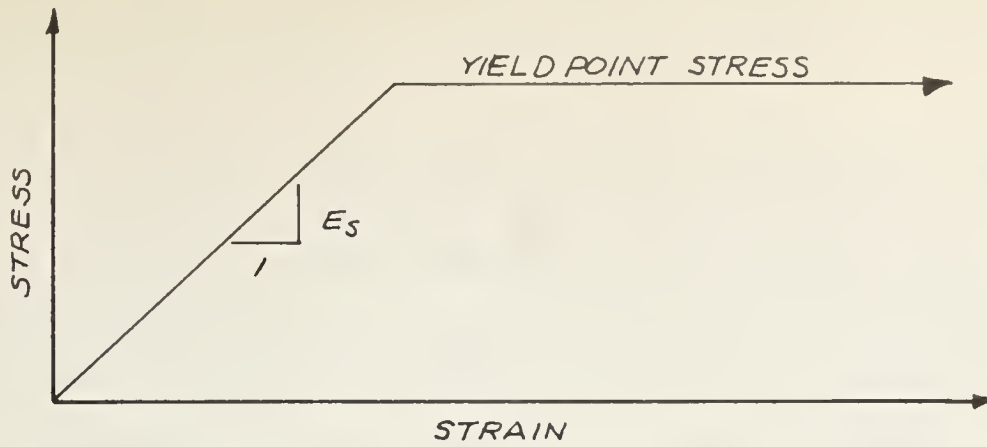


FIGURE 2-3 ASSUMED STRESS-STRAIN CURVE FOR STEEL

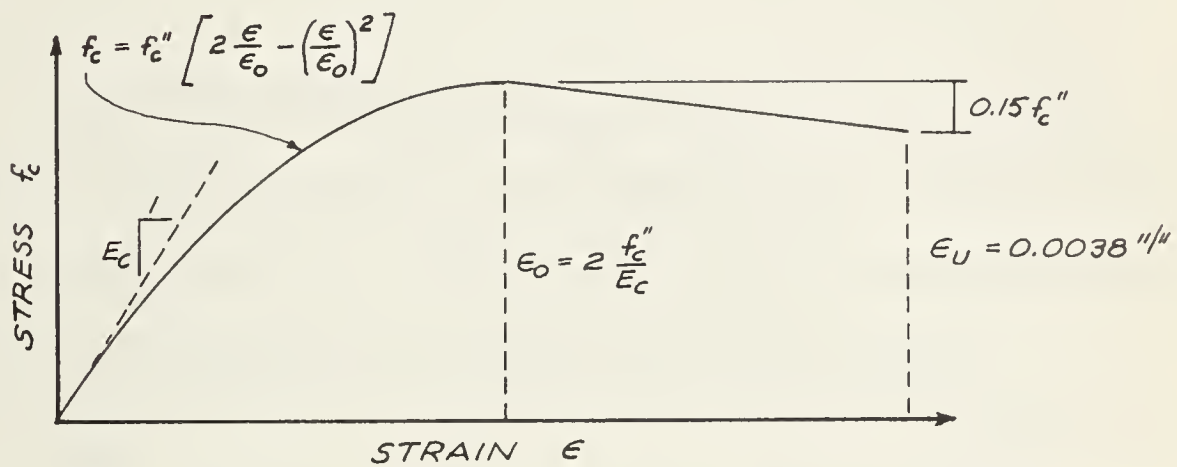


FIGURE 2-4 ASSUMED STRESS-STRAIN CURVE FOR CONCRETE

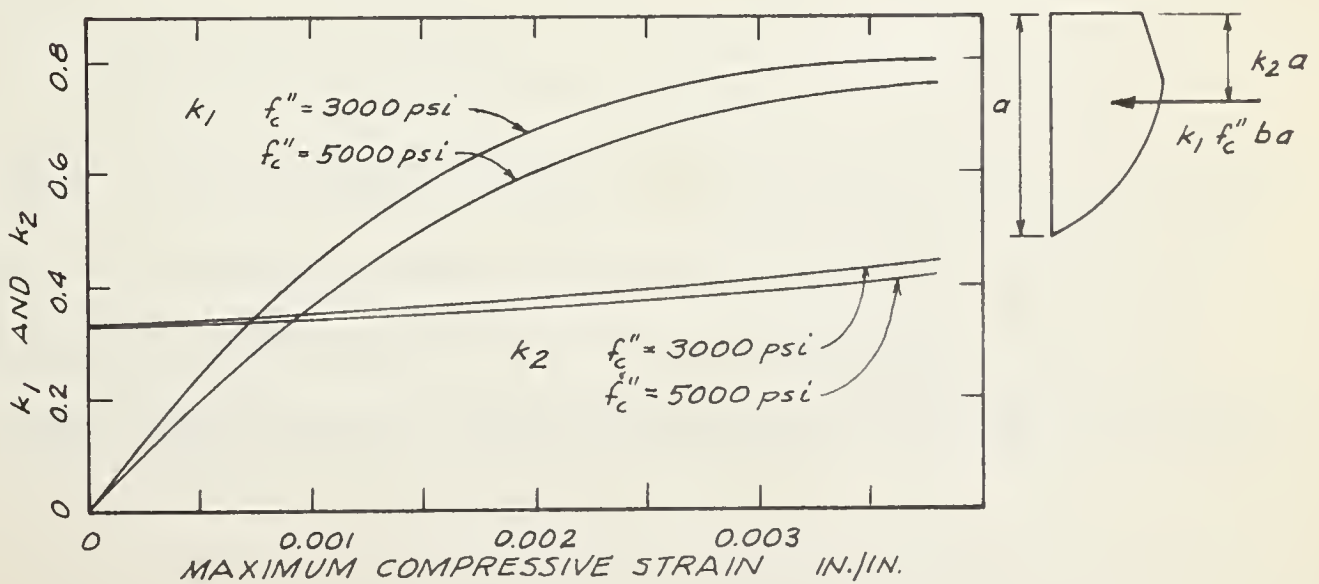


FIGURE 2-5 CONCRETE STRESS BLOCK PARAMETERS

compressive strain. Both coefficients were computed for various values of f_c'' and for strains ranging from zero to ϵ_u . The results were plotted as curves similar to those in FIGURE 2 - 5. For these computations the stress block was divided into a number of segments and the area of each segment was calculated. The coefficients were determined by summing the area and moment of the segments in the appropriate manner.

(iii) Maximum Concrete Compressive Stress In Columns. The maximum compressive stress in the Hognestad stress-strain curve is denoted by the symbol f_c'' in FIGURE 2 - 4. This stress is related to the standard 6 x 12 inch cylinder strength, f_c' , by the equation:

$$f_c'' = k_3 f_c' \quad (\text{EQ. 2 - 2})$$

Since the coefficient k_3 may have a value other than unity it must be evaluated in order that the stress-strain curve may be applied to real members.

In theory the magnitude of k_3 can be determined from test results by comparing measured and computed ultimate loads, deflections and moment-curvature curves. The agreement between measured and computed deflections (Chapter VI) was not close enough for k_3 to be determined, and curvature measurements were not included in the tests.

Hognestad (1951) adopted the value $k_3 = 0.85$ in his study of eccentrically loaded columns. This value was based in part on earlier tests of concentrically loaded columns (Richart, et al, 1957). These findings were based on a comparison of ultimate loads. In tests of long hinged columns cast horizontally, Chang and Ferguson (1963) obtained good agreement between measured and computed moment-curvature curves using $k_3 = 0.85$. In similar tests Breen (1962) found the value of k_3 to range between 0.85 and 1.00 and selected $k_3 = 0.85$ for use in evaluating statically indeterminate tests.

In view of the foregoing, interaction curves with $k_3 = 0.85$ were used in discussing the test results. However, interaction curves with $k_3 = 1.00$ have been plotted for comparison. When reference is made to interaction curves in the following chapters, and k_3 is not specified, it is understood that the curves with $k_3 = 0.85$ are meant. In the theoretical long column analysis of Chapter VI the value of k_3 was taken as 0.85.

(iv) Strain Distribution. Bernoulli's hypothesis that sections normal to the axis of the column that were plane before bending remain plane after bending was assumed to hold for reinforced concrete columns under combined bending and axial load, and for reinforced concrete beams in flexure. The validity of this assumption has been well documented with test results (Richart, et al, 1947; Hognestad, 1951).

(c) Method of Computation

Interaction curves were plotted for concrete strengths of 3000, 4000, and 5000 psi. Curves for the various test strengths were obtained by interpolation. The areas and dimensions of the column cross-section are shown in FIGURE 2 - 6.

Each original interaction curve was obtained by computing the coordinates of a number of random points and fitting a smooth curve between them. Computations were required for two basic cases. In Case (1), illustrated in FIGURE 2 - 7, the section is partially in tension and a cracked section was assumed. In Case (2), illustrated in FIGURE 2 - 8, the section is wholly in compression. The method of computation for each case is outlined in the following paragraphs.

Compressive strains, stresses and forces were taken as positive. All moments were referred to the centroidal axis. The sign convention is shown in FIGURES 2 - 7 and 2 - 8.

CASE (1) Cracked Section

- (1) A value of f'_c was assumed and ϵ_4 was taken equal to ϵ_u .
- (2) A value for ϵ_1 was assumed and ϵ_2 and ϵ_3 were computed from the geometry of the section.

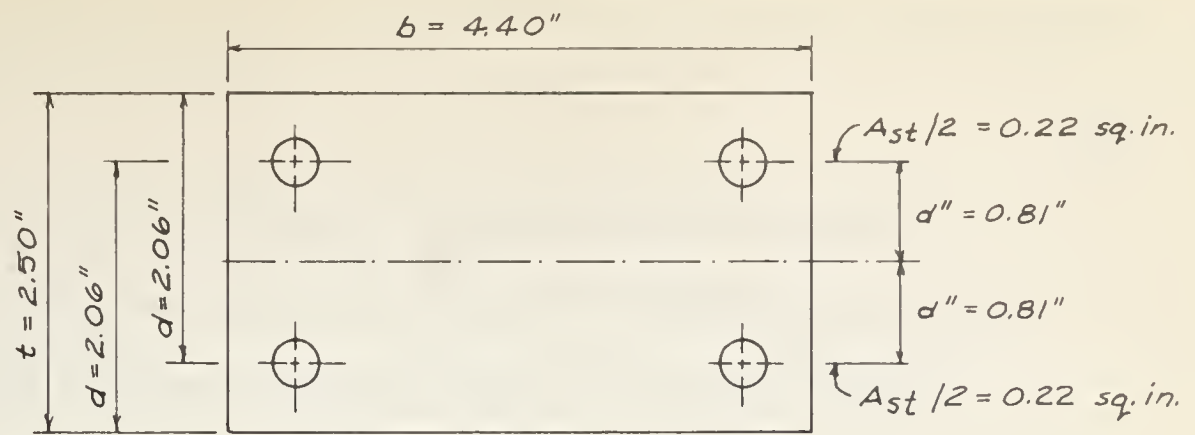


FIGURE 2-6 COLUMN CROSS-SECTION

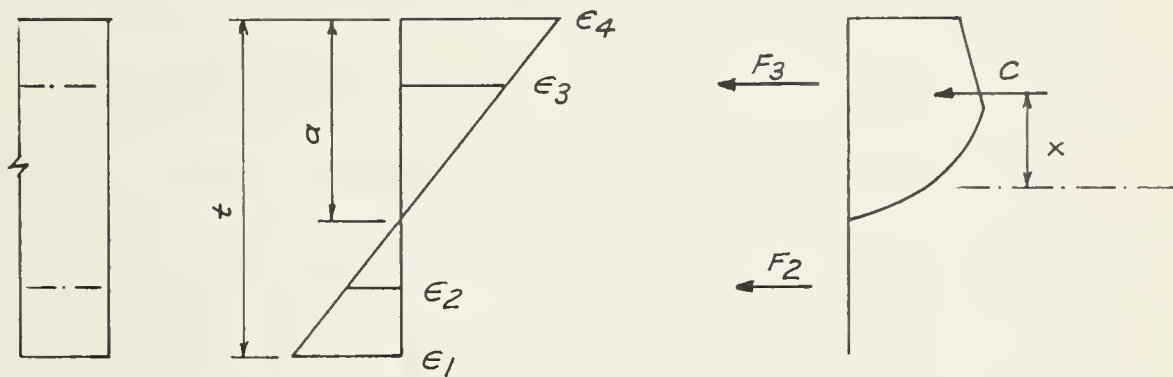


FIGURE 2-7 CASE (1) CRACKED SECTION

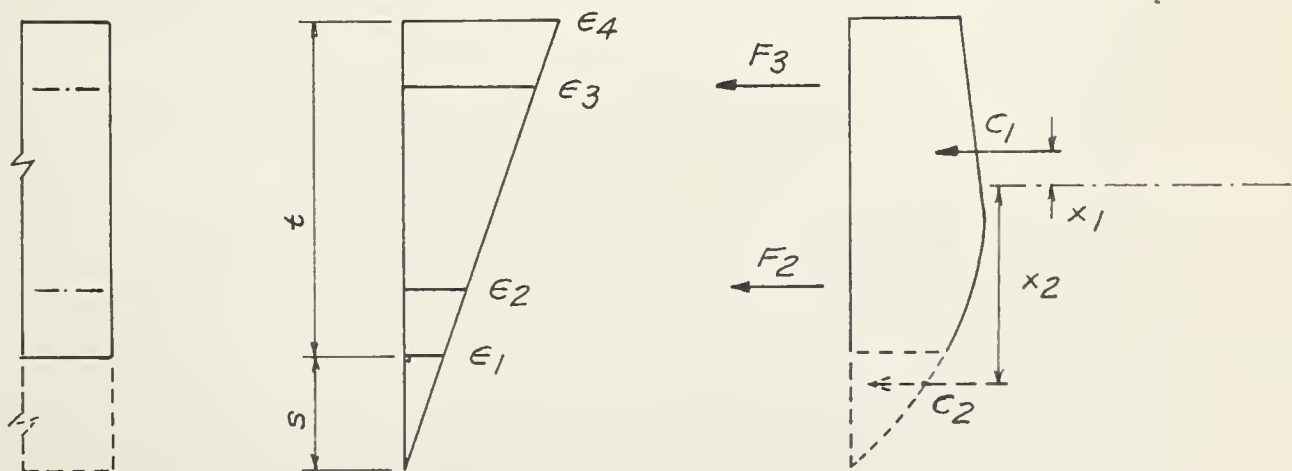


FIGURE 2-8 CASE (2) UNCRACKED SECTION

(3) Values of k_1 and k_2 were obtained from the curves (FIGURE 2 - 5) for the maximum compressive strain ϵ_4 .

(4) The concrete compression force, C , and its moment arm, x , were computed using the equations:

$$C = k_1 f_c'' b a \quad (\text{EQ. 2 - 3})$$

$$x = (t/2) - k_2 a \quad (\text{EQ. 2 - 4})$$

(5) The reinforcement forces, F_2 and F_3 were computed using the equations:

$$F_2 = \epsilon_2 E_s \quad (\text{EQ. 2 - 5})$$

$$F_3 = \epsilon_3 E_s \quad (\text{EQ. 2 - 6})$$

(6) The net axial force, P , was computed from:

$$P = F_2 + F_3 + C \quad (\text{EQ. 2 - 7})$$

(7) The net moment, M , was computed from:

$$M = (F_3 - F_2) d'' + Cx \quad (\text{EQ. 2 - 8})$$

(8) The coordinates (M, P) were plotted as a point on the interaction curve.

CASE (2) Uncracked Section

(1) A value for f_c'' was assumed and ϵ_4 was taken equal to ϵ_u .

(2) A value for ϵ_1 was assumed and ϵ_2 and ϵ_3 were computed from the geometry of the section.

- (3) Values of k_1 and k_2 were obtained from the curves (FIGURE 2 - 5) for the maximum compressive strain ϵ_4 .

- (4) The gross concrete compression force, C_1 , and its moment arm, x_1 , were computed from the equations:

$$C_1 = k_1 f_c'' b t \quad (\text{EQ. 2 - 9})$$

$$x_1 = (t/2) - k_2 t \quad (\text{EQ. 2 - 10})$$

- (5) Values of k_1 and k_2 were obtained from the curves (FIGURE 2 - 5) for the maximum compressive strain ϵ_1 .

- (6) The fictitious concrete compression force, C_2 , and its moment arm, x_2 , were computed from the equations:

$$C_2 = k_1 f_c'' b s \quad (\text{EQ. 2 - 11})$$

$$x_2 = k_2 (t - s) - (t/2) \quad (\text{EQ. 2 - 12})$$

- (7) The reinforcement forces F_2 and F_3 were computed from the equations:

$$F_2 = \epsilon_2 E_s \quad (\text{EQ. 2 - 5})$$

$$F_3 = \epsilon_3 E_s \quad (\text{EQ. 2 - 6})$$

- (8) The net axial force, P , was computed from:

$$P = F_2 + F_3 + C_1 - C_2 \quad (\text{EQ. 2 - 13})$$

- (9) The net moment, M , was computed from:

$$M = (F_3 - F_2) d'' + C_1 x_1 - C_2 x_2 \quad (\text{EQ. 2 - 14})$$

- (10) The coordinates (M , P) were plotted as a point on the interaction curve.

CHAPTER III

DETAILS OF TESTS

3.1 Details Of Test Specimens

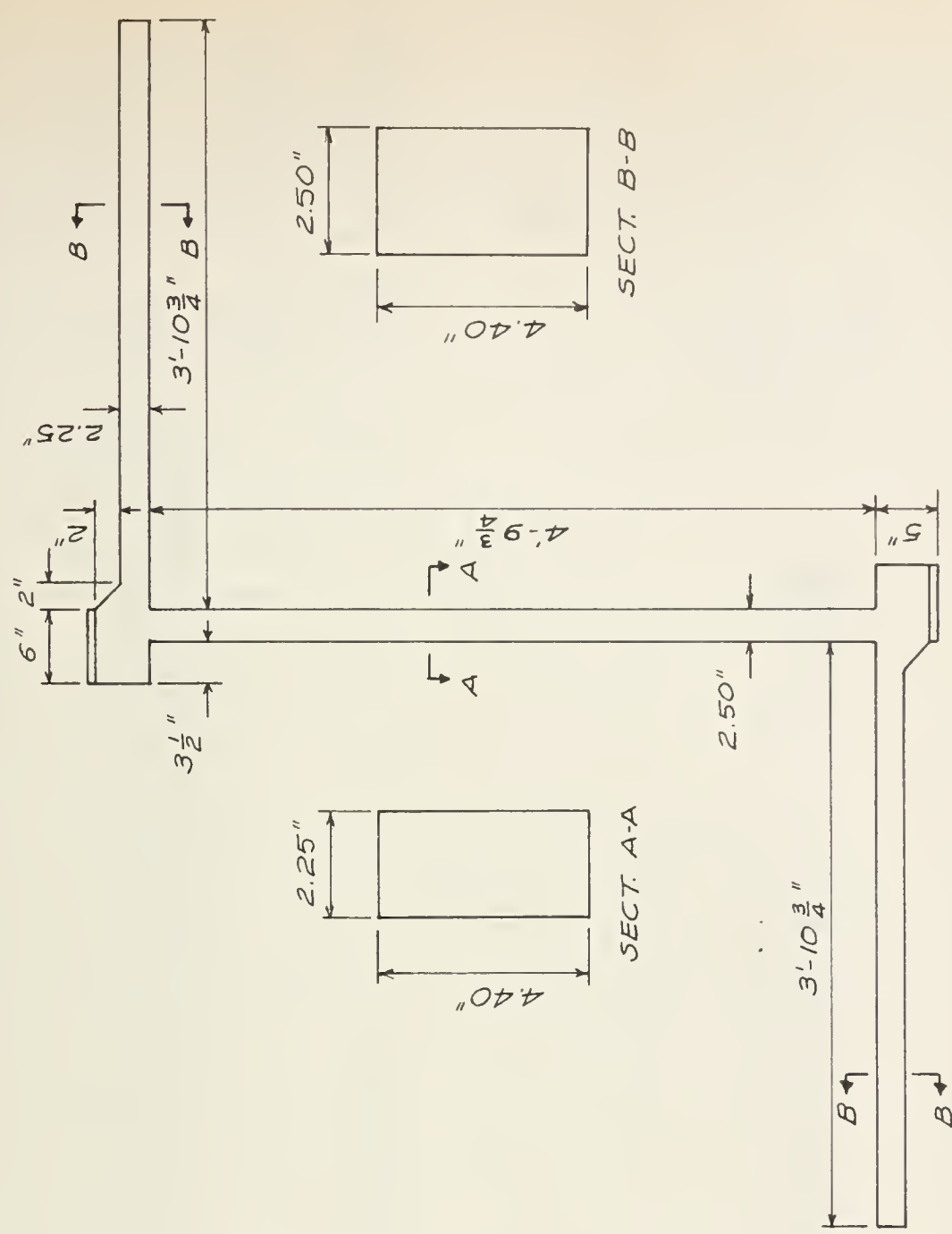
(a) Description

Eight specimens were fabricated for the testing program. The dimensions of the four hinged columns (Test Series A and B) are given in FIGURE 3 - 1 (a). The dimensions of the four restrained columns (Test Series C and D) are given in FIGURE 3 - 1 (b). The dimensions of the column portions were identical for all the specimens.

Details of the main column and beam reinforcement are shown in FIGURE 3 - 2. Details of the extra reinforcement placed in the column end blocks are shown in FIGURE 3 - 3 (c). The reinforcement was the same for all the test specimens. The longitudinal reinforcement in both the columns and the beams consisted of four #3 deformed bars, bent as shown. The reinforcement for a restrained column specimen is shown in FIGURE 3 - 4.

SCALES:
 $\frac{3}{4}'' = 1'-0''$
 $3'' = 1'-0''$

(b) TEST SERIES C AND D



(a) TEST SERIES A AND B

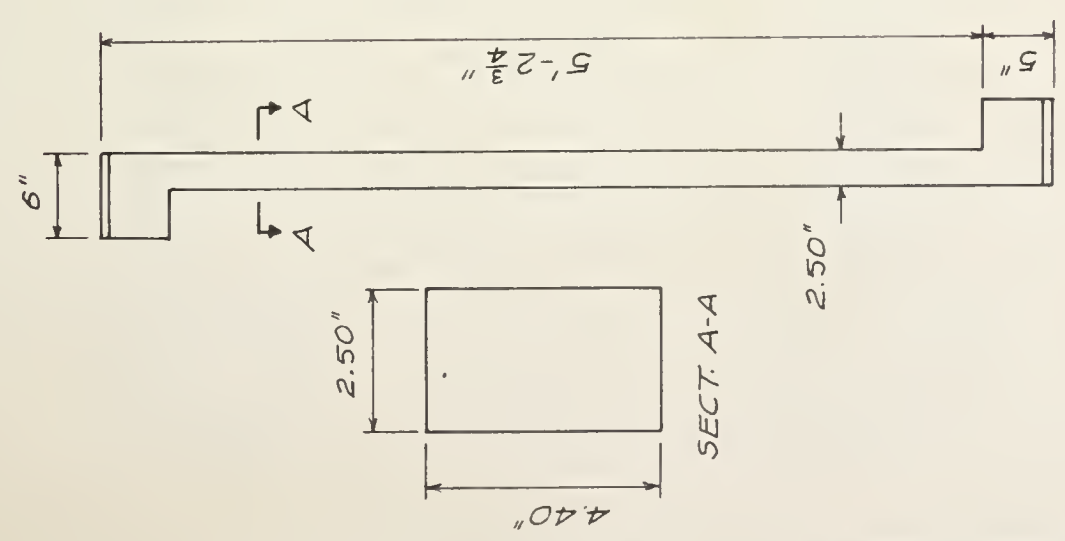
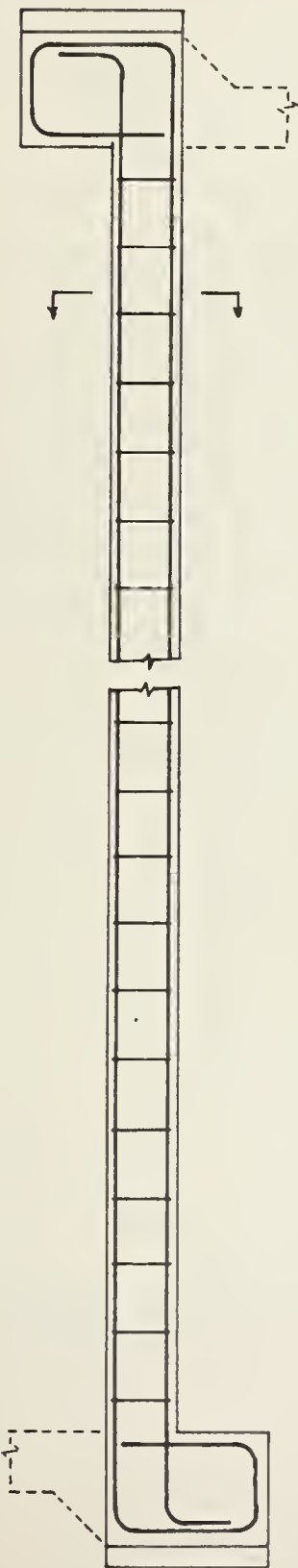


FIGURE 3-1 TEST SPECIMEN DIMENSIONS

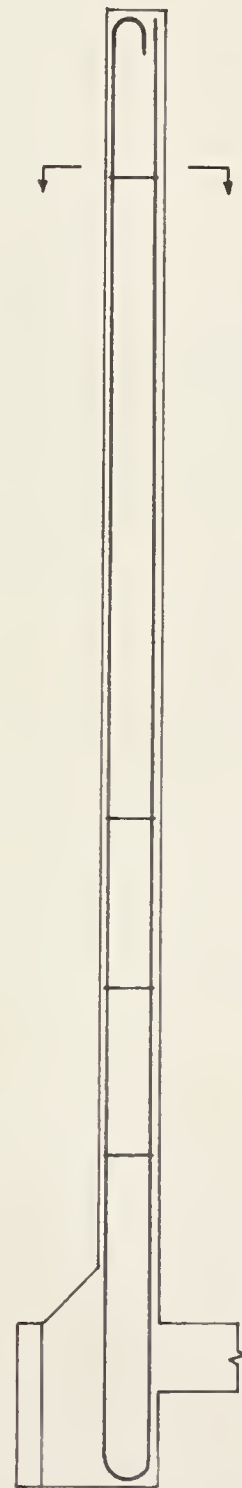


$\frac{1}{4}$ " COVER ON BARS
ALL SIDES

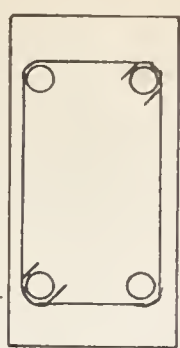


4 - #3 BARS
WIRE TIES @ $2\frac{1}{2}$ " O.C.

COLUMN REINFORCEMENT



$\frac{5}{8}$ "
 $\frac{1}{4}$ "

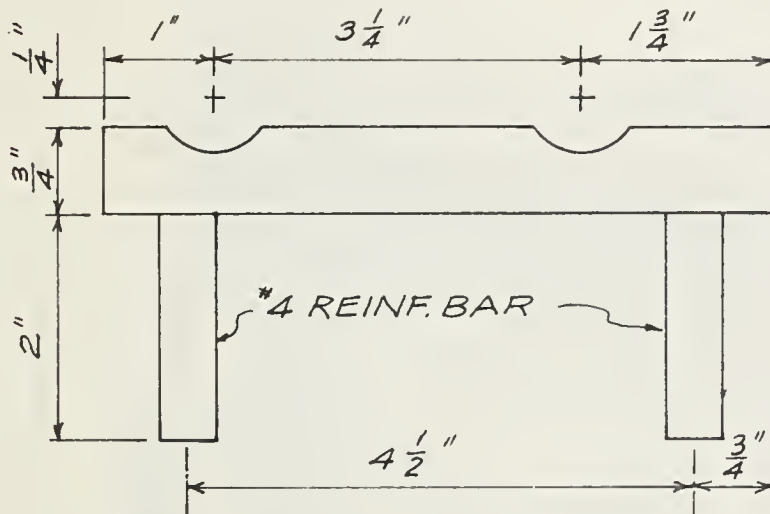
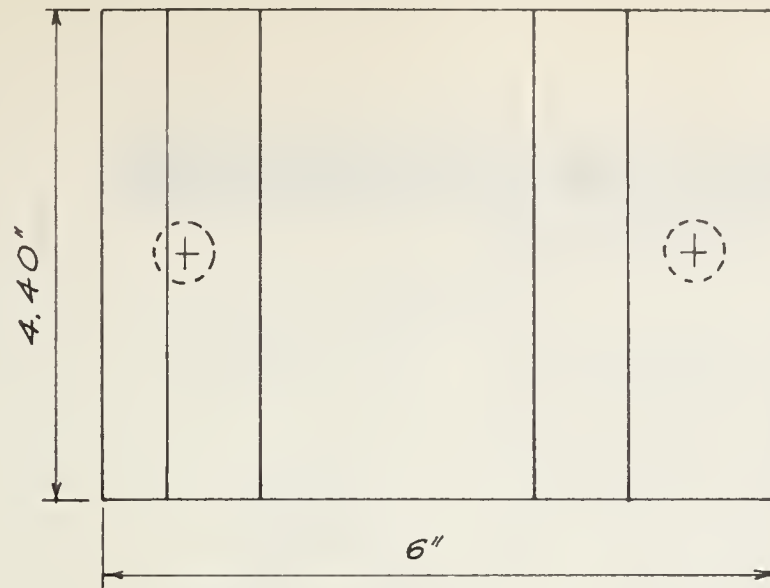


4 - #3 BARS
WIRE TIES AS SHOWN

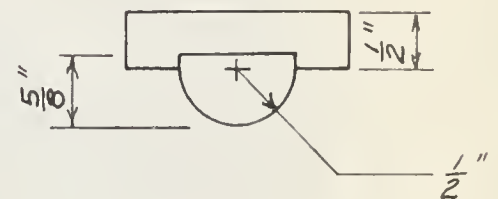
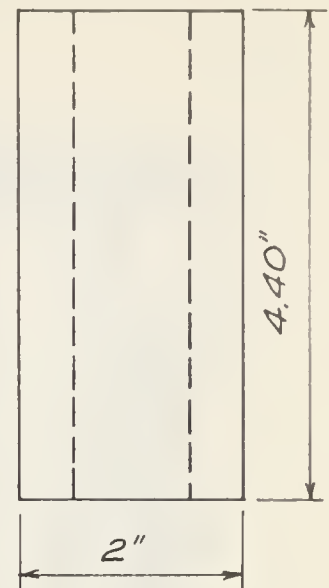
BEAM REINFORCEMENT

SCALE:
 $1\frac{1}{2}" = 1'-0"$

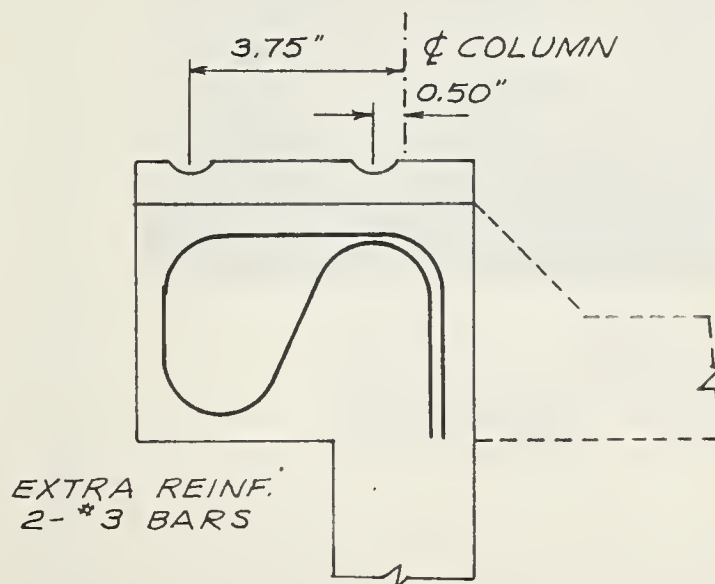
FIGURE 3 - 2 COLUMN AND BEAM REINFORCEMENT



(a) END BEARING PLATE
SCALE: HALF SIZE



(b) LOAD PIVOT
SCALE: HALF SIZE



(c) COLUMN END BLOCK
SCALE: 3" = 1'-0"

FIGURE 3-3 TEST SPECIMEN DETAILS



FIGURE 3-4
FORMWORK AND REINFORCEMENT FOR
RESTRAINED COLUMN SPECIMEN

Details of an end bearing plate are shown in FIGURE 3 - 3(a). The plates were fabricated from cold rolled steel. A plate was cast into each column end block as shown in FIGURE 3-3(c). The two end eccentricities used in the testing program were obtained by loading the columns through one or other of the two grooves in the plates.

(b) Reinforcement

(i) Material. The longitudinal reinforcement for all the columns and restraining beams was fabricated from 3/8 inch diameter (#3) deformed bars meeting ASTM Specification A 305. The bars were purchased locally in 20 foot lengths. Mill test reports for reinforcing bar specimens taken from each of eight ingots comprising the shipment gave the physical properties shown in TABLE 3-1. The median yield point stress, 46,400 psi was used in all computations.

TABLE 3 - 1			
REINFORCEMENT		PROPERTIES	
Item	Minimum Value	Maximum Value	Median Value
Yield Point psi	44,600	48,200	46,400
Ultimate Strength psi	60,900	63,600	62,700
Elongation In 8 inches percent	23	27	25

The column ties and restraining beam ties were fabricated from Number 10 gauge black annealed wire purchased in rolls.

(ii) Fabrication. The reinforcing bars and the ties were bent to shape using hand tools and a bench vise and were assembled into cages before being placed in the formwork. The beam reinforcement cage was narrower than the column cage, and fitted between the column bars in the restrained column specimens. In all cases the clear concrete cover over the column bars was the same on all four faces.

Special care was taken in bending the ties, which were used to hold the longitudinal bars in position. Small hexagonal machine nuts were used as spacers to maintain the required clearance between the reinforcement and the formwork when the concrete was cast.

(c) Concrete

(i) Materials. The cement used was Type One Portland Cement manufactured by Inland Cement Company Limited. It was purchased locally in paper sacks and stored in the original containers until used.

The fine aggregate was a washed river sand and had a fineness modulus of 2.54. The coarse aggregate was a washed crushed river gravel with 3/8 inch maximum size.

Several trial mixes were made and tested at seven days in order to determine the final mix proportions. Since mechanical vibrating equipment was not available, and concrete cover over the column ties was only 1/4 inch, a six inch slump was chosen to facilitate compaction. Small changes were made to the mix proportions as the work progressed to improve workability. The final mix proportions for each test specimen are given in TABLE 3 - 2.

TABLE 3 - 2
CONCRETE MIX PROPORTIONS

TEST SPECIMEN	WATER/ CEMENT Gallons per sack - (Canadian)	MIX PROPORTIONS BY WEIGHT		
		CEMENT	FINE AGGREGATE	COARSE AGGREGATE
A1	5.9	1.00	2.29	1.94
A2	5.9	1.00	2.46	2.21
B1	6.3	1.00	2.43	2.14
B2	5.9	1.00	2.39	2.21
C1	6.4	1.00	2.47	2.27
C2	5.7	1.00	2.30	2.11
D1	6.2	1.00	2.45	2.21
D2	6.5	1.00	2.41	2.19

(ii) Fabrication. The formwork used was constructed of 3/4 inch paper coated plywood on a plywood base stiffened with 2 by 6 inch wood stringers. A view of the formwork is shown in FIGURE 3 - 4. A system of blocks, wedges, and clamps was provided to ensure correct dimensions and alignment. One set of formwork was used for all the specimens, with the restraining beams blocked off when not required. The formwork was cleaned and checked for accuracy before each concrete pour.

All concrete was mixed in an electrically powered drum mixer of approximately three cubic feet capacity. The concrete was then transported from the mixing room to the casting room. Considerable segregation occurred while in transit and the concrete was re-mixed by hand before placing. After placing, the concrete was thoroughly tamped with a metal rod. Three standard 6 x 12 inch cylinders were cast with each specimen.

About one hour after casting each specimen was given a final trowelling and covered with plastic sheeting. After 24 hours the side forms were loosened and the specimen was covered with wet burlap. Three days after casting, the specimen was removed from the formwork and cured an additional four days under wet burlap. Each specimen was then stored in air until tested. The concrete cylinders were cured

and stored with the specimens, and tested the same day as the specimens. Concrete strengths are given in TABLE 3 - 3.

TABLE 3 - 3
CONCRETE STRENGTHS

Test Specimen	Date Cast	Age at Test Days	Cylinder Strength - psi			
			1	2	3	Average
A1	3, Nov., 1961	28	4780	5130	4750	4880
A2	10, Nov., 1961	28	4760	4810	4640	4740
B1	7, Nov., 1961	28	4140	4250	4230	4210
B2	14, Nov, 1961	28	4810	4630	4760	4730
C1	29, Jan., 1962	32	3710	3860	3950	3840
C2	1, Feb., 1962	30	4560	4550	4120	4410
D1	22, Jan., 1962	32	3220	3700	3970	3630
D2	25, Jan., 1962	33	4250	4520	4890	4550

3.2 Hinged Column Tests

(a) Loading System

The hinged columns were tested in a 200,000 pound Baldwin testing machine. A view of the test arrangement is shown in FIGURE 3 - 5. Each specimen was tested in an upright position, with the thrust line coincident with the centerline of the testing machine. Load was

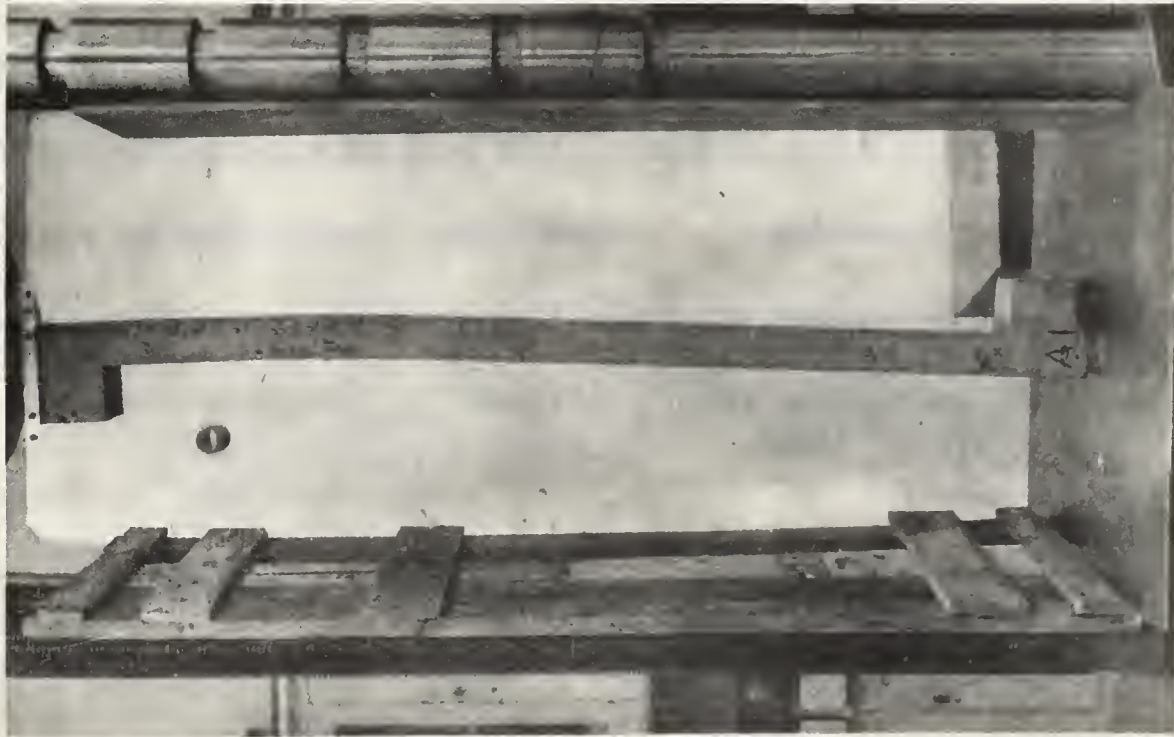


FIGURE 3-5
SPECIMEN AI AFTER FAILURE

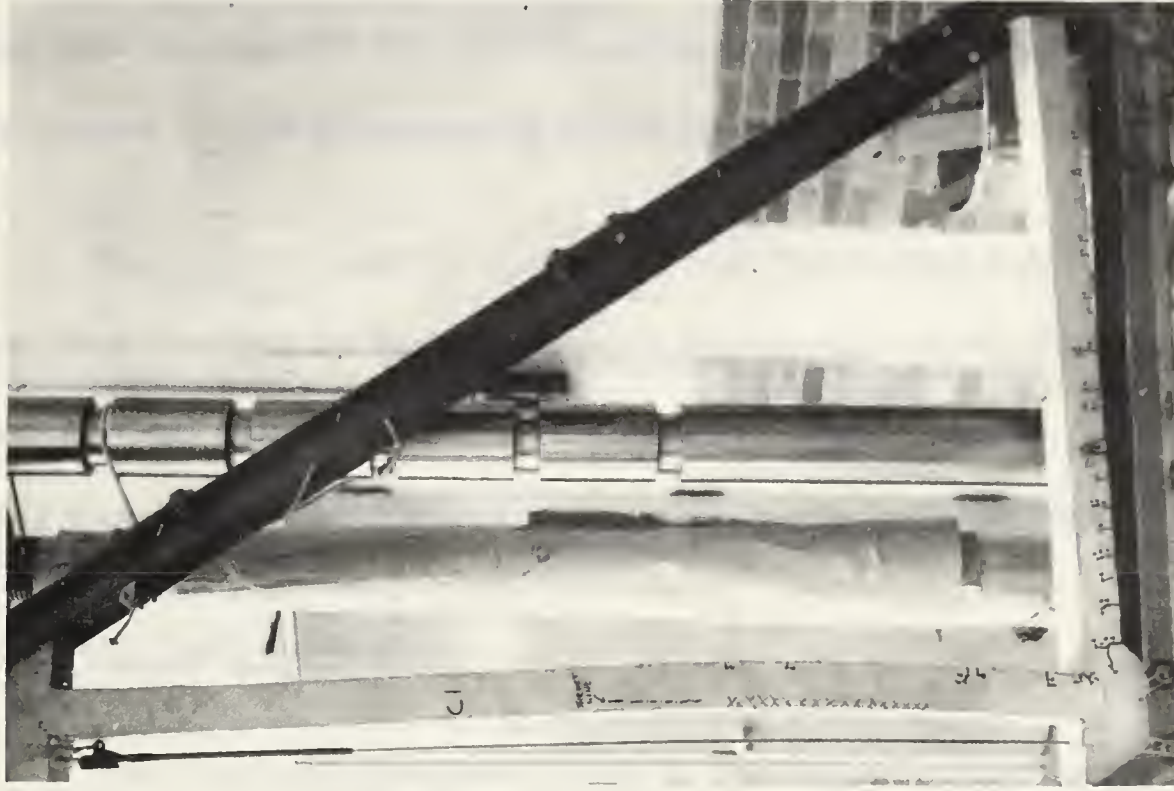


FIGURE 3-6
SPECIMEN CI AFTER FAILURE



FIGURE 3-7
SPECIMEN AI TENSION
FACE OF FAILURE ZONE

applied to the column end bearing plates through two cylindrical load pivots (FIGURE 3 - 3(b)) which fitted into grooves in the bearing plates. The grooves were greased to reduce friction. The load pivots were held in place against the testing machine head and platten by friction. A ball joint was used at the testing machine head to compensate for any inaccuracies in the alignment of the bearing surfaces.

The applied load was regulated with the testing machine controls. When creep occurred during observation periods the vernier control was opened a small amount to maintain a constant load. No specific rate of loading was used, but care was taken to apply the loads smoothly.

(b) Instrumentation

The only measurements made in the hinged column tests were the magnitude of the applied load and the lateral deflections of the column at each load level. The applied load readings were obtained directly from the testing machine load dial. The dial could be read to the nearest 50 pounds in Test Series A and 10 pounds in Test Series B. During the time required to make the measurements at any given load level, the load varied by about plus or minus 75 pounds in Test Series A and about 25 pounds in Test Series B.

The lateral deflections were measured at six stations located as shown in FIGURE 3 - 8. At each station small finishing nails were glued to the column with rigid setting cement. A fine monofilament nylon line was anchored at the lower end bearing plate and run over a smooth pin in the upper end bearing plate, as shown in FIGURE 5 - 19. A weight was attached to the line to keep it taut. Deflection measurements were made with a steel rule bearing against each nail and passing under the reference line. The rule was read at its intersection with the reference line. The rule was graduated in hundredths of an inch and measurements were recorded to the nearest graduation.

(c) Experimental Procedure

Each specimen was set in place in the testing machine and carefully centered. A clamping load of about 75 pounds was applied to hold the specimen in position. Initial lateral deflection readings were taken and recorded.

Increments of load were then applied. Lateral deflection readings were taken and recorded. Surfaces were examined for tension cracks with a magnifying glass. Cracks were traced with a marking crayon and the depth at each load increment was marked. At various load levels photographs were taken to record the appearance of the test specimen. Loading was continued in increments until failure occurred, after four to eight increments.

At higher load levels a second set of lateral deflection readings was taken just before the following load increment was added to determine whether deflections were increasing under constant load as a result of the effects of creep.

3.3 Restrained Column Tests

(a) Loading System

The restrained columns were tested in the same testing machine as the hinged columns. A partial view of the test arrangement is shown in FIGURE 3 - 6. The testing frame described in Appendix A was used to support the free ends of the restraining beams. The load pivots were aligned and held in position in the same manner as in the hinged column tests. A load cell was clamped to the free end of each restraining beam and they acted against the testing frame to provide the beam reactions.

Load application was regulated with the testing machine controls in the same manner as in the hinged column tests.

(b) Instrumentation

The measurements made in the restrained column tests were the magnitude of the applied load, and beam reactions and the lateral

deflections of the column and beams at each load level. The applied load readings were obtained directly from the testing machine load dial. The dial could be read to the nearest 50 pounds. During the time required to make measurements at any given load level, the load varied by about plus or minus 75 pounds. The beam reaction readings were obtained using two Kyowa two-ton load cells and an electronic strain indicator. The load cells had a sensitivity of 4.50 and 4.38 pounds per dial division on the strain indicator.

Lateral deflections were measured at six column stations and eight beam stations in the same manner as in the hinged column tests. The nylon reference lines were attached to the specimen at locations shown in FIGURE 3 - 9. The location of all measuring stations and reaction points are also shown in FIGURE 3 - 9.

Instrumentation for measuring the lateral displacement of the beam-column joints relative to the load pivots was not included. The computation of these displacements, used in reducing the observed test data, is given in Appendix C.

During the test it was necessary to adjust the beam reaction supports so that no moments were induced in the test specimen by differential deflection of the two ends of a restraining beam due to axial shortening of the column. A dial guage was installed adjacent to the

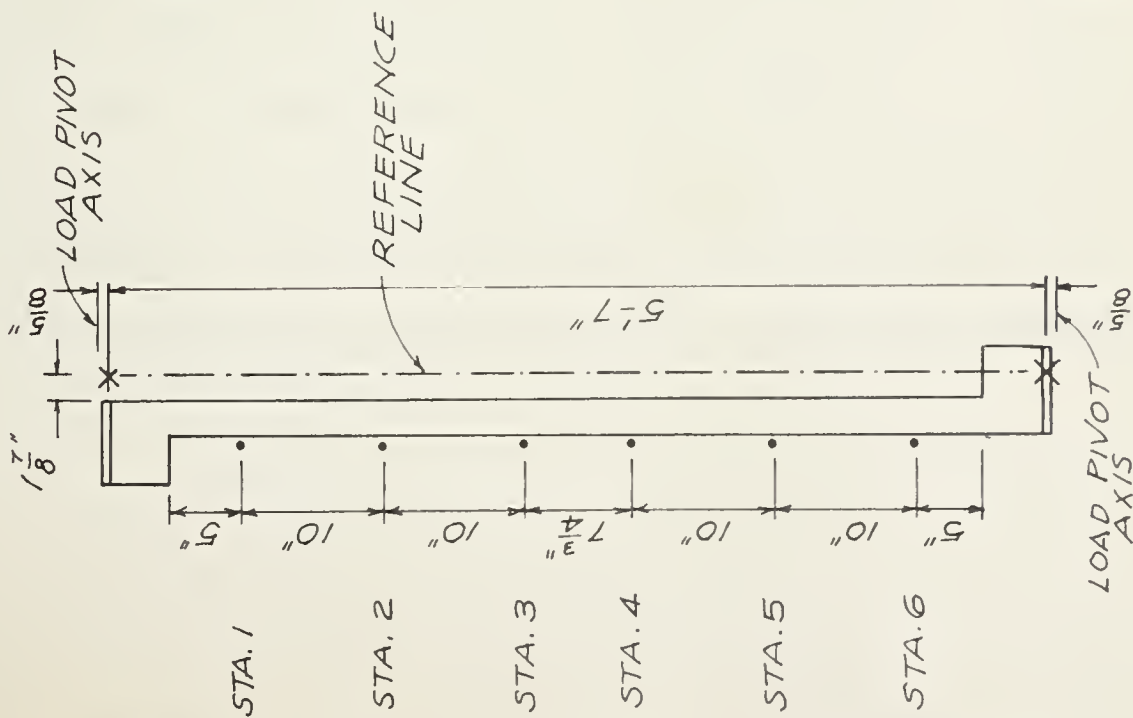


FIGURE 3-8 HINGED COLUMN MEASURING POINTS

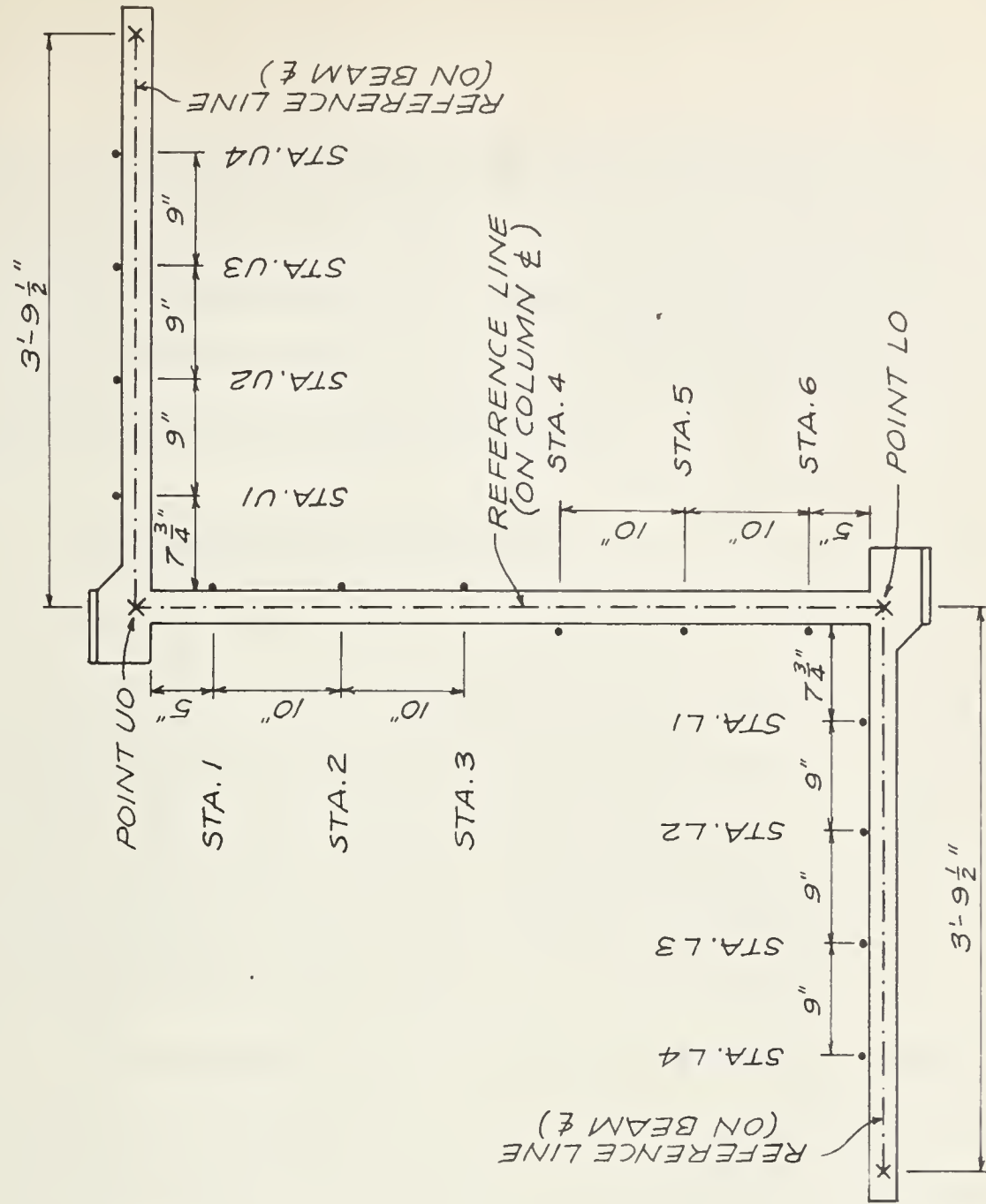


FIGURE 3-9 RESTRAINED COLUMN MEASURING POINTS

column to give the axial shortening at each load level. At each beam support a dial gauge was attached to the testing frame, bearing against the end of the restraining beam. Using these dials, the beam supports were adjusted after each load increment by an amount equal to the column shortening during that increment.

(c) Experimental Procedure

The testing frame was assembled around each specimen and the unit set in place in the testing machine and carefully centered. A clamping load of about 100 pounds was applied to hold the testing frame in position. The beam support adjusting bolts were set to just clear the load cells clamped to the beams. Initial lateral deflection, dial gauge and strain indicator readings were taken and recorded.

Increments of load were then applied with the testing machine. At each load level the axial shortening of the column was determined and the beam support adjusting bolts were adjusted a like amount. Following this, deflection and load cell readings were taken and recorded. Surfaces were examined for tension cracks with a magnifying glass. Cracks were traced with a marking crayon and the depth at each load level indicated. At various load levels photographs were taken to record the appearance of the test specimen. Since the restrained column

tests were rather lengthy, only one set of readings was taken at each load level to reduce the possible effects of creep on the test results. Loading was continued in increments, until failure occurred, after six to ten load increments.

3.4 Presentation of Test Results

The results of the tests described in this chapter are presented in Chapters IV and V and discussed in Chapters VI and VII. The observed test data is tabulated in Appendix B and the reduced test data is tabulated in Appendix C.

Four types of graphs (1 to 4, below) were used to present the results of both the hinged and restrained column tests. Two additional types of graphs (5 and 6, below) were required for the restrained column tests. On these graphs, points representing measured test data were plotted as filled and open circles. The open circles represent a single test observation. The filled circles represent two observations which had the same value. This resulted when two sets of deflection readings were taken at one load level and no creep deflections had occurred. The results of the theoretical analysis of Chapter VI were plotted as thin dashed lines. These curves are discussed in Chapter VI. The measured ultimate column loads are indicated on the graphs by dashed lines marked "Failure Load."

The six types of graphs mentioned previously are:

(1) Key Diagram. Key Diagrams, such as FIGURES 4 - 1 and 4 - 8, were plotted for each test series. The diagram shows the location of points for which deflections, moments, and reactions were plotted in the other graphs. The typical pattern of tension cracks at the last observation before failure, and the location of failure sections are also shown.

(2) Deflection Profile Diagram. Measured deflected configurations at various load levels are shown for each specimen in Deflection Profile Diagrams, such as FIGURES 4 - 2 and 4 - 9. The reference lines for the deflections are shown in FIGURES 3 - 8 and 3 - 9. For the restrained columns, the beam and column profiles are offset for clarity.

(3) Load-Deflection Graph. Measured lateral deflections at Column Stations 2 and 5 were plotted against corrected axial column load in Load-Deflection Graphs, such as FIGURES 4 - 4 and 4 - 11. Stations 2 and 5 were chosen since they were representative of the behavior of the upper and lower portions of the columns. For the restrained columns, the deflections at Beam Stations U2 and L2 were also plotted.

(4) Load-Moment Diagram. Measured bending moments at each column station were plotted against corrected axial column load in Load-Moment Diagrams, such as FIGURES 4 - 6 and 4 - 17. The moments were computed from test data in accordance with the analysis described in Appendix C.

Portions of the computed interaction curves described in Chapter II were also plotted in these figures, together with a small key plot to indicate the portion of the curves which are shown. Interaction curves are shown for both $k_3 = 0.85$ and $k_3 = 1.00$, although only the curves based on $k_3 = 0.85$ were used in interpreting the test results.

(5) Beam Reaction Graph. For each restrained column specimen the measured beam reactions were plotted against corrected axial column load in Beam Reaction Graphs such as FIGURE 4 - 13. Since the restraining moments are a direct multiple of the beam reactions, these graphs indicate the trend of the restraining moments.

(6) Moment Distribution Diagram. For each restrained column, the measured distribution of moment at each beam-column joint is plotted against corrected axial column load in Moment Distribution Diagrams such as FIGURE 4 - 15. At each load level the applied moment, M_A , was equal to the sum of the column moment, M_C , and the restraining moment, M_R , as shown by the curves.

In discussing this diagram reference is made to the ratio M_C/M_A as a convenient method of indicating the effect on the column of the distribution of moment at each beam-column joint. Although numerical values of this ratio are not shown it is believed the variation of M_C/M_A with column load can be visualized from the curves plotted on the Moment Distribution Diagrams.

CHAPTER IV

RESULTS OF TESTS OF COLUMNS WITH LARGE ECCENTRICITY

4.1 Introduction

The results of Test Series B and D are presented in this chapter. Both test series had the same nominal end eccentricities, but the columns of Test Series B were hinged while those of Test Series D were restrained. The test results are presented in one chapter in order that the effect of end restraints may be shown. The nominal end eccentricities were such that the columns were expected to fail as a result of initial yielding of the tension reinforcement.

4.2 Test Series B

(a) General

Test Series B comprised tests of two similar specimens designated B1 and B2. The columns were hinged and had nominal end eccentricities of 3.75 inches which corresponded to eccentricity ratios

$e/t = 1.5$ at the end blocks, and $e/t = 1.27$ at the ends of the column section. The average concrete strengths were 4210 psi for Specimen B1 and 4730 psi for Specimen B2. Results of the tests are summarized in FIGURES 4 - 1 to 4 - 7.

The general behavior of both specimens was similar, as shown by the plotted test results and observed behavior, and the results of both tests are discussed together. The loading apparatus and instrumentation performed as expected and no difficulties were encountered.

(b) Outline Of Observed Test Behavior

(i) Specimen B1. The first observations were made at 2.00 kips nominal load. Roughly equal lateral deflections had occurred at both ends of the column, as shown by the deflection profile in FIGURE 4 - 2. Tension cracks appeared over a length of about 12 inches at the upper and lower ends.

At 4.00 kips nominal load, deflections had increased equally at both ends, as shown in FIGURE 4 - 2. Earlier cracks progressed and several new cracks appeared.

The last observations before failure were at 6.00 kips nominal load. Lateral deflections at the lower end were still about the same as at the upper end, as shown by the deflection profile in FIGURE 4 - 2.

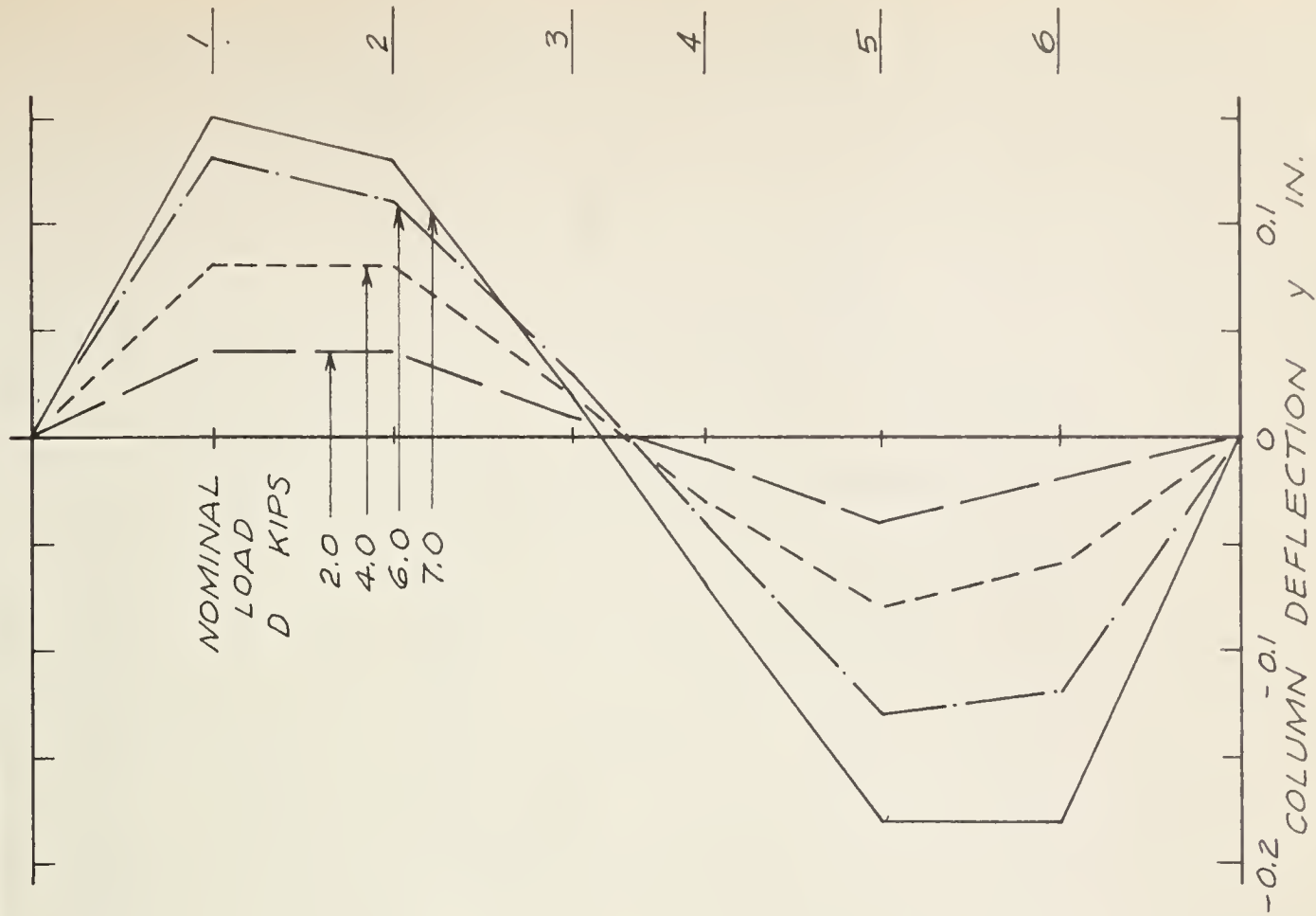
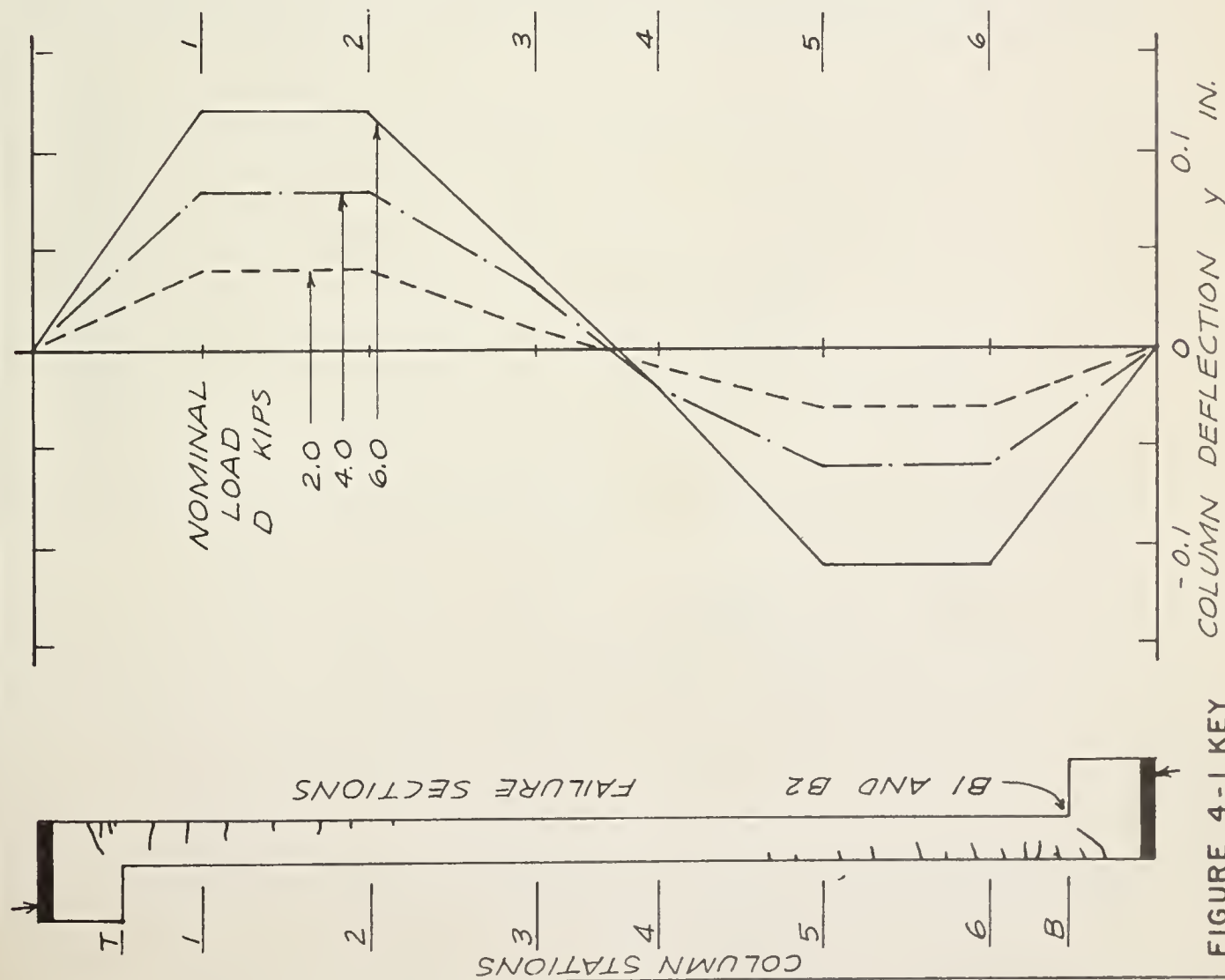


FIGURE 4-2 DEFLECTION PROFILE
DIAGRAM, SPECIMEN B1

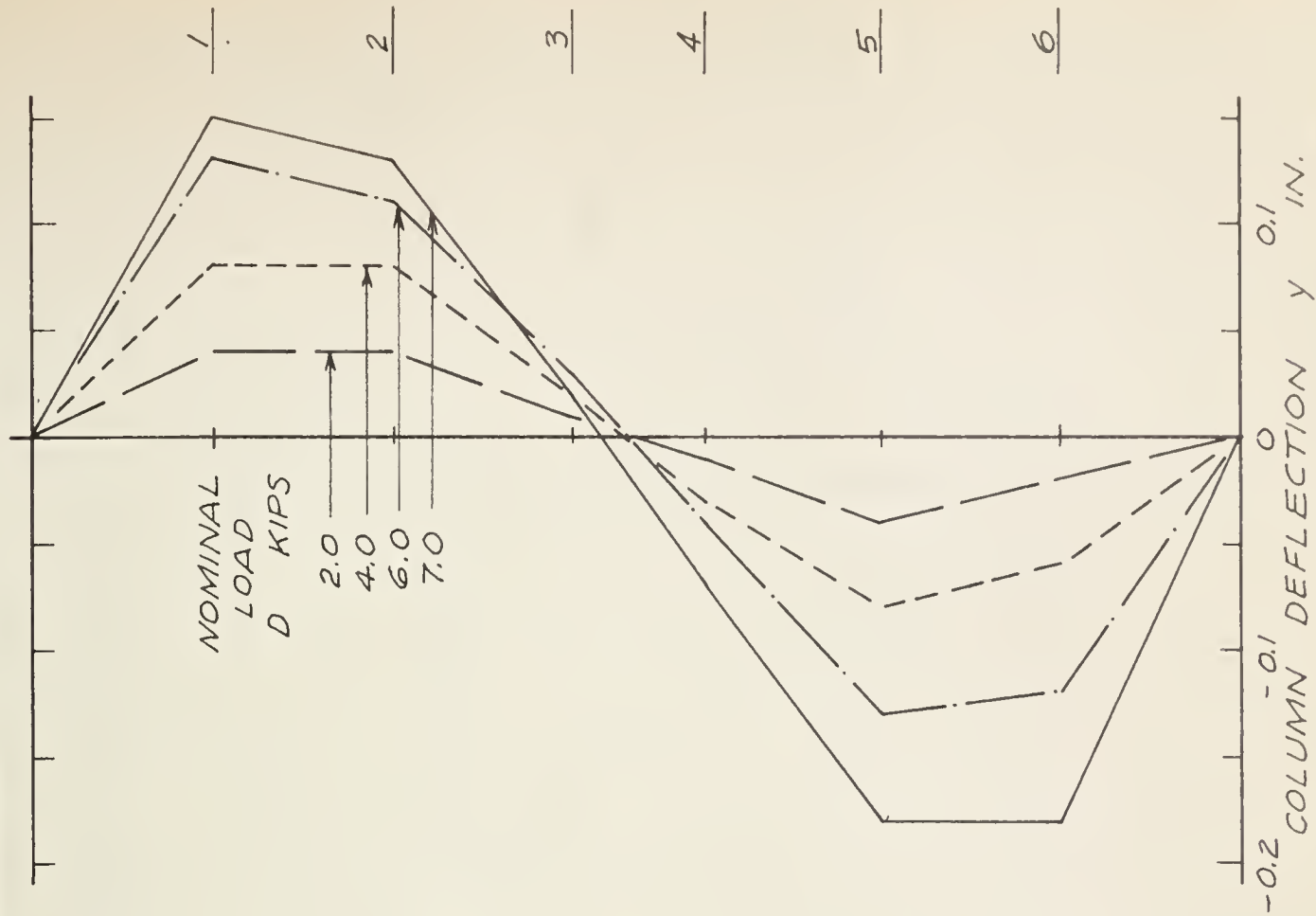


FIGURE 4-3 DEFLECTION PROFILE
DIAGRAM, SPECIMEN B2

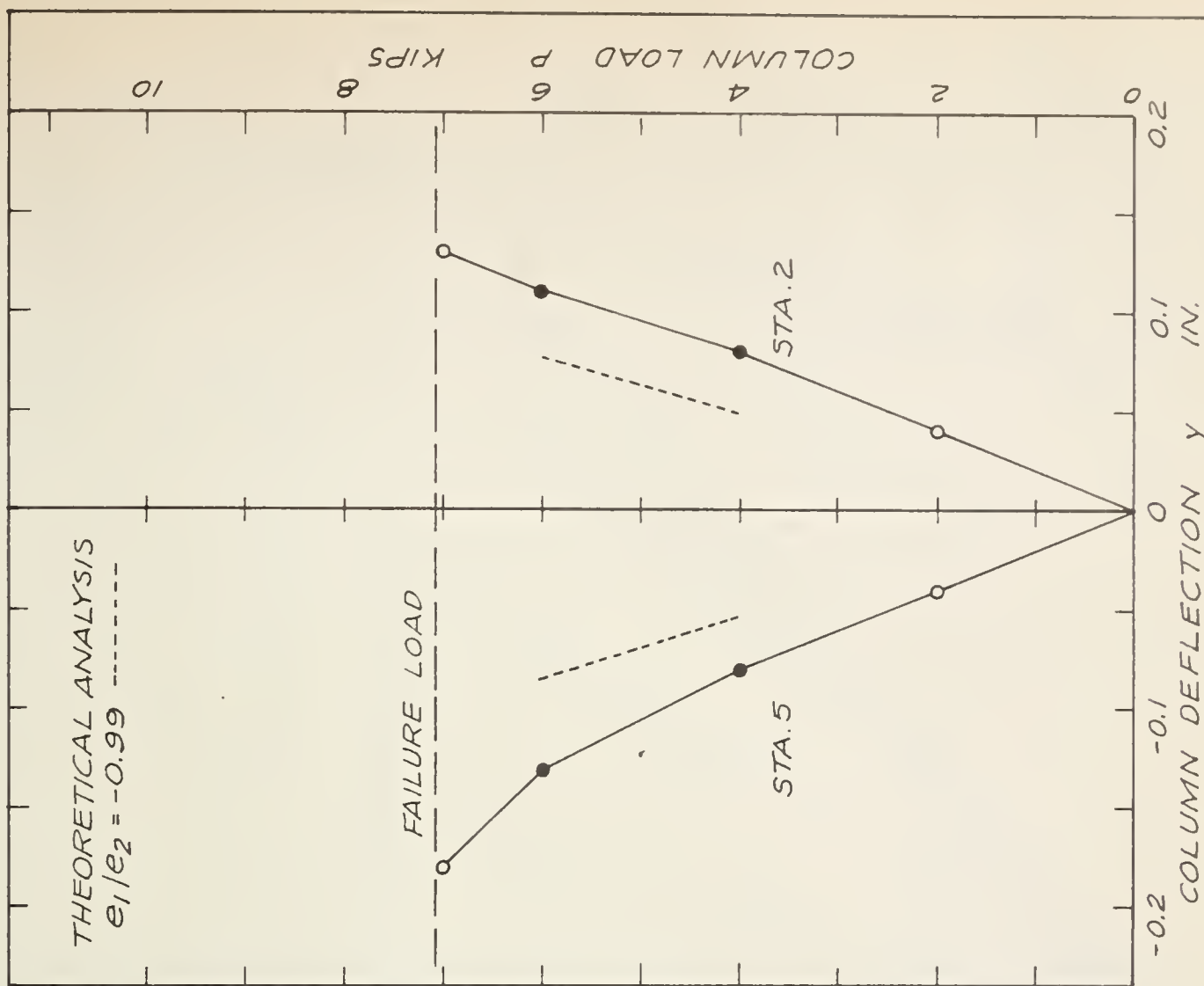


FIGURE 4-5 LOAD - DEFLECTION GRAPH, SPECIMEN B2

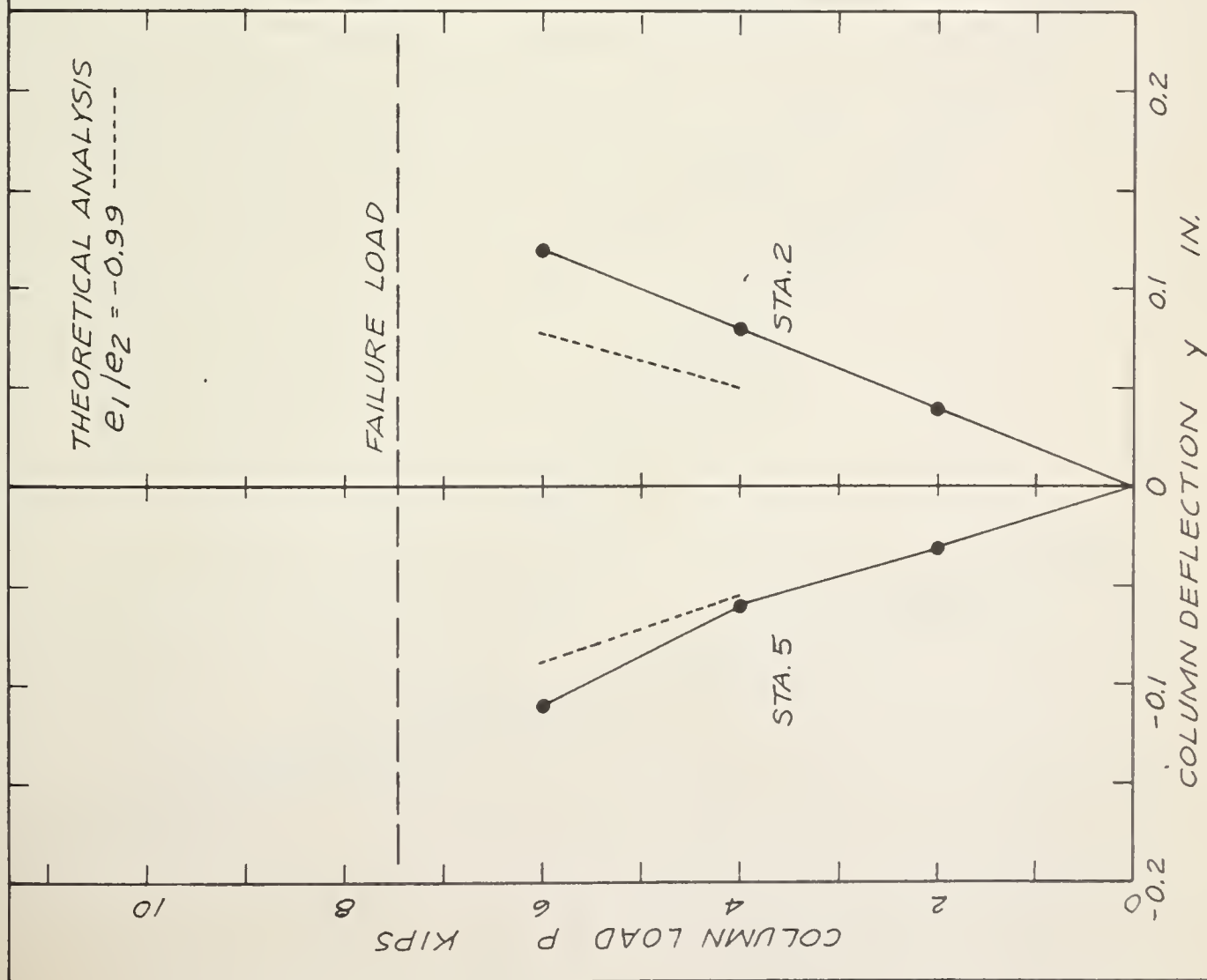


FIGURE 4-4 LOAD - DEFLECTION GRAPH, SPECIMEN B1

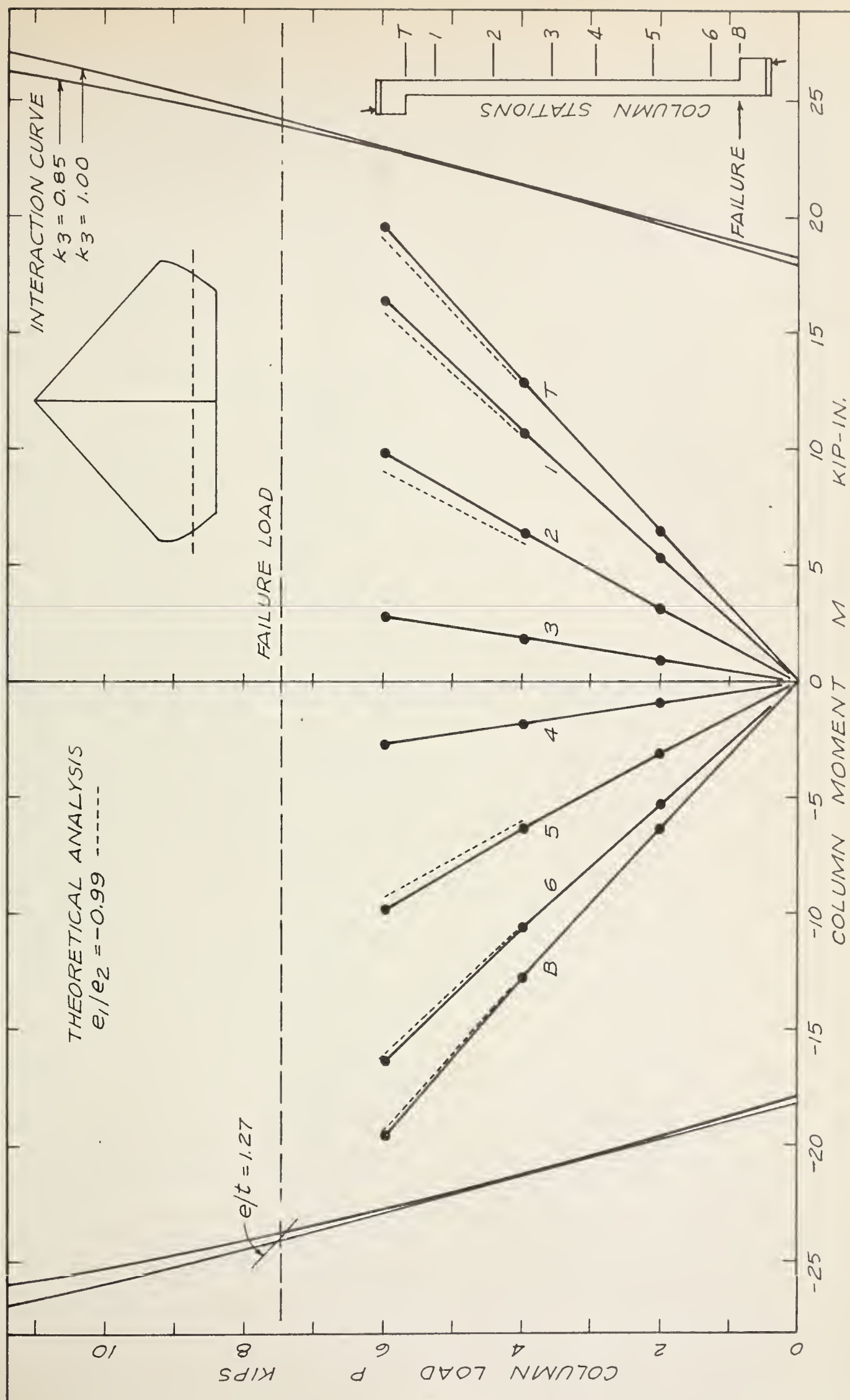


FIGURE 4-6 LOAD-MOMENT DIAGRAM, SPECIMEN B1

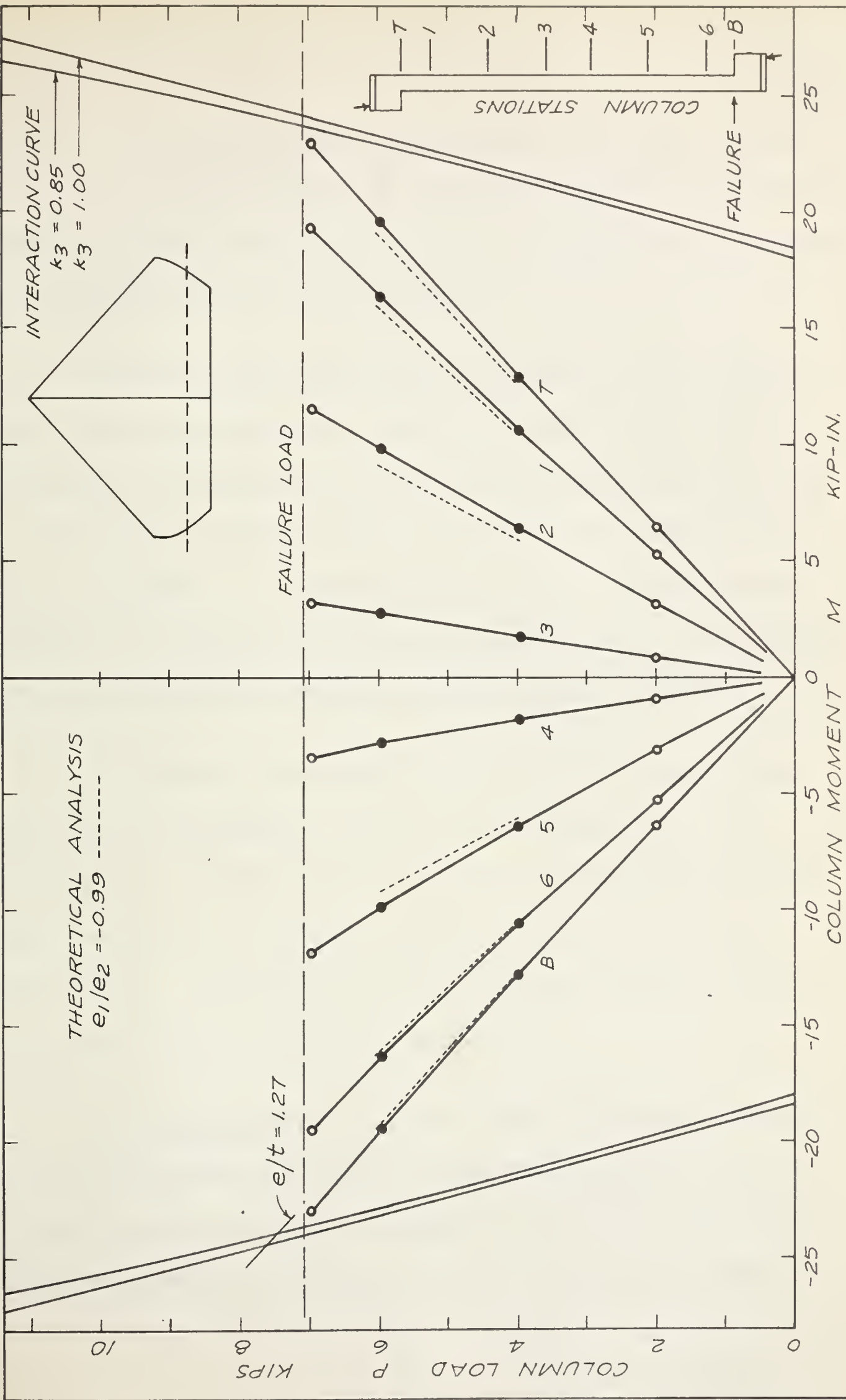


FIGURE 4-7. LOAD-MOMENT DIAGRAM, SPECIMEN B2

However, the tension cracking was more severe at the lower end, as cracks penetrated about 80 percent of the column thickness near Station B and only about 60 percent near Station T. This was the first indication of the probable location of the failure zone.

Failure occurred while the next increment of load was being added. The load dial reached a reading of 7.50 kips when crushing of the concrete and widening of the tension cracks was observed at Station B. The pattern of cracking shortly before failure was similar to that shown in FIGURE 4 - 1. Straining was continued but the load dropped gradually to 7.0 kips which could not be exceeded again. The appearance of the failure zone after additional straining is shown in FIGURE 4 - 19.

The ultimate column load was reported as 7.50 kips nominal load, which corresponded to 7.45 kips corrected axial load. The column failed by initial yielding of the tension reinforcement and subsequent crushing of the concrete compression block, and was a typical tension failure. The failure section was located at Station B, adjacent to the lower end block, as shown in FIGURE 4 - 1.

(ii) Specimen B2. At 2.00, 4.00 and 6.00 kips nominal load the test observations were similar to those for Specimen B1. At 6.00 kips nominal load, the tension cracking at the lower end of the column was more severe than at the upper end which indicated the probable

location of the failure zone. Deflection profiles are shown in FIGURE 4 - 3.

Loading proceeded slowly after 6.00 kips load. At 7.00 kips nominal load, lateral deflections of the lower portion of the column became somewhat larger than in the upper portion, as shown in FIGURE 4 - 3. Slight crushing of concrete at the compression face and widening of the tension cracks was observed near Station B. There was no drop of the load dial, although an increased strain rate was required to maintain the load while a hurried set of deflection readings were taken.

Failure occurred while the next increment of load was being added. The load dial reached a reading of 7.10 kips when considerable crushing was observed at Station B. The pattern of cracking shortly before failure was similar to that shown in FIGURE 4 - 1. The appearance of the specimen immediately after failure is shown in FIGURE 4 - 20. The nominal load of 7.10 kips could not be exceeded with additional straining.

The ultimate column load was reported as 7.10 kips nominal load which corresponded to 7.06 kips corrected axial load. The column failed by initial yielding of the tension reinforcement and subsequent crushing of the concrete compression block, and was a typical tension failure. The failure section was located at Station B adjacent to the lower end block as shown in FIGURE 4 - 1.

(c) Discussion Of Test Series B

Load-Deflection Graphs are shown in FIGURES 4 - 4 and 4 - 5 for Specimens B1 and B2, respectively. In both tests the deflections at Stations 2 and 5 were roughly equal to each other at all loads reflecting the symmetrical behavior described in Section 4.2(b). The projected maximum deflection at ultimate load was about five percent of the nominal end eccentricity. At no time did the sum of the initial eccentricity, e_i , and deflection, y , at any point exceed the nominal end eccentricity. The rate of change of deflection with load was generally constant throughout the tests, although there was a very slight increase in the rate at Station 5 at higher loads. This indicated there was relatively little change in column stiffness during the tests. Deflections were measured at the beginning and end of each observation period, and the readings did not change at constant load, indicating that creep did not affect the deflections in this test series.

Load-Moment Diagrams are shown in FIGURES 4 - 6 and 4 - 7 for Specimens B1 and B2, respectively. The load-moment curves for corresponding stations in the upper and lower portions of each column are similar, as expected from the symmetry of the deflection profiles. Each load-moment curve is nearly linear since the P_y -moments were small at all load levels.

In both tests the failure section was located at Station B, at the bottom end of the column. This is in agreement with the Load-Moment Diagrams which show that the largest moments in the lower portion of each column occurred at Station B. Although the moments at Stations T and B were approximately equal, the lower end of the columns apparently had slightly less strength causing failure to occur at Station B rather than at Station T.

In both tests of Series B the ultimate column load was determined by material failure, and not instability. The behavior was similar to that in Case (c), described in Section 2.1(c), in which the failure section was located at one extreme end of the column. The test observations indicated that material failure occurred simultaneously with maximum load, which is characteristic of a material failure. Also, the projection of the load-moment curve for the failure section has a positive slope where it intersects the interaction curve, which indicates a material failure, as discussed in Section 2.1(c).

In order to compare the measured strength of the column cross-section with that predicted by the interaction curve, it was assumed that projection of the last segment of the load-moment curve for the failure section represented the actual test conditions. At ultimate load, for Specimen B1, the "measured" moment was 5 percent greater than that

predicted by the interaction curve. For Specimen B2, the "measured" moment was 3 percent less than predicted.

4.3 Test Series D

(a) General

Test Series D comprised tests of two similar specimens designated D1 and D2. The columns were restrained and had nominal end eccentricities of 3.75 inches which corresponded to eccentricity ratios $e/t = 1.5$ at the end blocks, and $e/t = 1.27$ at the ends of the column section. The average concrete strengths were 3840 psi for D1 and 4410 psi for D2. Results of the tests are summarized in FIGURES 4 - 8 to 4 - 18.

The general behavior of both specimens was similar, as shown by the plotted results and observed behavior, and the results of both tests are discussed together. The loading apparatus and instrumentation performed as expected and no difficulties were encountered.

(b) Outline of Observed Test Behavior

(i) Specimen D1. The first observations were made at 1.50 kips nominal load. The deflected configuration was approximately

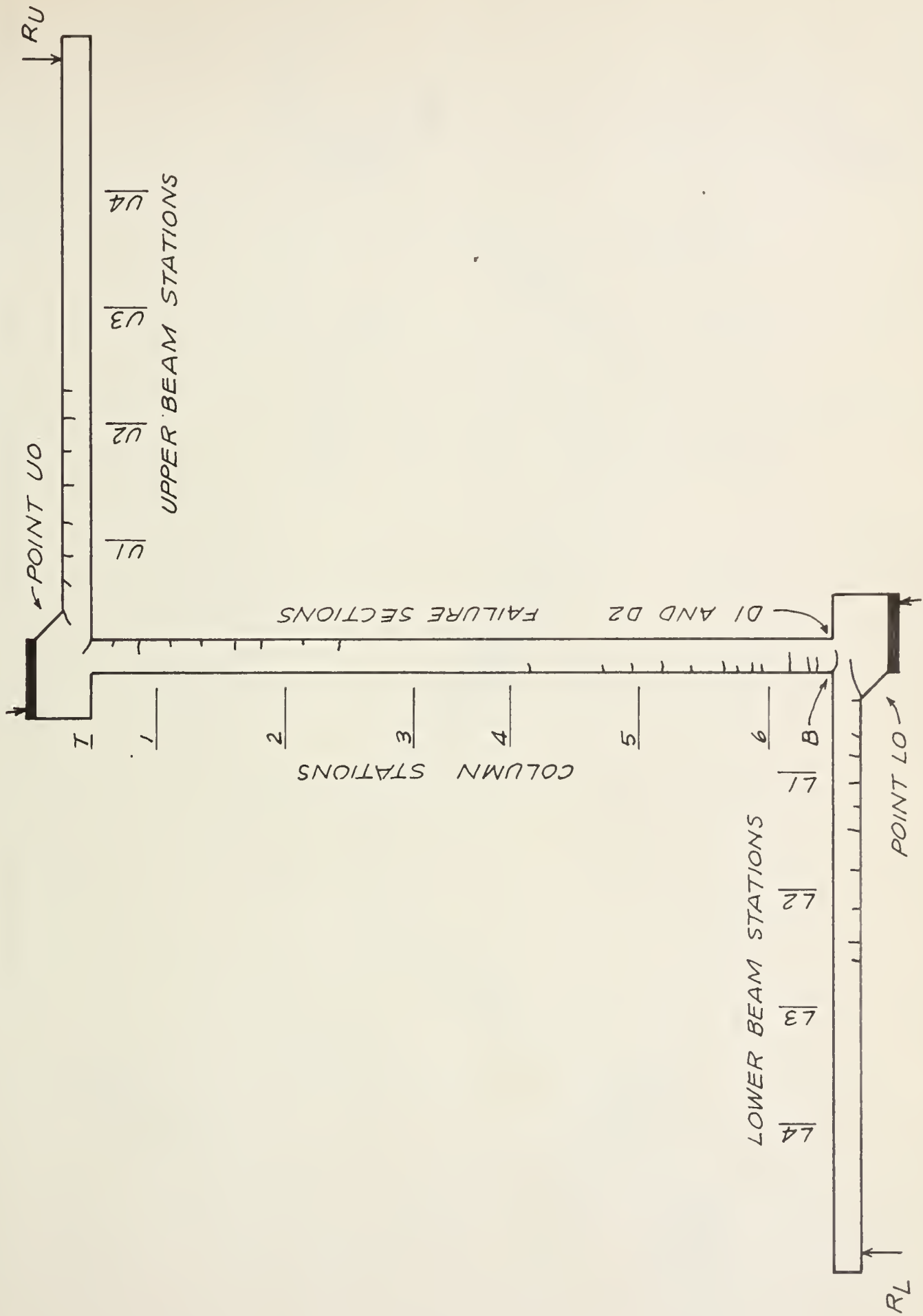


FIGURE 4-8 KEY DIAGRAM, TEST SERIES D

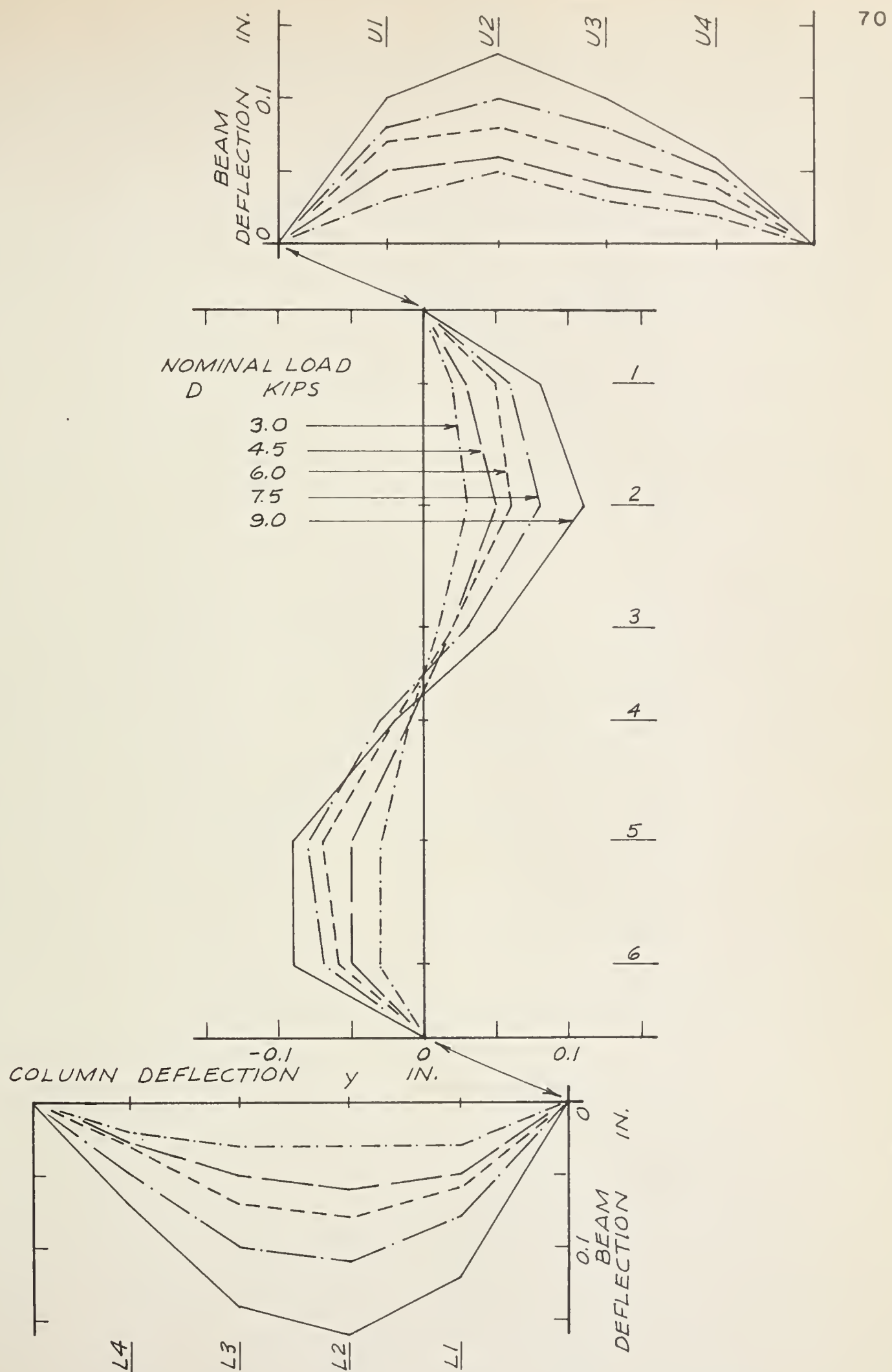


FIGURE 4-9 DEFLECTION PROFILE DIAGRAM, SPECIMEN D1

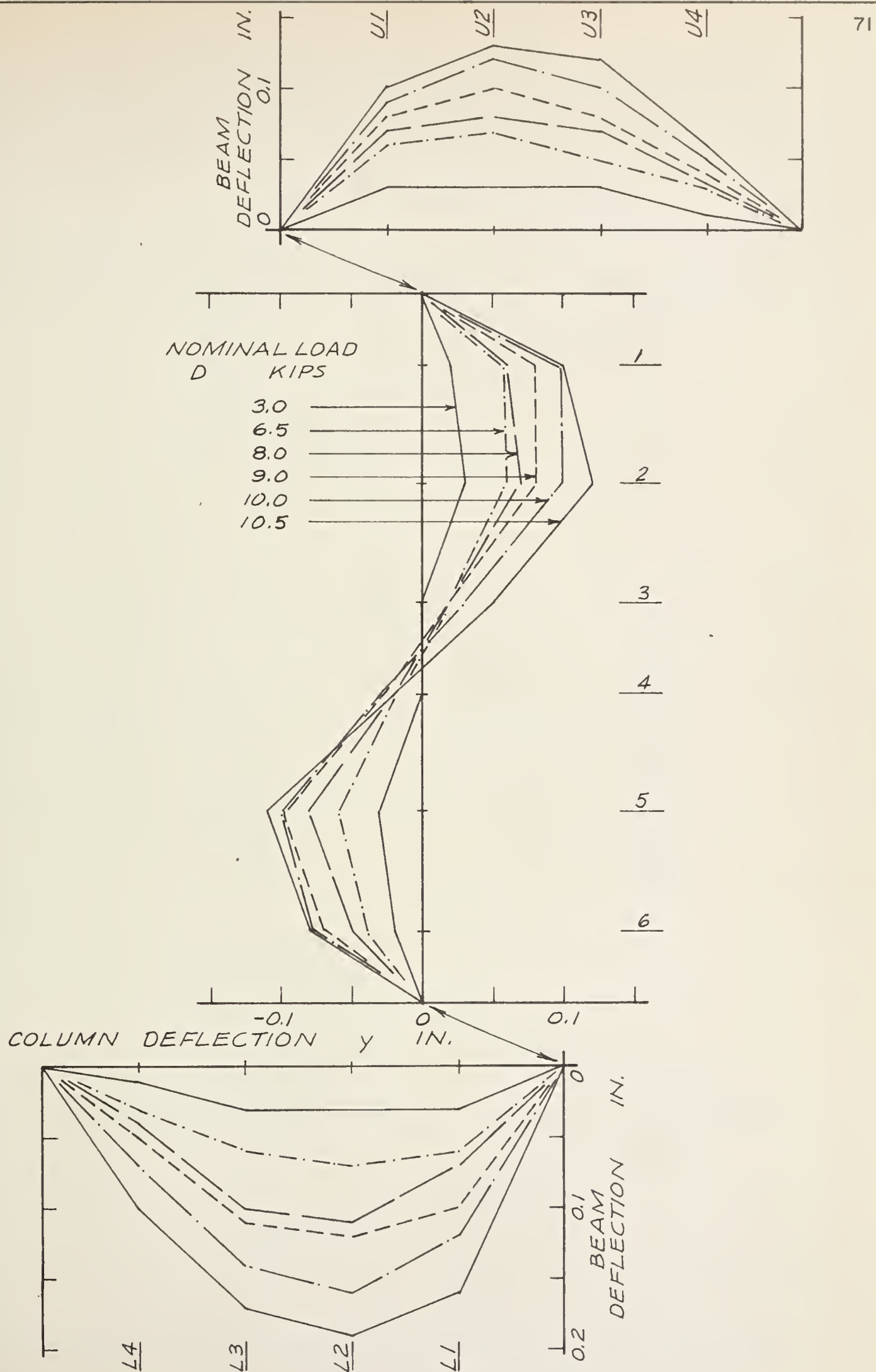


FIGURE 4-10 DEFLECTION PROFILE DIAGRAM, SPECIMEN D2

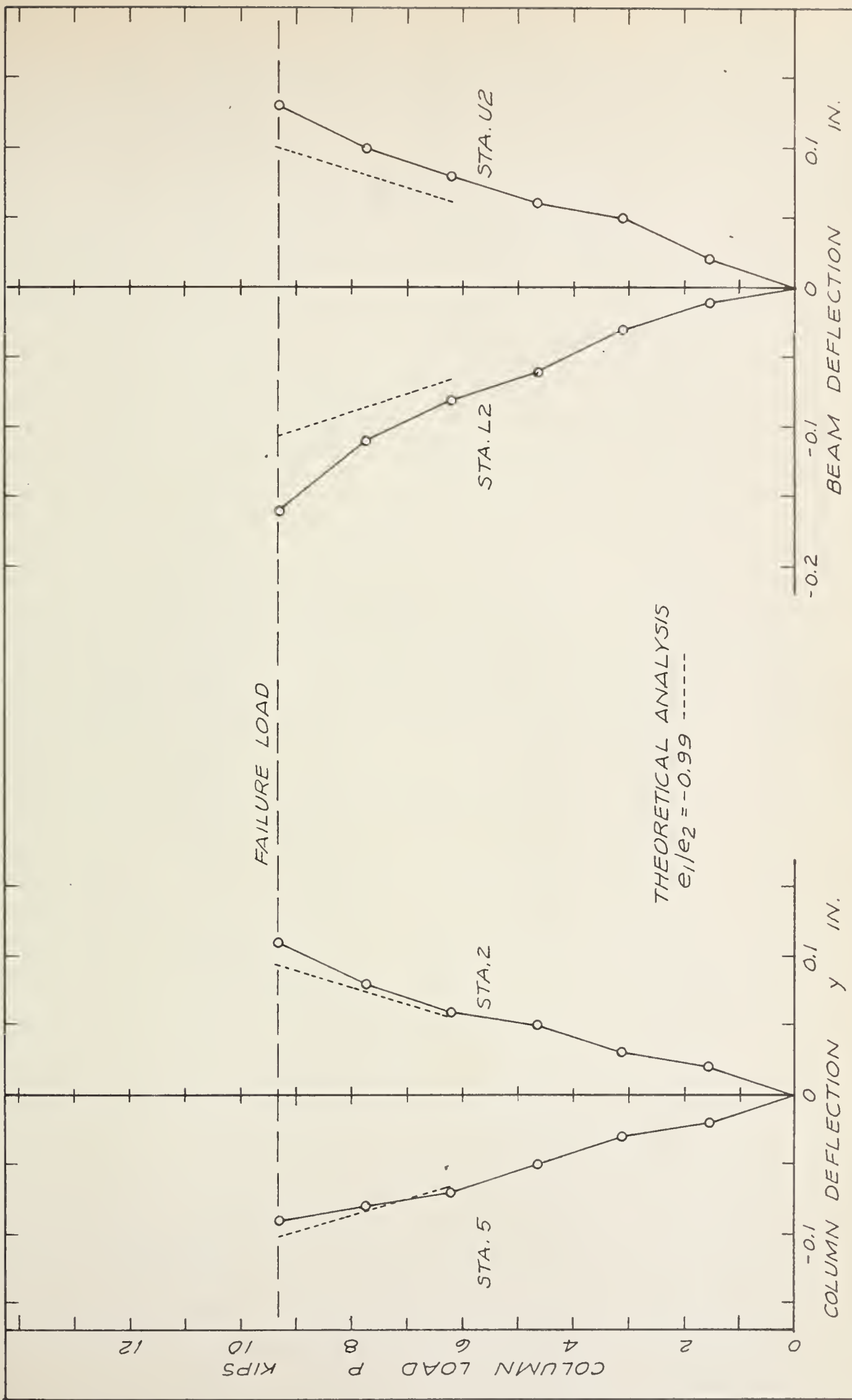


FIGURE 4-11 LOAD-DEFLECTION GRAPH, SPECIMEN D1

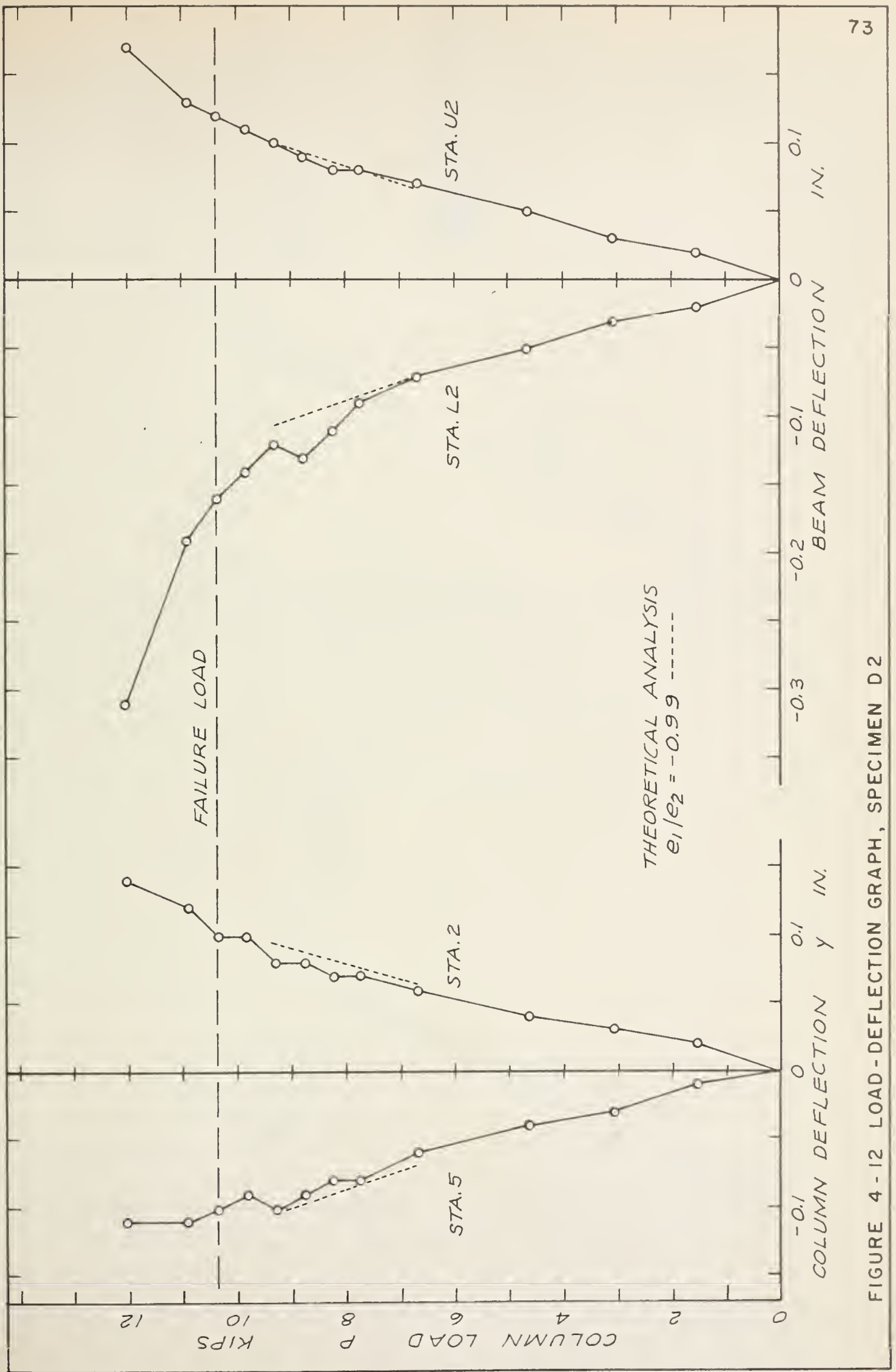


FIGURE 4-12 LOAD-DEFLECTION GRAPH, SPECIMEN D2

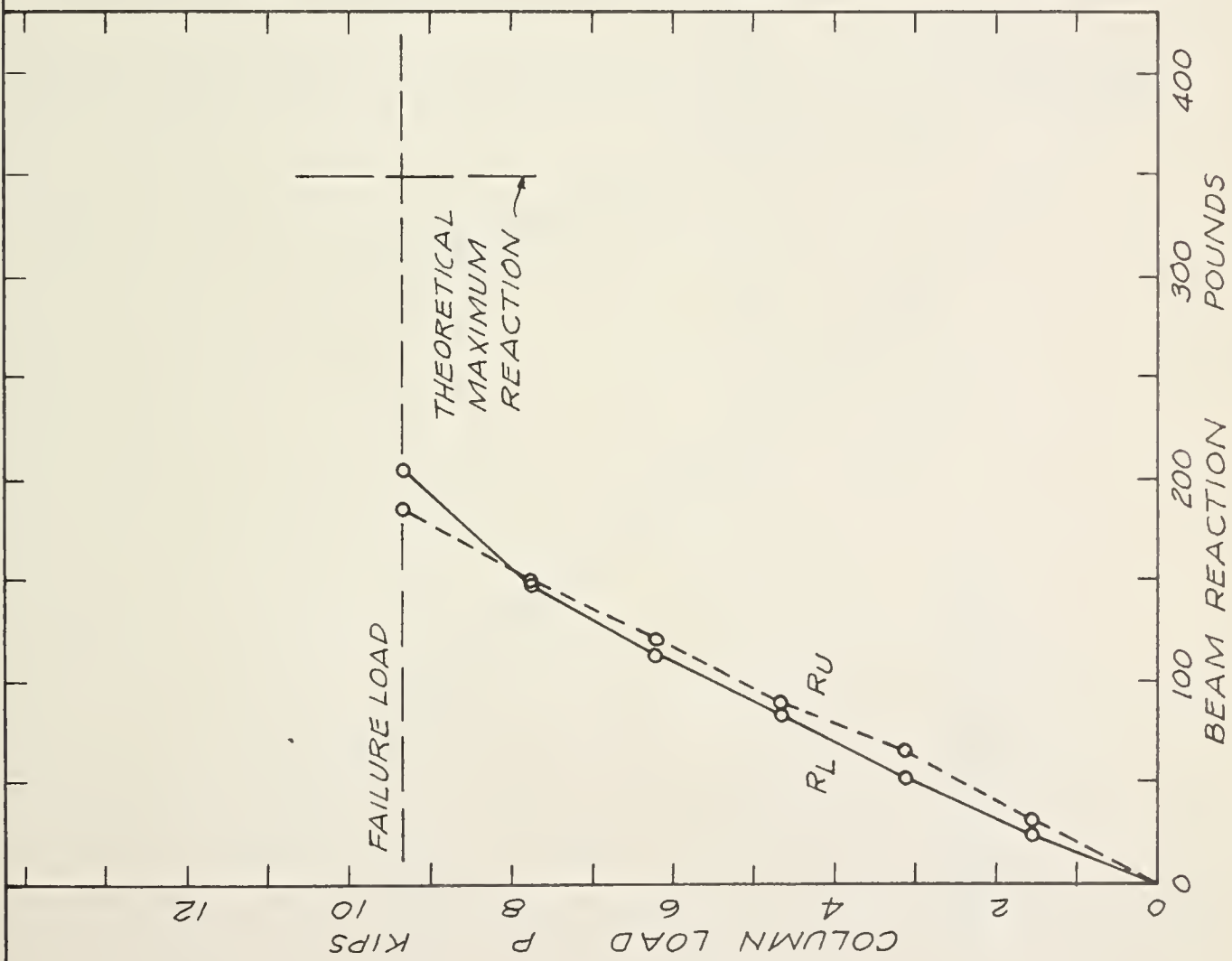


FIGURE 4-13 BEAM REACTION GRAPH,
SPECIMEN D1

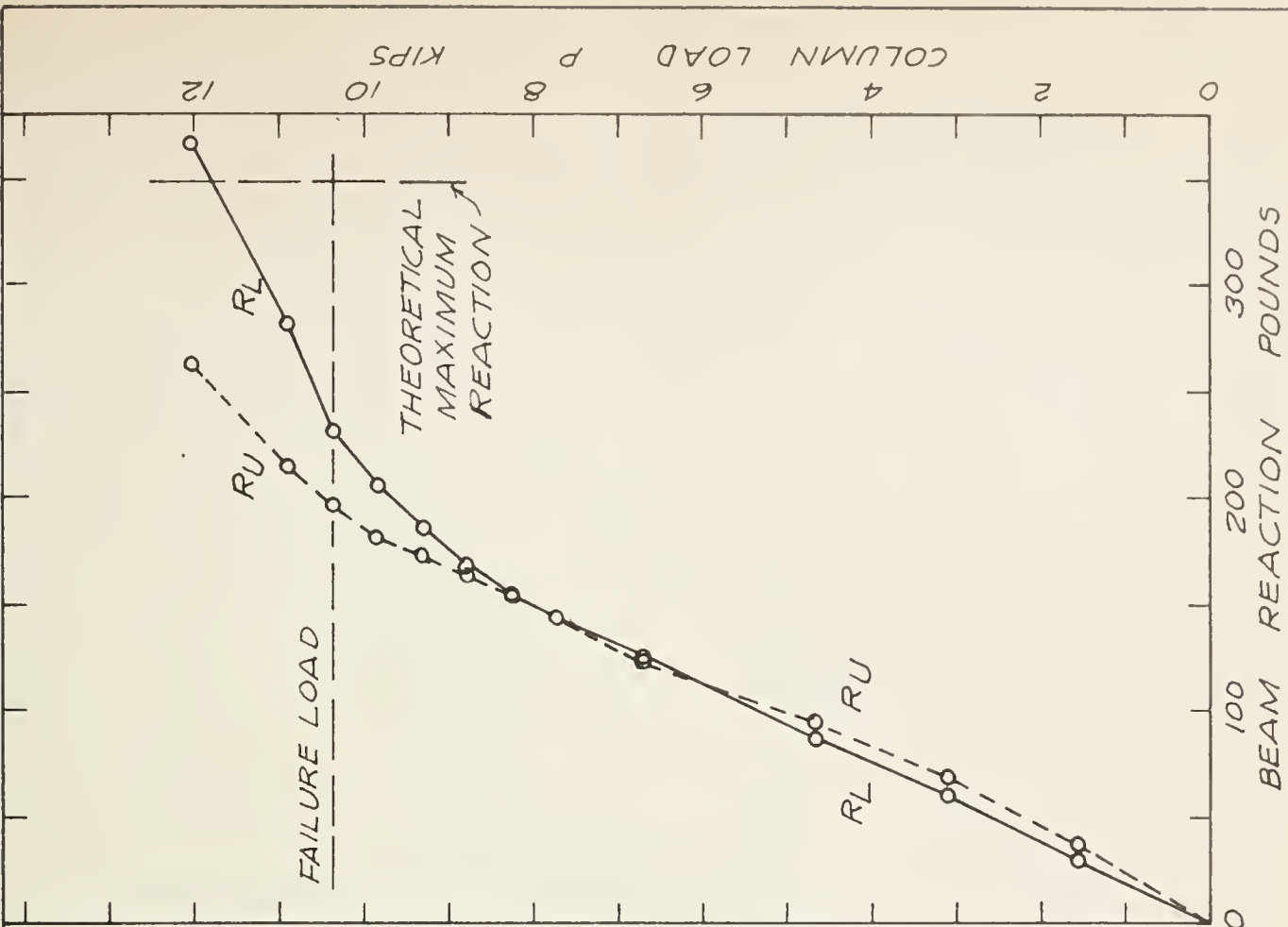


FIGURE 4-14 BEAM REACTION GRAPH,
SPECIMEN D2

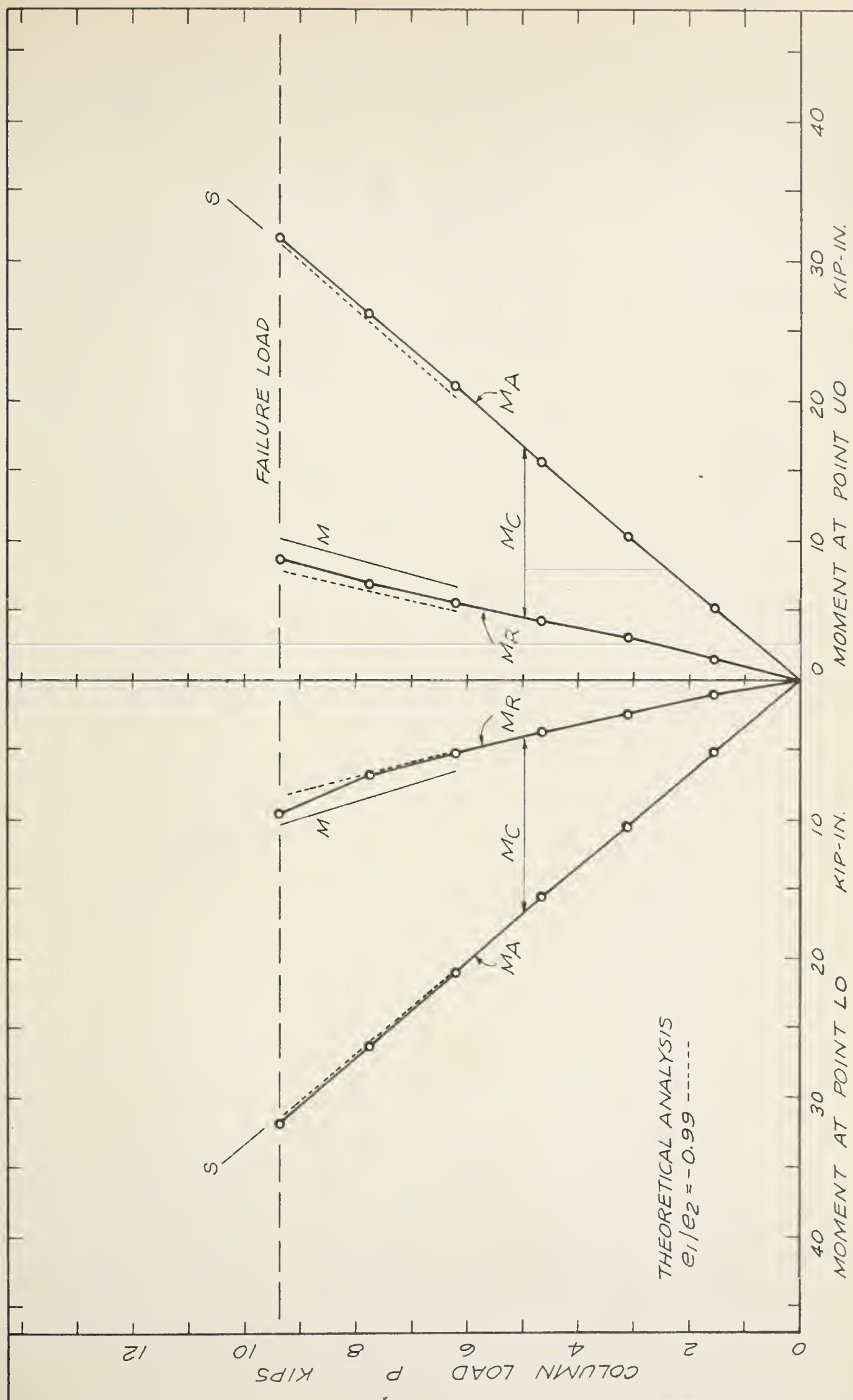


FIGURE 4-15 MOMENT DISTRIBUTION DIAGRAM, SPECIMEN D1

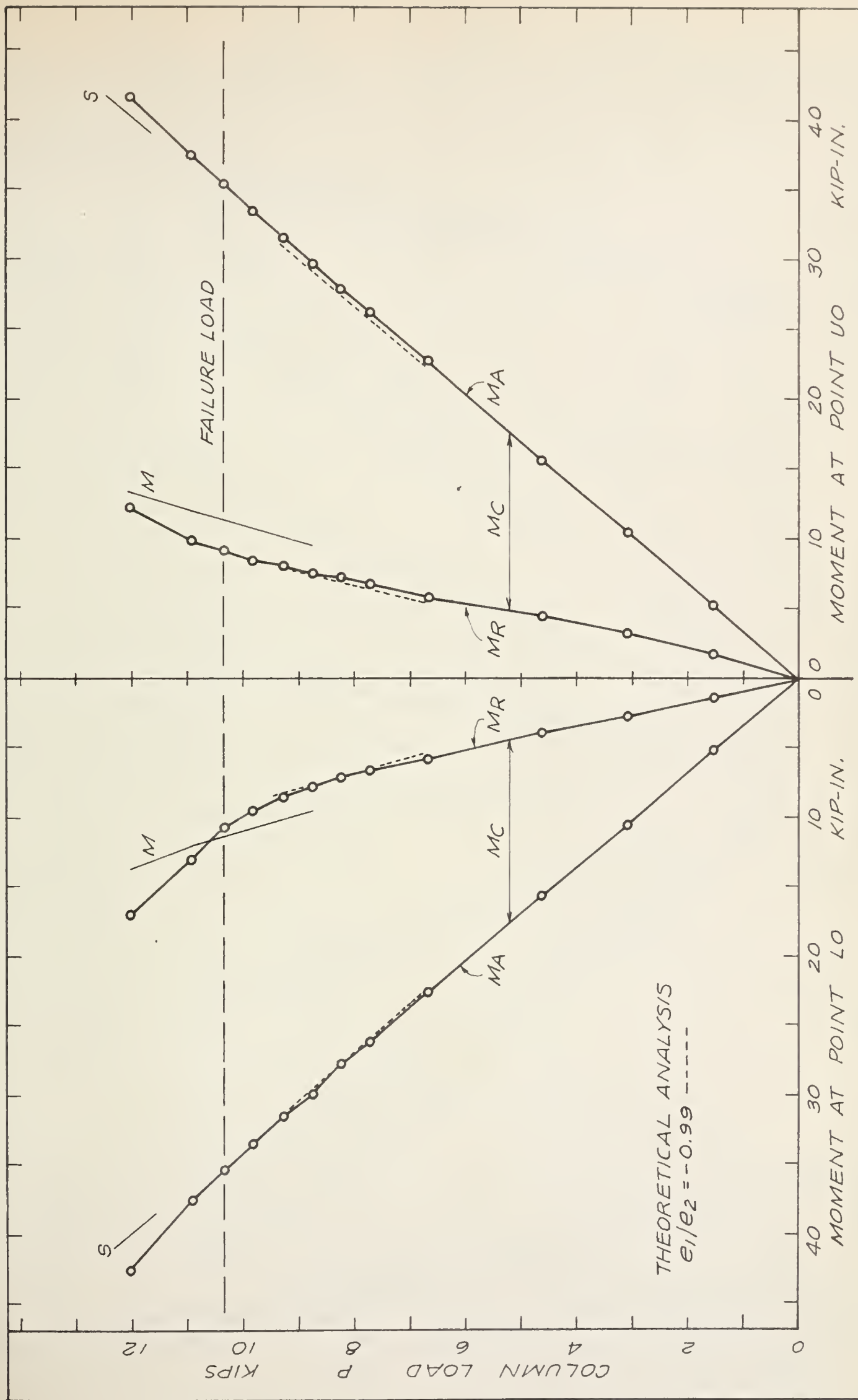


FIGURE 4 - 16 MOMENT DISTRIBUTION DIAGRAM , SPECIMEN D2

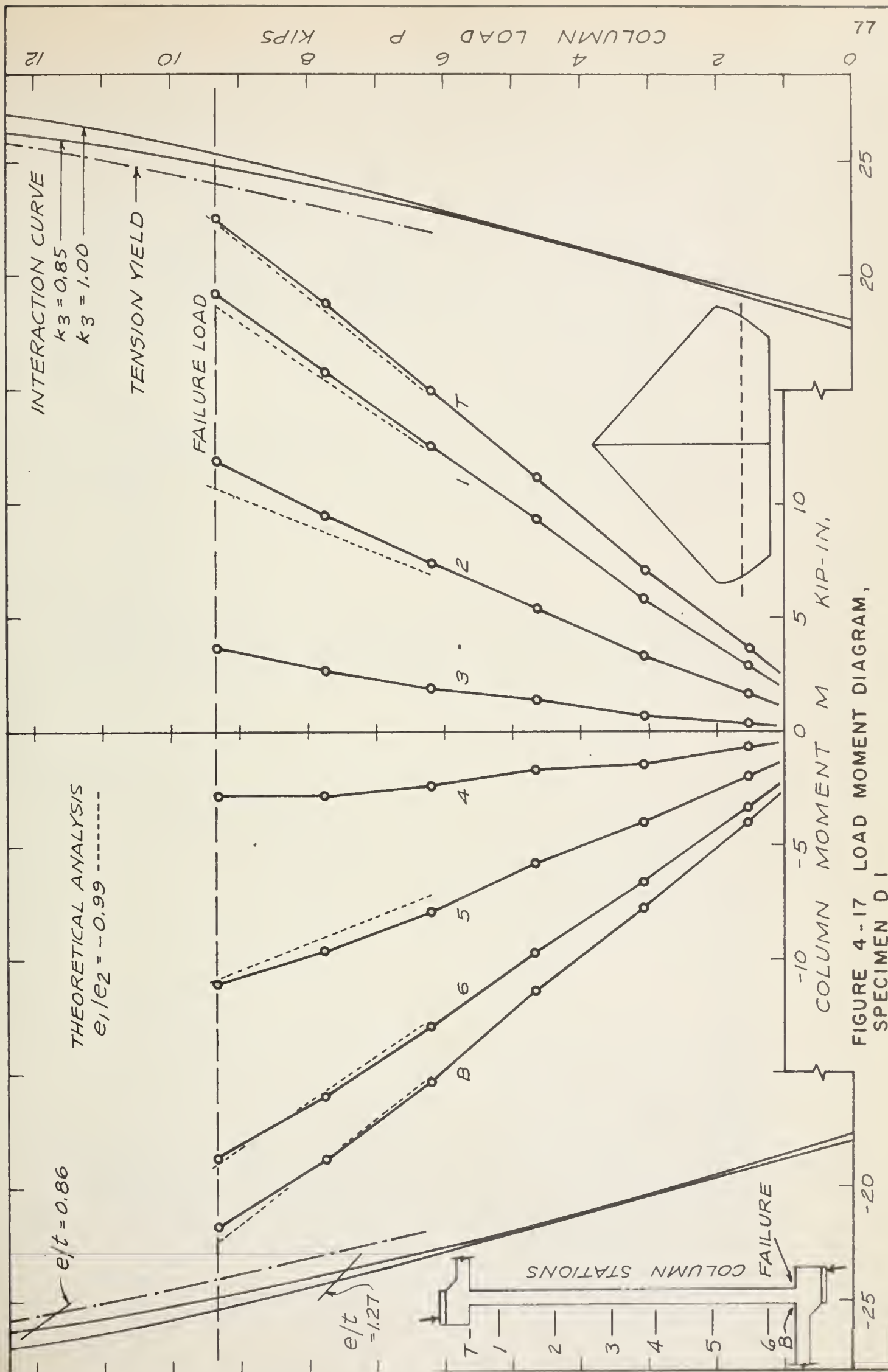


FIGURE 4-17 LOAD MOMENT DIAGRAM, SPECIMEN D 1

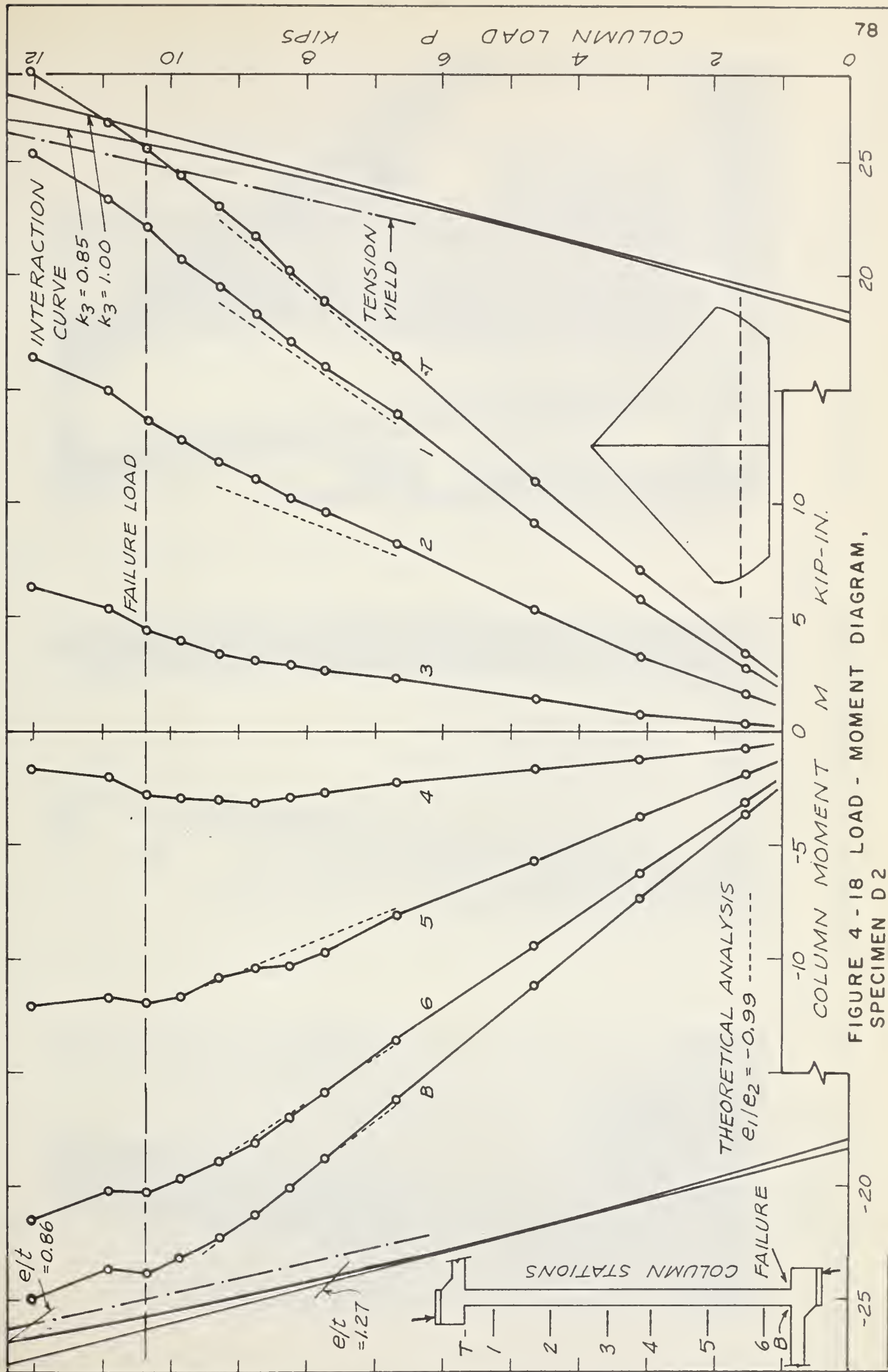




FIGURE 4-19
SPECIMEN B1 FAILURE ZONE

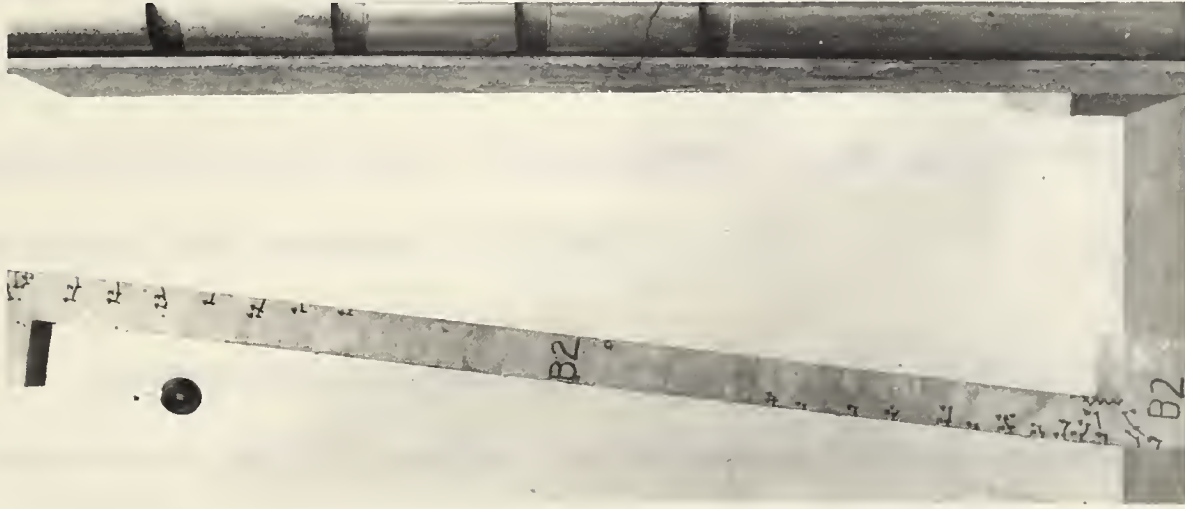


FIGURE 4-20
SPECIMEN B2 AFTER FAILURE



FIGURE 4-21
SPECIMEN D1 AT 7.50 KIPS LOAD

antisymmetrical, as shown by the deflection profile of FIGURE 4 - 9. Tension cracks were found in the high moment regions of the column and beams.

At 3.00 kips and 4.50 kips nominal load, the deflected configuration remained approximately antisymmetrical, as shown in FIGURE 4 - 9. There was a general increase in the extent of cracking.

At 6.00 kips and 7.50 kips nominal load, the deflected configuration remained approximately antisymmetrical, as before. There was a definite increase in the number and depth of tension cracks in the lower portion of the column and the lower beam, which indicated the probable location of the failure zone. The appearance of the specimen at 7.50 kips nominal load is shown in FIGURE 4 - 21.

Loading was continued at a slow rate with continual inspection for concrete crushing. Loading was stopped at 9.00 kips nominal load for a routine set of readings. Crushing of the concrete was observed at the compression face at Station B, together with widening of the tension cracks. No crushing was believed to have occurred until this load was reached. The pattern of cracking shortly before failure was similar to that shown in FIGURE 4 - 8. There was no sign of distress at the upper end of the column or in the upper beam. The lower beam had

wide tension cracks, some of which were inclined toward the column reflecting the effect of shear. No concrete crushing was visible in the lower beam.

It was possible to maintain the load at 9.00 kips with a slightly increased strain rate. The beam reactions were adjusted and a set of readings recorded, giving a close approximation of the conditions at column failure. The deflected shape is shown in FIGURE 4 - 9.

Since some load capacity remained, loading was continued. At 10.85 kips nominal load, the lower beam failed by crushing of the compression block adjacent to the column. The load could not be exceeded as the concrete of the column and beam compression areas continued to crush and spall.

The ultimate column load was reported as 9.00 kips, which corresponded to 9.33 kips corrected axial load. The column failed by initial yielding of the tension reinforcement and subsequent crushing of the concrete compression block, and was a typical tension failure. The failure section was located at Station B adjacent to the lower end block, as shown in FIGURE 4 - 8.

(ii) Specimen D2. From the beginning of the test to 7.50 kips nominal load the test observations were similar to those for Specimen D1.

At 7.50 kips nominal load, the tension cracking at the lower end of the column and in the lower beam was more severe than at the upper end, which indicated the probable location of the failure zone. Deflection profiles are shown in FIGURE 4 - 10. The appearance of the specimen at 7.50 kips nominal load is shown in FIGURE 5 - 20.

At 8.00 kips and 8.50 kips nominal load, the deflected configuration remained approximately antisymmetrical as shown in FIGURE 4 - 10. There was a continued increase in cracking in the lower portion of the column and the lower beam.

At 9.00 kips and 9.50 kips, deflections of the lower beam became slightly larger than those of the upper beam, as shown in FIGURE 4 - 10. Tension cracks in the lower portion of the column and lower beam continued to widen. A thorough inspection of compression surfaces was made at 9.75 kips load and no concrete crushing was found.

Loading was continued, with continual inspection of compression surfaces. Loading was stopped at 10.00 kips nominal load for a routine set of readings which were taken and recorded. After about 5 minutes at this load crushing of the concrete was observed at the compression face at Station B, together with widening of the tension cracks. No crushing was believed to have occurred until this load was reached. The

pattern of cracking shortly before failure was similar to that shown in FIGURE 4 - 8. The deflected shape is shown in FIGURE 4 - 10. There was no sign of distress at the upper end of the column or in either beam.

Since the specimen was still intact loading was continued. At 10.50 kips nominal load no additional failures were found, but tension cracks at the upper end of the column had widened considerably. There was continued crushing and spalling of the concrete at the original failure zone. A set of readings was taken and recorded. The deflected shape is shown in FIGURE 4 - 10.

Observations were made at 11.50 kips nominal load. Tension cracks at the upper end of the column had become very wide but no crushing was found. The lower beam had large diagonal cracks and horizontal splitting at the level of the tension reinforcement in the high moment region, but no flexural crushing was found.

The maximum load reached in the test was 11.85 kips nominal load, which could not be exceeded or maintained. There were no additional failures at this load, but the original column failure section had become badly spalled.

Straining was continued as the indicated load decreased. At 10.5 kips load, crushing occurred at the compression face of the lower

beam adjacent to the column. No crushing was found in the upper beam or upper end of the column when the test was ended.

The ultimate column load was reported as 10.00 kips nominal load, which corresponded to 10.36 kips corrected axial load. The column failed by initial yielding of the tension reinforcement and subsequent crushing of the concrete compression block, and was a typical tension failure. The failure section was located at Station B adjacent to the lower end block, as shown in FIGURE 4 - 8.

(c) Discussion Of Test Series D

Load-Deflection Graphs are shown in FIGURES 4 - 11 and 4 - 12 for Specimen D1 and D2, respectively. Up to the ultimate column load, the deflections at Column Stations 2 and 5 were roughly equal to each other as were those at Beam Stations U2 and L2 reflecting the symmetrical behavior described in Section 4.3(b). The maximum column deflection at ultimate load was about three percent of the nominal end eccentricity. This was considerably less than the maximum deflection in Test Series B, even though the columns of Test Series B failed at lower loads, and shows the effect of the end restraints. The rate of change of column deflection with load was generally constant up to ultimate column load. This indicated there was relatively little change in overall column stiffness during this load range.

Beam Reaction Graphs are shown in FIGURES 4 - 13 and 4 - 14 for Specimen D1 and D2, respectively. In both tests the upper and lower beam reactions were roughly equal up to about 90 percent of ultimate column load. At ultimate load the lower beam reaction was from 10 to 18 percent larger than the upper beam reaction. This difference was probably due to a slight reduction in the stiffness of the lower end of the column near the failure section. This would result in the lower beam taking a relatively greater portion of the applied moment.

As described in Chapter III, the beam supports were adjusted during the tests to eliminate induced moments due to differential settlement of the two ends of each beam. In the test of Specimen D2, column failure occurred after the supports had been adjusted for the column shortening which took place during the load increment. However, in the test of Specimen D1, the column failure occurred while the supports were still at the setting for the previous load reading. The tabulated test data at the failure load was obtained after the supports were adjusted. The column shortening which took place during this load increment was only 0.008 inches, and a very approximate analysis indicated this differential settlement would have a negligible effect on the magnitude of the beam reactions. For the columns of Test Series D, the practice of adjusting the level of the beam supports appeared to have little effect on the failure loads.

At the ultimate column load the beam reactions in both tests were less than the theoretical maximum based on the ultimate moment capacity of the restraining beam, shown in FIGURES 4 - 13 and 4 - 14 by the lines marked "THEORETICAL MAXIMUM REACTION". Since the yield moment for the beams was only slightly smaller than the ultimate moment the calculations indicate the beams were well below the point of yielding. From this and from the test observations it was clear that the restraints were in full effect when the ultimate column load was reached.

As shown in FIGURE 4 - 14, the lower beam reaction of Specimen D2 exceeded the theoretical maximum reaction by five percent at $P = 12.05$ kips. Although the beam had not failed at this load, failure did occur after the column load had increased slightly to 12.40 kips, and then dropped to about 10.5 kips.

The Moment Distribution Diagrams for Specimens D1 and D2 are shown in FIGURES 4 - 15 and 4 - 16, respectively. Up to about 90 percent of ultimate column load the ratio of column moment to applied moment, M_C/M_A , was nearly constant at both Point UO and Point LO. As ultimate column load was approached, M_C/M_A decrease slightly at Point LO in both tests, as the lower restraining beam relieved the column of a portion of the moment increase. This was apparently due to a decrease in stiffness at the lower end of the columns, where the failure

sections were located. However, the relief provided by the lower beam was relatively small and at ultimate load the lower end of the column was subjected to nearly the same eccentricity as at smaller loads.

The Moment Distribution Diagrams show that the eccentricity of the applied load at Points UO and LO, as given by M_A/P , increased slightly as the ultimate column load was approached. The increase was due to the lateral displacement of Points UO and LO, denoted Δ , and the effects of the interaction of the beam reactions. The effect of the latter factor was small compared to the effect of the displacement, Δ . These factors are shown in the expression for M_A in Appendix C (EQ. C-12 and C-14). The lines marked "S" represent the initial applied load eccentricity (3.28 inches), and the difference in moment between the M_A -curves and Line S indicates the combined effect of these two factors.

Load-Moment Diagrams are shown in FIGURES 4 -17 and 4 - 18 for Specimens D1 and D2, respectively. Up to about 90 percent of ultimate column load the load-moment curves for corresponding stations in the upper and lower portions of each column are similar. This was expected from the symmetry of the deflection profiles and of the distribution of moment at the upper and lower beam-column joints. As the ultimate column load was approached, the moment at Station B did not increase at as great a rate as at Station T. This was due to the decreasing value

of M_C/M_A at Point LO, which was ascribed to decreasing stiffness at the lower end of the column. Consequently, at ultimate column load, the Load-Moment Diagrams indicate smaller moments at Station B, than at Station T. This is seemingly in disagreement with the observed location of the failure section, at Station B, since it would normally be expected that the moments at the failure section would be larger than at any other point in the column. However, due to unavoidable variations in materials and fabrication, it is likely that one end of the columns would have somewhat less strength than the other end. If it is assumed that lower strength is associated with less stiffness, this would explain the larger restraining moments and hence smaller column moments at the lower end of the column at ultimate load.

In both tests of Series D the ultimate column load was determined by material failure and not instability. The behavior was similar to that in Case (c), described in Section 2.1(c), in which the failure section was located at the extreme end of the column. The test observations indicated that there was no decrease in load before material failure occurred, and this is characteristic of a material failure. Also, the load-moment curves for the failure sections had a positive slope when column failure occurred, indicating a material failure, as discussed in Section 2.1(c).

The measured strength of the column cross-section was compared with that given by the interaction curves on the basis of measured and predicted moment at the failure section at ultimate column load. For Specimen D1 the measured moment at Station B was twelve percent less than that predicted by the interaction curve. For Specimen D2 the measured moment at Station B was seven percent less than predicted. In addition, for Specimen C2, at 12.05 kips load, Station T sustained a moment twelve percent greater than that given by the interaction curve without failure.

The agreement in this test series was not as good as in Test Series B, although the variations appear to be within reasonable limits of test accuracy.

The column of Test Series B and D were similar, except that the former were hinged and the latter were restrained. The effect of the end restraints may be seen in a comparison of the results of the two test series. In both test series the columns failed at the end of the column section, adjacent to an end block. In neither case were the column deflections large enough to shift the point of maximum moment away from the end of the column. At the same load levels, the maximum column deflections in Test Series D were about one-half those in Test Series B, due to the effects of the end restraints. In order to compare the ultimate column loads, they

were made non-dimensional by dividing by the quantity $f_c''bt$, giving average values of 0.17 in Test Series B and 0.26 in Test Series D.

The higher load capacities in Test D were the result of the restraining beams relieving the columns of a portion of the applied end moments.

CHAPTER V

RESULTS OF TESTS OF COLUMNS WITH SMALL ECCENTRICITY

5.1 Introduction

The results of Test Series A and C are presented in this chapter. Both series had the same nominal end eccentricities, but the columns of Series A were hinged while those of Series C were restrained. The test results are presented in one chapter in order that the effect of end restraints may be shown. The nominal end eccentricities were such that the columns were expected to fail as a result of initial crushing of the concrete.

5.2 Test Series A

(a) General

Test Series A comprised tests of two similar specimens designated A1 and A2. The columns were hinged and had nominal end eccentricities of 0.50 inches, which corresponded to eccentricity ratios $e/t = 0.2$ at the end blocks, and $e/t = 0.17$ at the ends of the column

section. The average concrete strengths were 4880 psi for A1 and 4740 psi for A2. Results of the tests are presented in FIGURES 5 - 1 to 5 - 7.

The general behavior of both specimens was similar, as shown by the plotted test results and observed behavior, and the results of both tests are discussed together. The loading apparatus performed as expected and no difficulties were encountered.

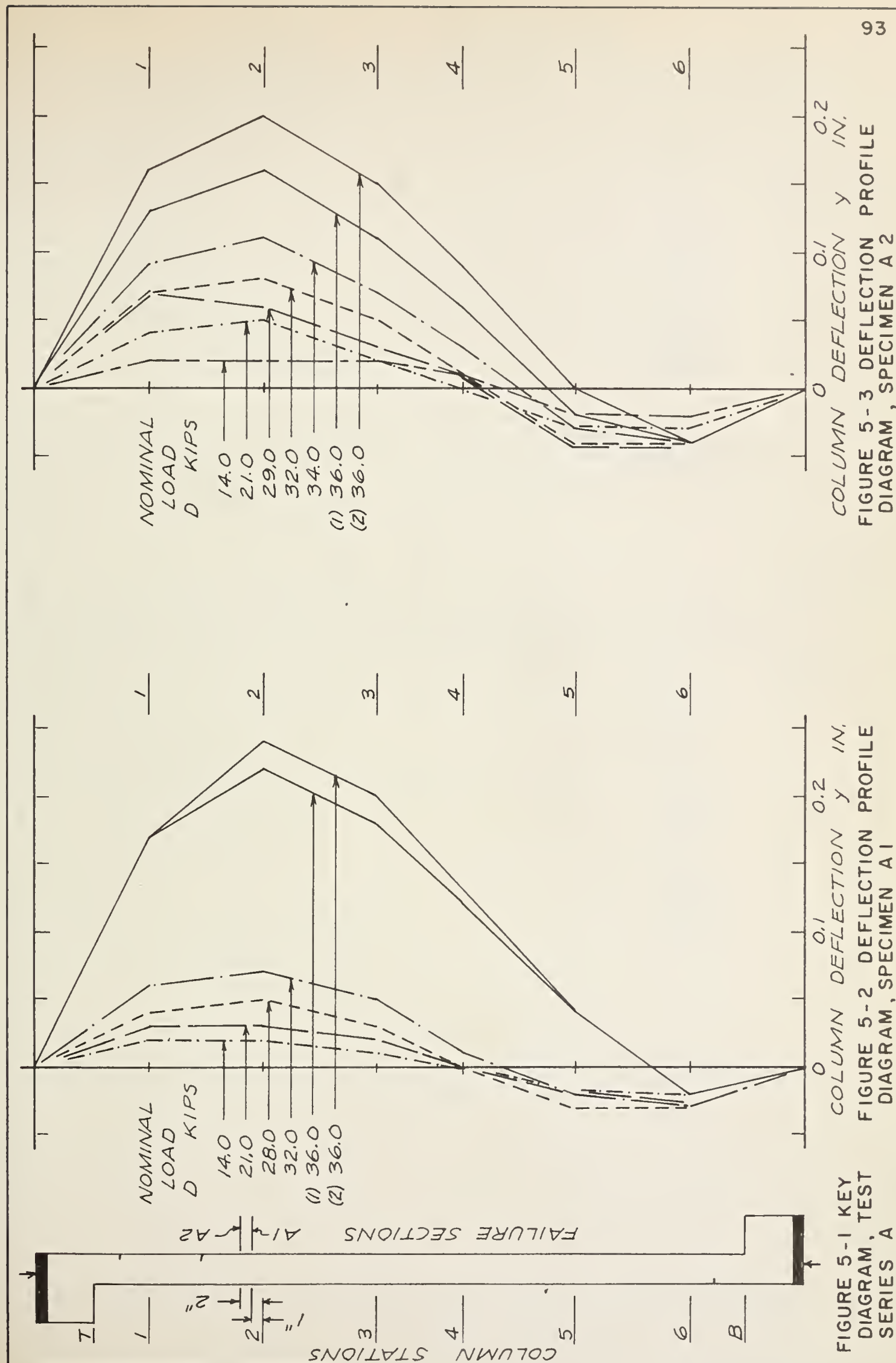
(b) Outline Of Observed Test Behavior

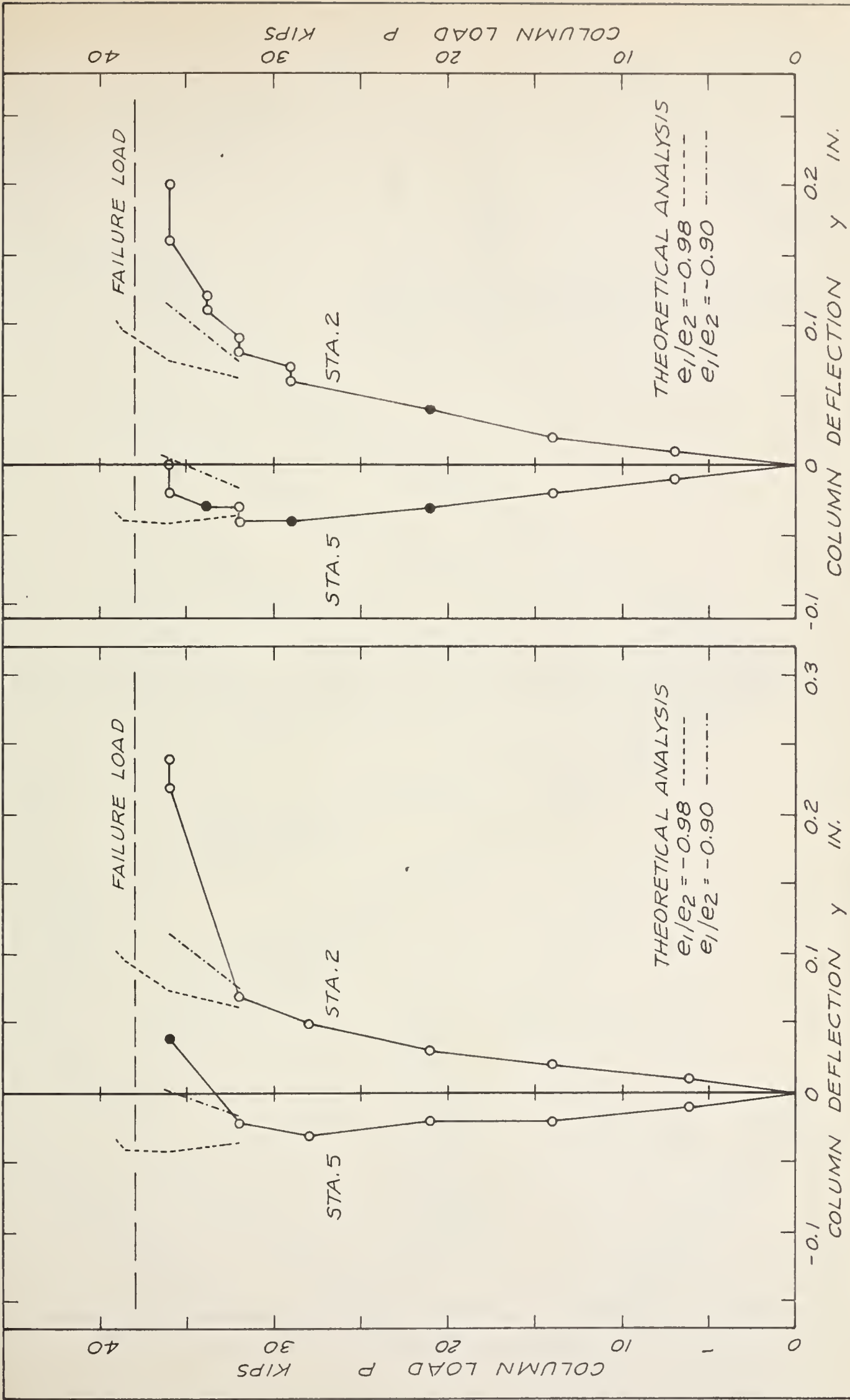
(i) Specimen A1. The first observations were made at 7.05 kips nominal load. The deflected shape was approximately antisymmetrical. No tension cracks were found.

At 14.00 kips nominal load, lateral deflections remained nearly equal at the upper and lower ends of the column, as shown in FIGURE 5 - 2. No tension cracks were found.

The first tension cracking appeared at 21.00 kips nominal load. One small crack was found in the tension face at both the upper and lower ends of the column.

At 28.00 kips nominal load the deflected shape had become noticeably unsymmetrical, with the larger deflections occurring at the upper end of the column, as shown in FIGURE 5 - 2. This was the first





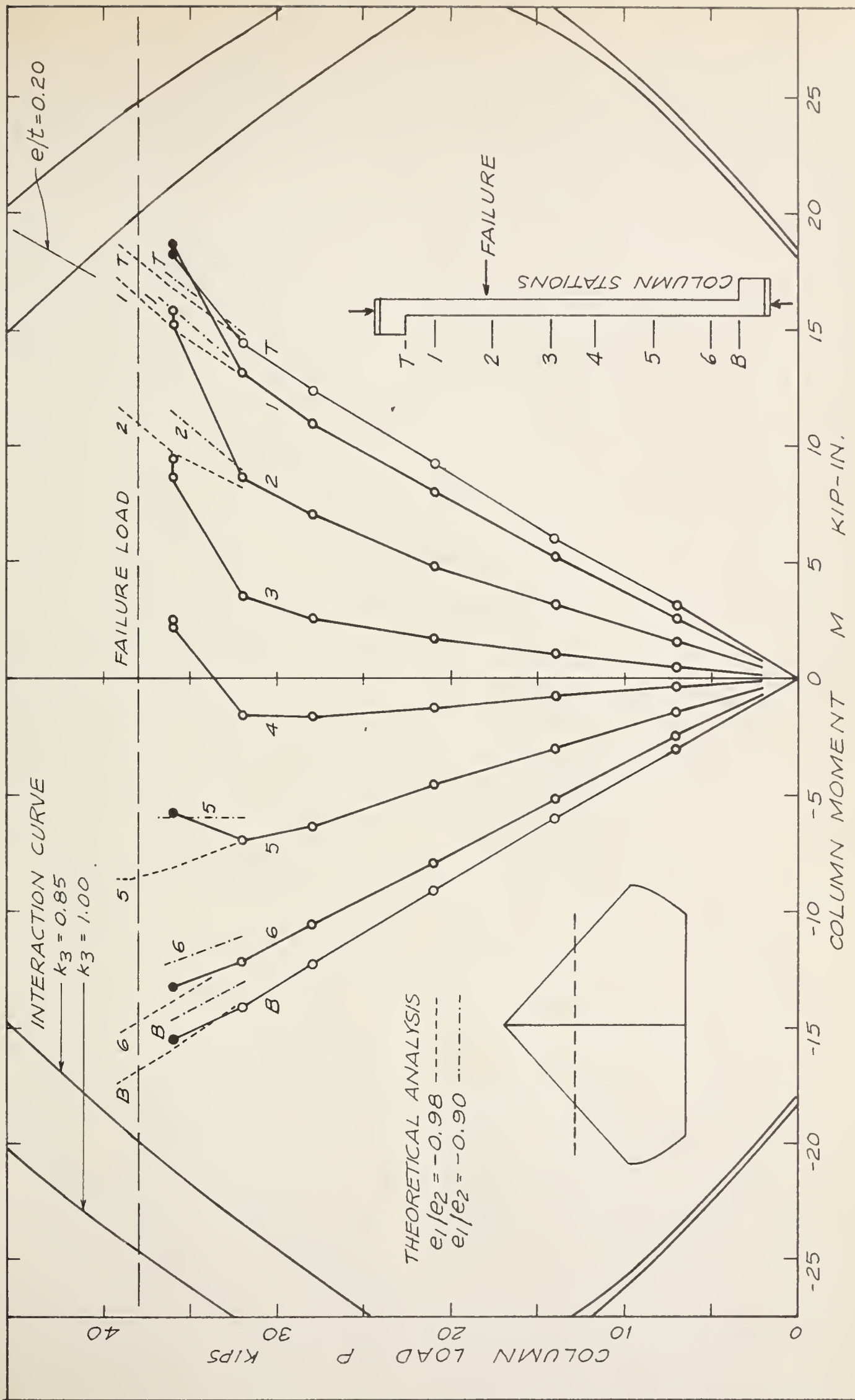


FIGURE 5-6 LOAD-MOMENT DIAGRAM, SPECIMEN A1

definite departure from the antisymmetrical condition, and indicated that failure would probably occur in the upper portion of the column. One new crack appeared in the upper portion of the column.

At 32.00 kips nominal load the unsymmetrical trend of the lateral deflections continued. There was little increase in the extent of cracking.

The last observations before failure were made at 36.00 kips nominal load. A vertical crack was found in the upper end block, and is visible in FIGURE 3 - 5. The crack had no effect on the column strength. The effects of creep were noticeable, as lateral deflections increased at constant load. The increase is shown by the two deflection profiles for 36.00 kips load, in FIGURE 5 - 2. The deflected shape had become very unsymmetrical, with the maximum deflection of the upper portion about ten times that of the lower.

Failure occurred while the next increment of load was being added. The load dial reached a maximum reading of 37.95 kips, when crushing of the concrete was observed. This load could not be maintained or exceeded. Crushing occurred on the compression face over a length of about four inches, centered one inch above Station 2. Crushing did not penetrate the full depth of the cross-section. Short cracks were

observed on the tension face at the failure zone. The pattern of cracking shortly before failure was similar to that shown in FIGURE 5 - 1. The appearance of the specimen immediately after failure is shown in FIGURE 3 - 5. Straining was continued, and at about 34.00 kips load the full cross-section crushed at the original failure zone. The appearance of the tension side of the failure zone after additional straining is shown in FIGURE 3 - 7.

The ultimate column load was reported as 37.95 kips nominal load, which corresponded to 37.95 kips corrected axial load. The column failed by initial crushing of the concrete and was a typical compression failure. The failure section was located as shown in FIGURE 5 - 1.

(ii) Specimen A2. From the beginning of the test to 21.00 kips nominal load the test observations were similar to those for Specimen A1. The first tension cracks appeared at 21.00 kips load. Deflection profiles are shown in FIGURE 5 - 3.

At 29.00 kips nominal load, the deflected shape had become noticeably unsymmetrical with the larger deflections occurring at the upper end of the column, as shown in FIGURE 5 - 3. This was the first definite departure from the antisymmetrical condition, and indicated that failure would probably occur in the upper portion of the column. The effect of creep was first noticed at this load as lateral deflections

increased at constant load. The second deflection profile was omitted from FIGURE 5 - 3, but the increase in deflections may be seen in FIGURE 5 - 5. Vertical cracks were found in the loading brackets as shown in FIGURE 5 - 19.

At 32.00 kips and 34.00 kips nominal load the previously observed trend of deflections continued. The increase in deflection due to creep may be seen in FIGURE 5 - 5. There was little increase in the extent of cracking.

The last observations before failure were made at 36.00 kips nominal load. During the seven minutes required for observations lateral deflections increased as much as 25 percent under constant load. The increase is shown by the two deflection profiles for 36.00 kips load, in FIGURE 5 - 3. The deflected shape had become very unsymmetrical, with the maximum deflection of the upper portion about five times that of the lower.

Failure occurred while the dial reading was being adjusted to 38.00 kips for a routine set of readings. This load could not be maintained or exceeded. Crushing of the concrete was observed on the compression face over a length of about five inches, centered two inches above Station 2. Crushing did not penetrate the full depth of the cross-section. Short cracks were observed on the tension face at the

failure zone. The pattern of cracking shortly before failure was similar to that shown in FIGURE 5 - 1. The appearance of the failure zone immediately after failure is shown in FIGURE 5 - 19.

The ultimate column load was reported as 38.00 kips nominal load, which corresponded to 38.00 kips corrected axial load. The column failed by initial crushing of the compression block, and was a typical compression failure. The failure section was located as shown in FIGURE 5 - 1.

(c) Discussion Of Test Series A

Load-Deflection Graphs are shown in FIGURES 5 - 4 and 5 - 5 for specimens A1 and A2, respectively. In both cases the failure section was located near Station 2, while Station 5 was the symmetrically located point in the lower portion of the column. The lateral deflection at Stations 2 and 5 were nearly equal up to about 70 percent of ultimate load. As the ultimate load was approached, the deflection at Station 2 increased at a much greater rate than before, while the deflection at Station 5 decreased. The point of zero deflection moved well into the lower half of the column, as the deflected shape became very unsymmetrical. A conservative straight-line projection of the load-deflection curves indicated that at ultimate load the deflection at Station 2 was from 50 to 60 percent of the nominal end eccentricity. In both

tests, the small value of the slope of the load-deflection curve for Station 2, near the ultimate load, indicated decreasing column stiffness as well as the effect of P_y -moments. Deflections were measured at the beginning and end of each observation period and the change at constant load is shown by the horizontal segments of the curves. The deflections resulting from the effects of creep added considerably to the total deflection at Station 2, near the failure section, in both tests.

Load-Moment Curves are shown in FIGURES 5 - 6 and 5 - 7 for Specimens A1 and A2, respectively. As can be seen from the key interaction curves in the lower left part of the figures, the eccentricities in Test Series A corresponded to a compression failure. Up to about 70 percent of ultimate column load, the load-moment curves for corresponding stations in the upper and lower portions of each column are similar, as expected from the symmetry of the deflection profiles. Each load-moment curve is nearly linear since P_y -moments were small up to this load level.

As ultimate load was approached, the moments at the stations in the upper portion of the columns began to increase at a much greater rate than before due to the increase in magnitude of the P_y -moments. At the same time, moments at stations in the lower portion of the columns began to decrease, and in some cases changed sign, as a result of the

lowering of the point of zero deflection. The effect of creep deflections on the moments is shown by the horizontal segments of the load-moment curves.

In both tests the failure section was located near Station 2, while the maximum moment was at Station 1 at the last observation before failure. However, a comparison of the slopes of the load-moment curves for these stations shows that moments were increasing at a greater rate at Station 2 than at Station 1. From the trend of the curves it appears that the moment at Station 2 would have exceeded that at Station 1 at ultimate load. This is in agreement with the observed locations of the failure section.

In both tests of Series A the ultimate column load appeared to be determined by material failure and not instability. The behavior was similar to that in Case (b), described in Section 2.1(c), in which the failure section was located away from the column end. This conclusion was based primarily upon test observations, since the plotted data was inconclusive. The test observations indicated that material failure occurred simultaneously with maximum column load, which is characteristic of a material failure. The slopes of the load-moment curves for Station 2, near the failure section, were rapidly decreasing as the ultimate load was approached. However, it appears likely the slopes

were positive at failure, which would also indicate a material failure, as discussed in Section 2.1(c).

It was not possible to directly compare the measured strength of the column cross-section with that predicted by the interaction curve since the load-moment curves could not be accurately projected. However, at the last observation before failure all the measured moments fell within the limits of the interaction curve. Also, the trends indicated that the load-moment curves for the failure sections could quite reasonably have intersected the interaction curves at close to the measured ultimate load. To this extent, reasonable agreement was indicated between measured and predicted strengths.

5.3 Test Series C

(a) General

Test Series C comprised tests of two similar specimens designated C1 and C2. The columns were restrained and had nominal end eccentricities of 0.50 inches, which corresponded to eccentricity ratios $e/t = 0.2$ at the end blocks and $e/t = 0.17$ at the ends of the column section. The average concrete strengths were 3630 psi for A1 and 4550 psi for A2. Results of the tests are presented in FIGURES 5 - 8 to 5 - 18.

The general behavior of both specimens was similar, as shown by the plotted test results and observed behavior, and the results of both tests are discussed together. The loading apparatus performed as expected and no difficulties were encountered.

(b) Outline Of Observed Test Behavior

(i) Specimen C1. The first observations were made at 7.00 kips nominal load. The deflected shape was approximately antisymmetrical. No tension cracks were found.

At 14.00 kips and 21.00 kips nominal load the deflected shape remained approximately antisymmetrical, as shown in FIGURE 5 - 9. Tension cracks appeared in the high moment regions of both beams but none were found in the column.

At 27.00 kips nominal load, the lower portion of the column and the lower beam had deflected considerably more than the upper end, as shown in FIGURE 5 - 9. From this trend it appeared that failure would probably occur in the lower portion of the column. The first tension cracks appeared in the column, near the lower end. There was an increase in tension cracking in the lower beam while the upper beam showed little change.

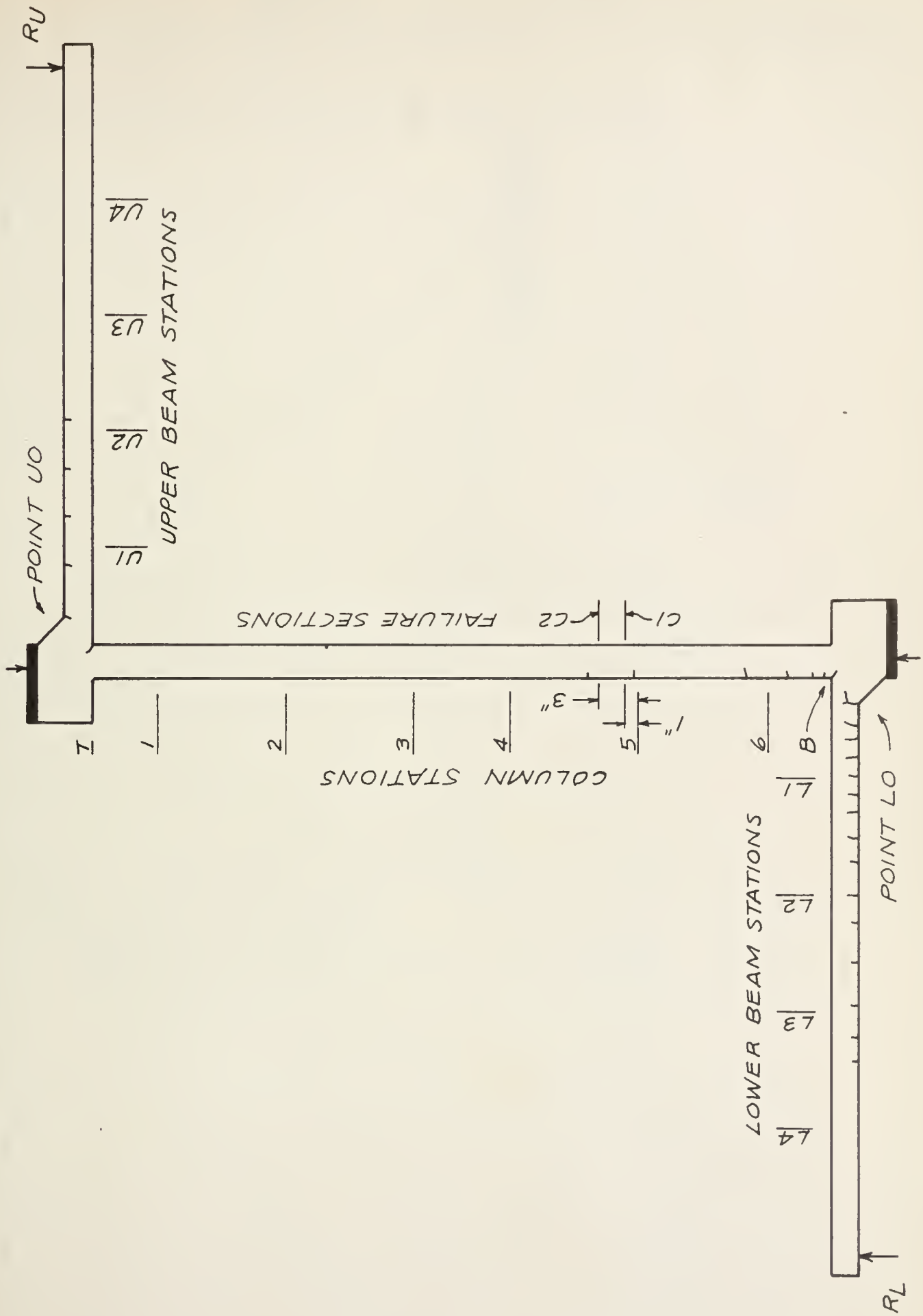


FIGURE 5-8 KEY DIAGRAM, TEST SERIES C

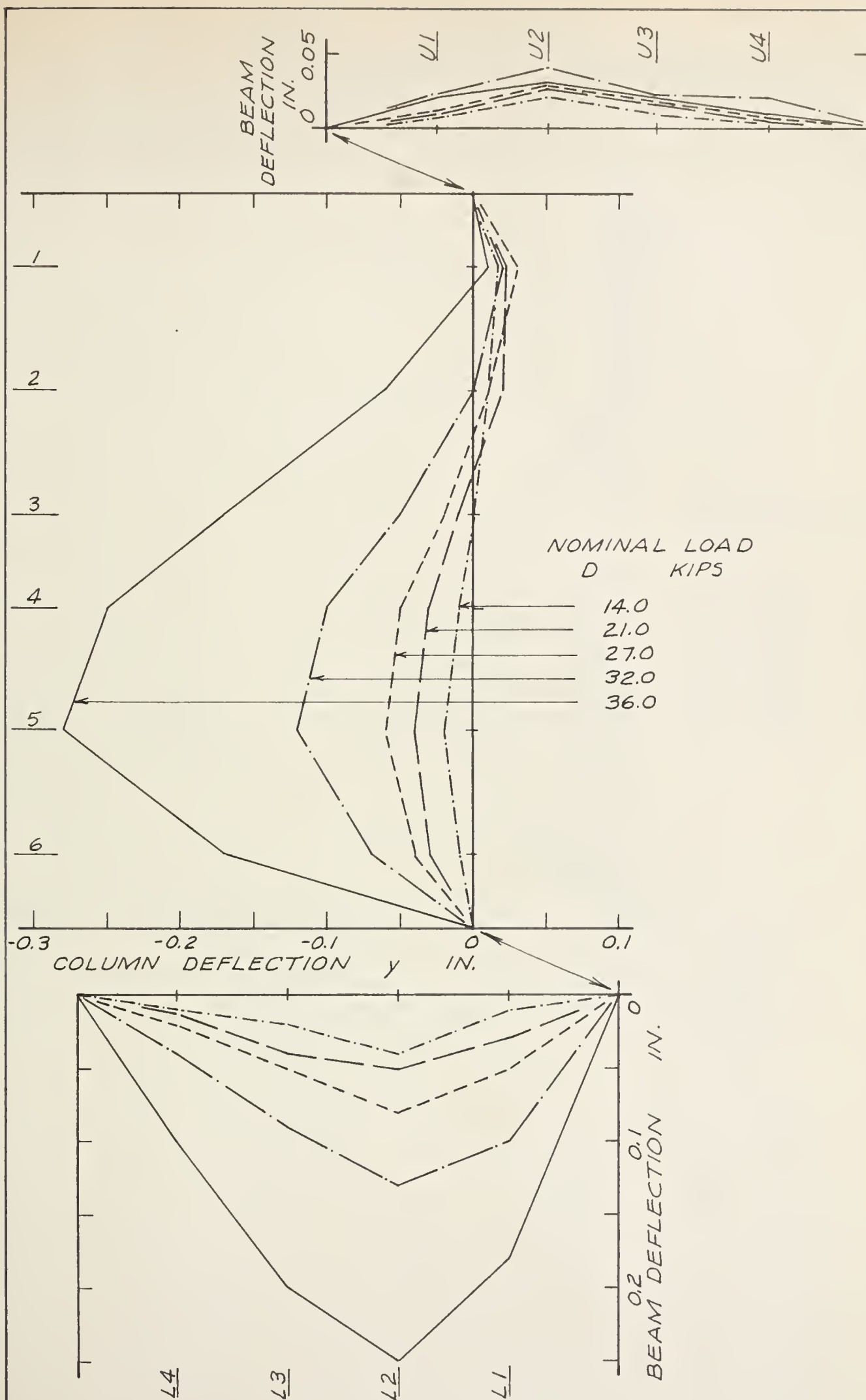


FIGURE 5 - 9 DEFLECTION PROFILE DIAGRAM , SPECIMEN C I

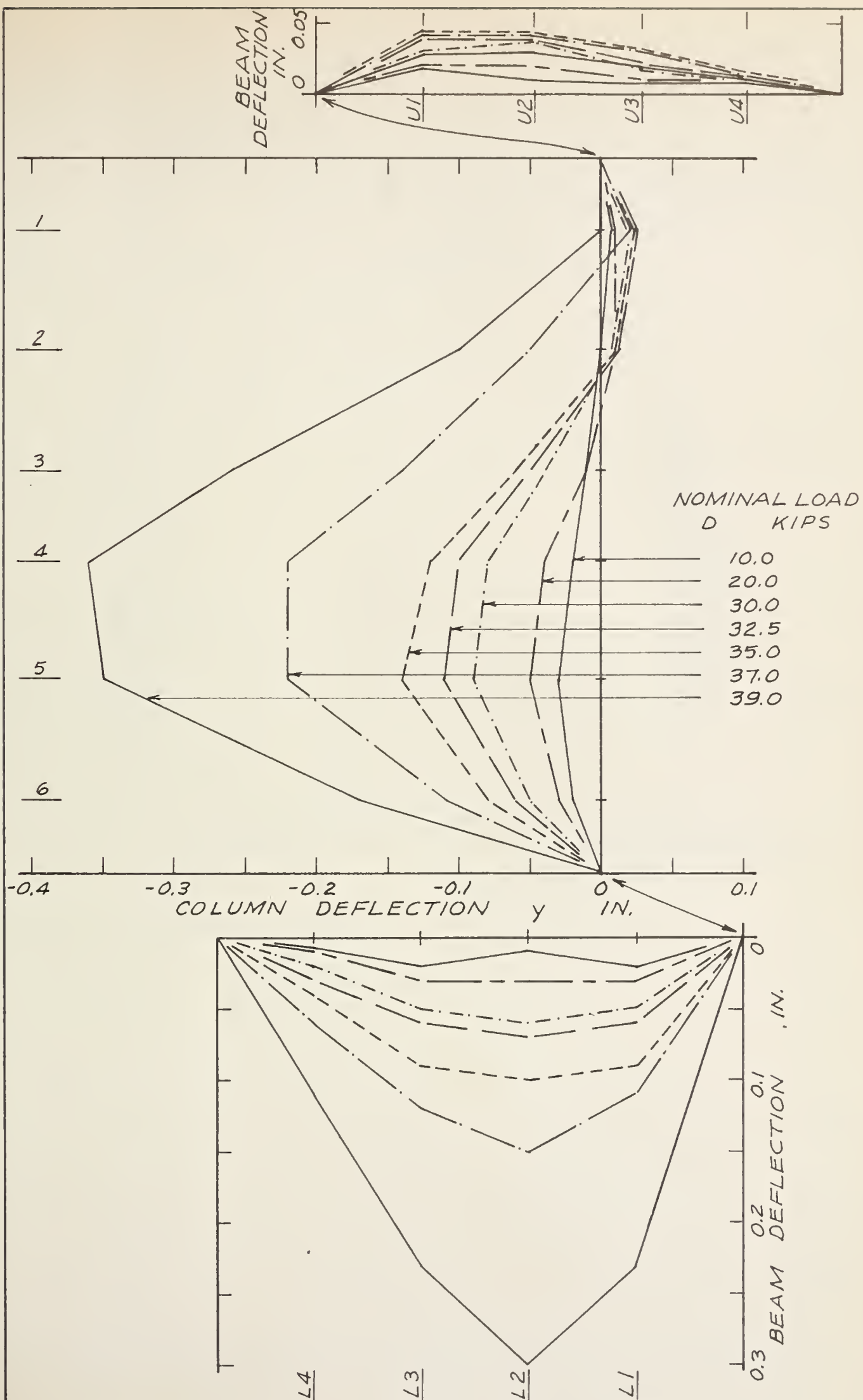


FIGURE 5 - 10 DEFLECTION PROFILE DIAGRAM, SPECIMEN C 2

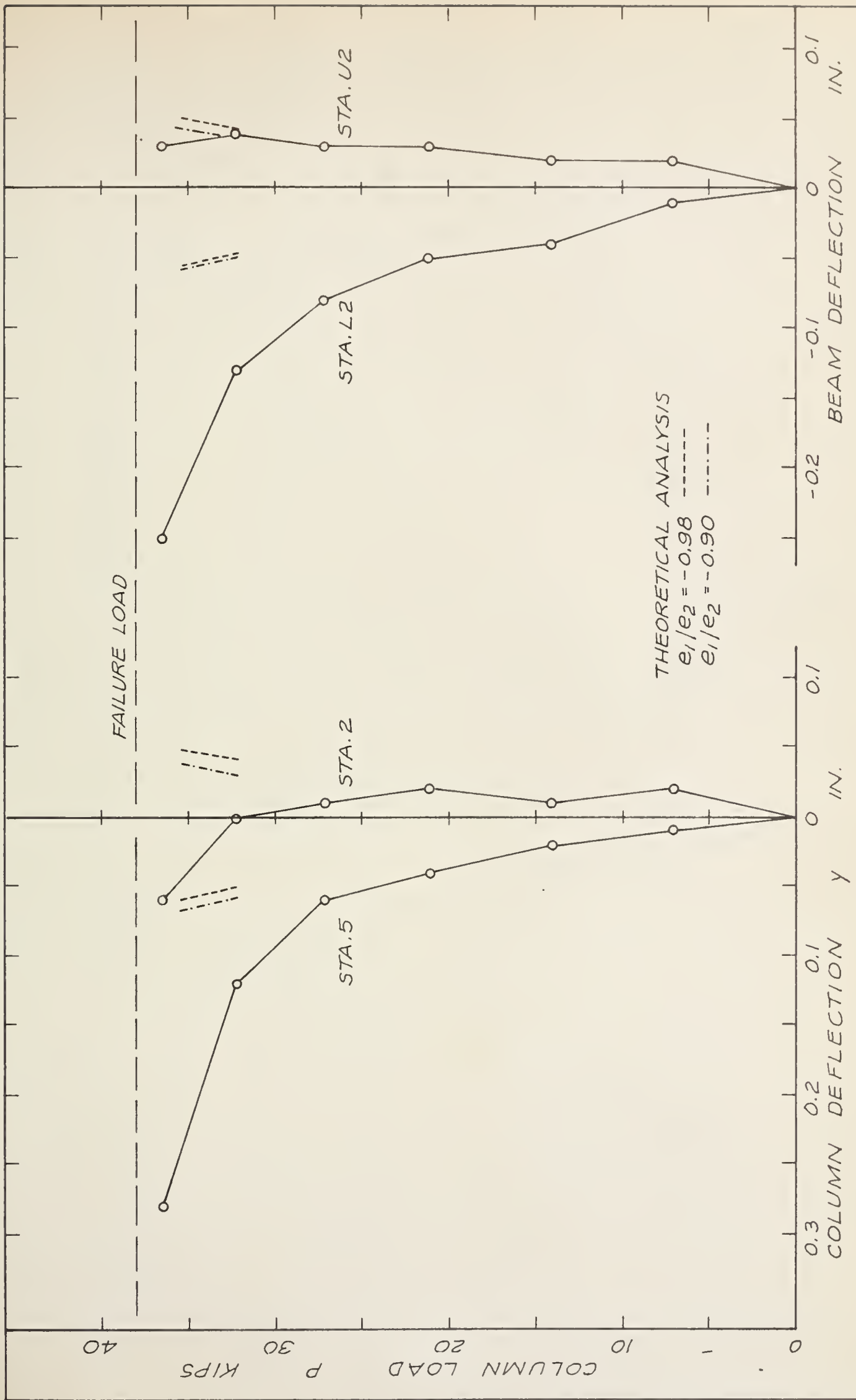


FIGURE 5-11 LOAD - DEFLECTION GRAPH, SPECIMEN C 1

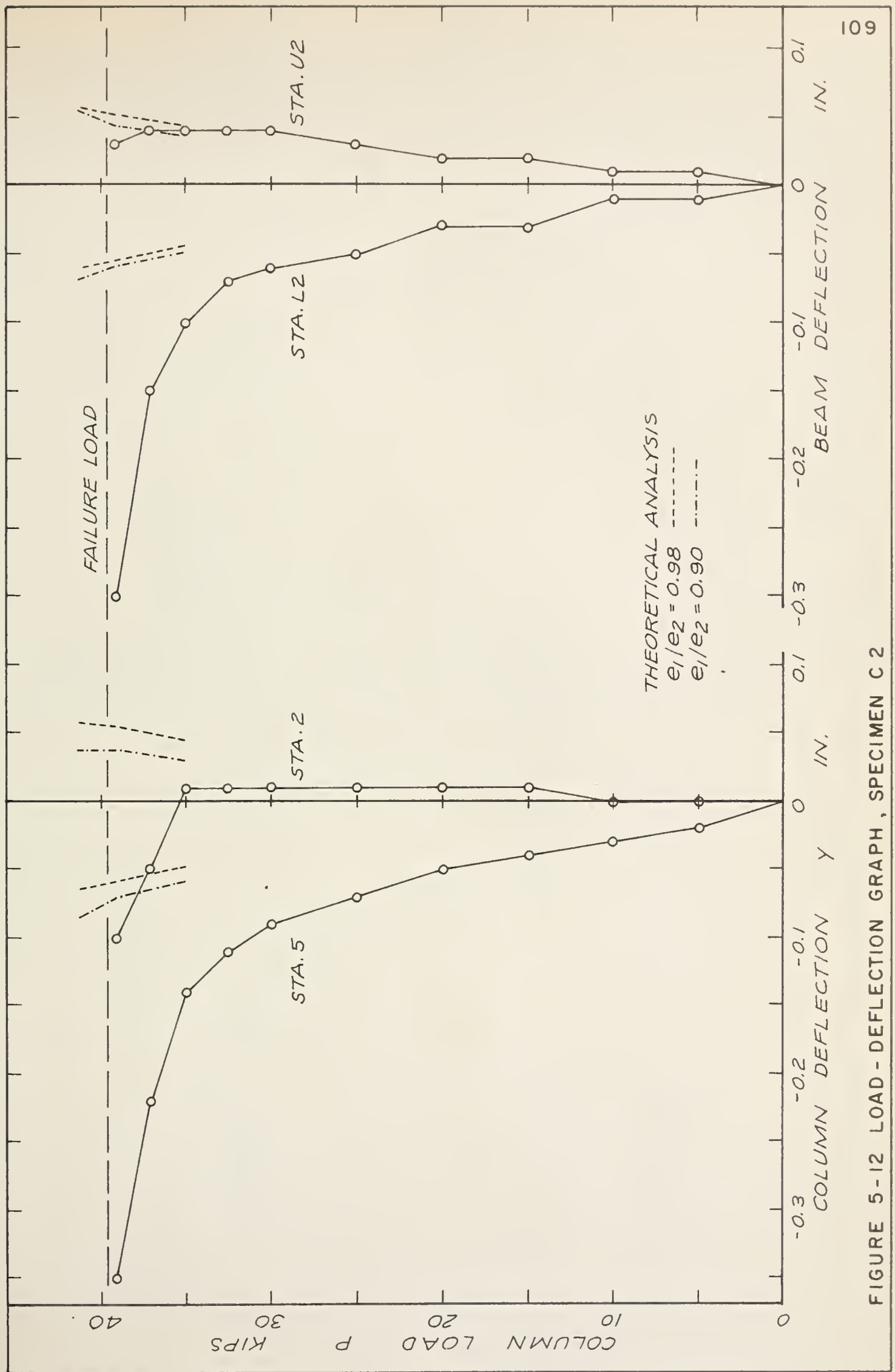


FIGURE 5-12 LOAD - DEFLECTION GRAPH, SPECIMEN C 2

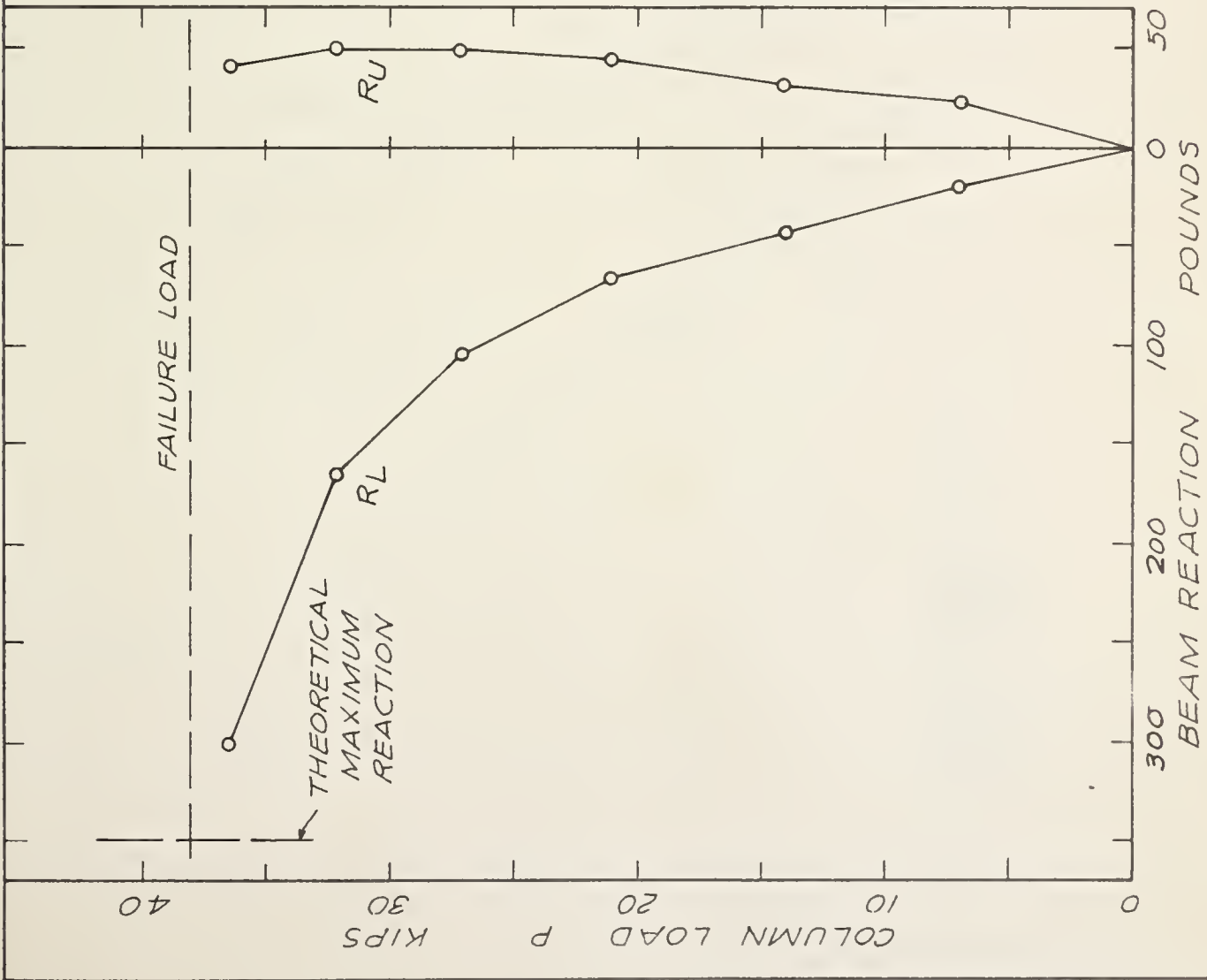


FIGURE 5-13 BEAM REACTION GRAPH,
SPECIMEN C1

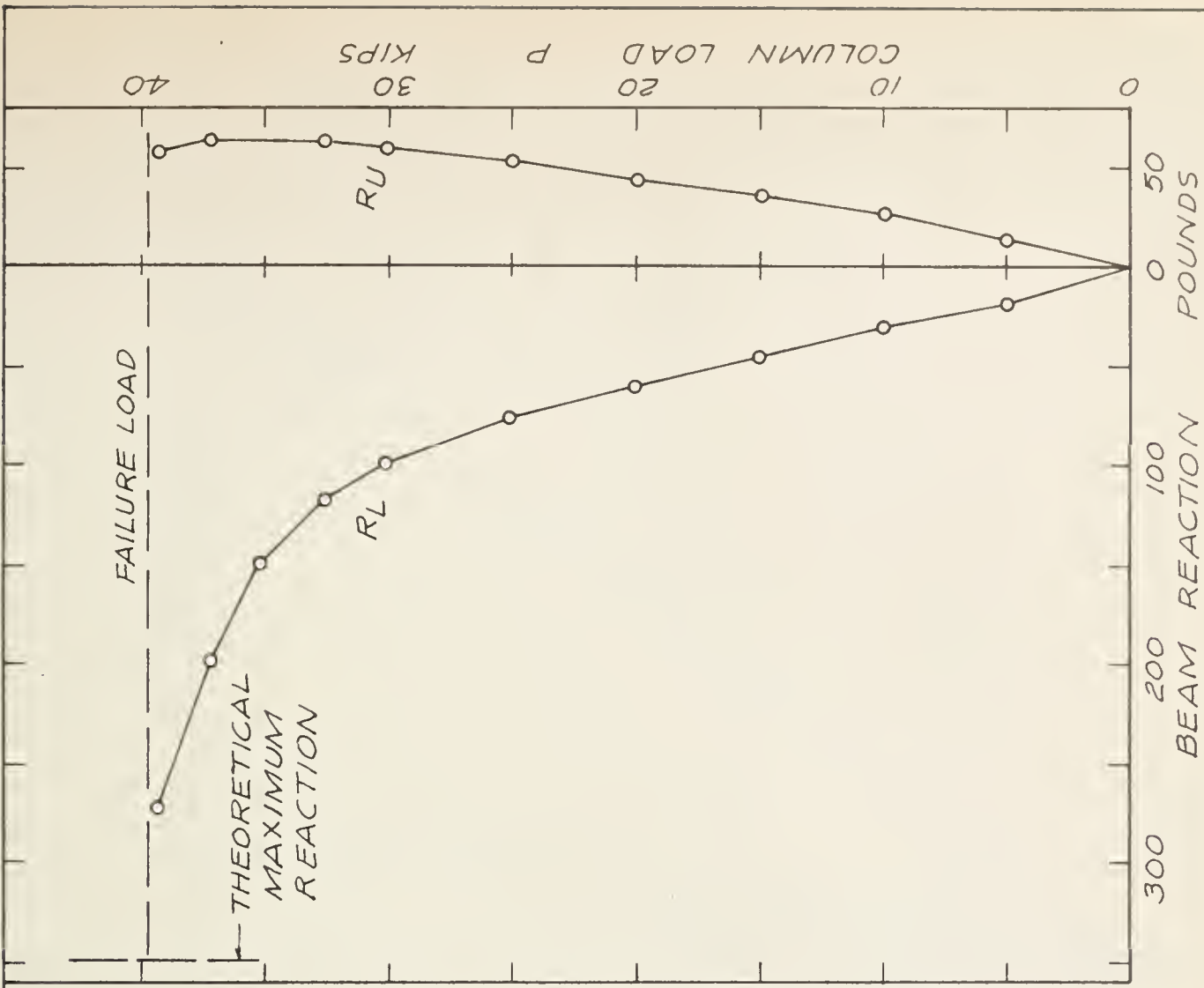


FIGURE 5-14 BEAM REACTION GRAPH,
SPECIMEN C2

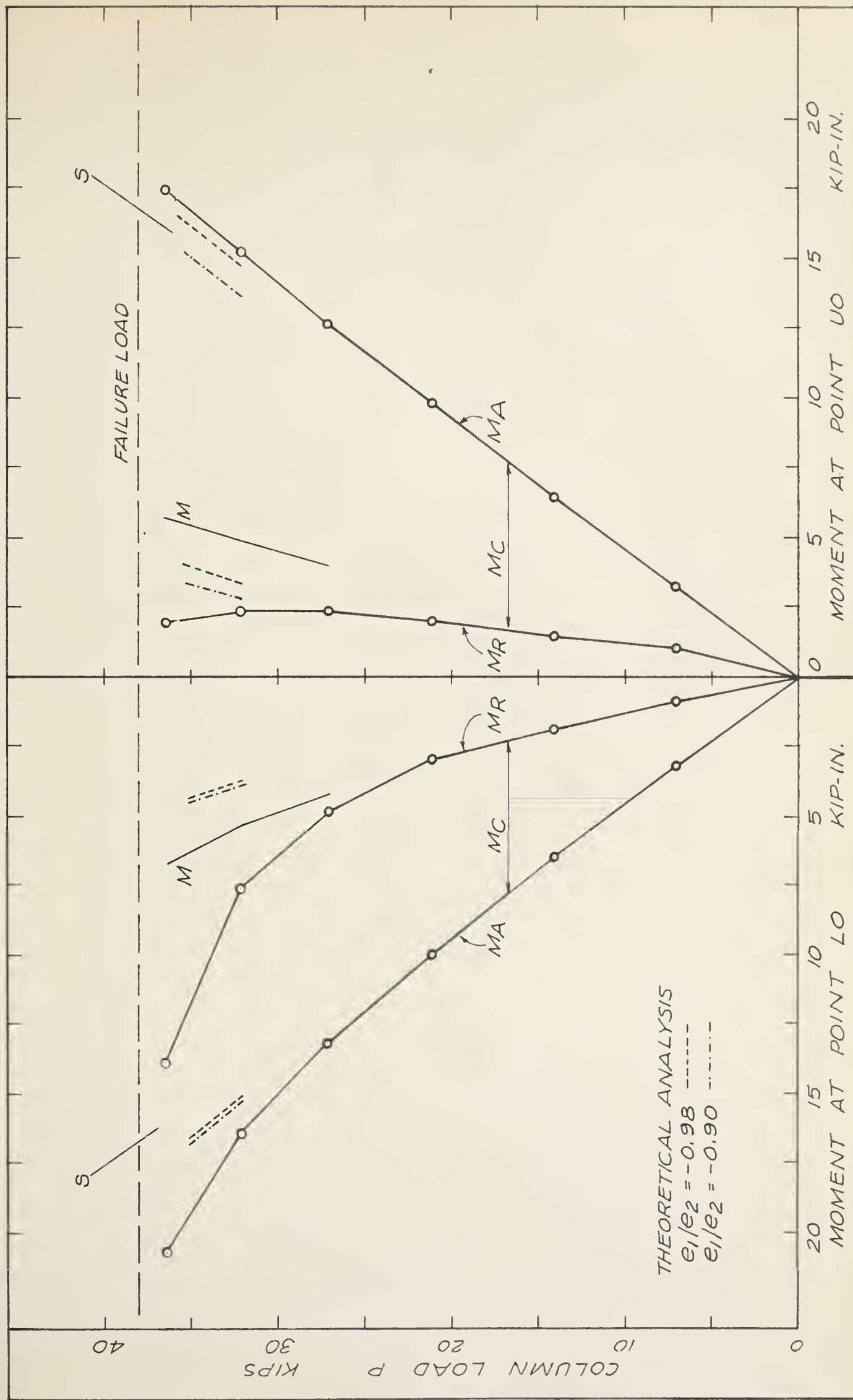


FIGURE 5-15 MOMENT DISTRIBUTION DIAGRAM, SPECIMEN C1

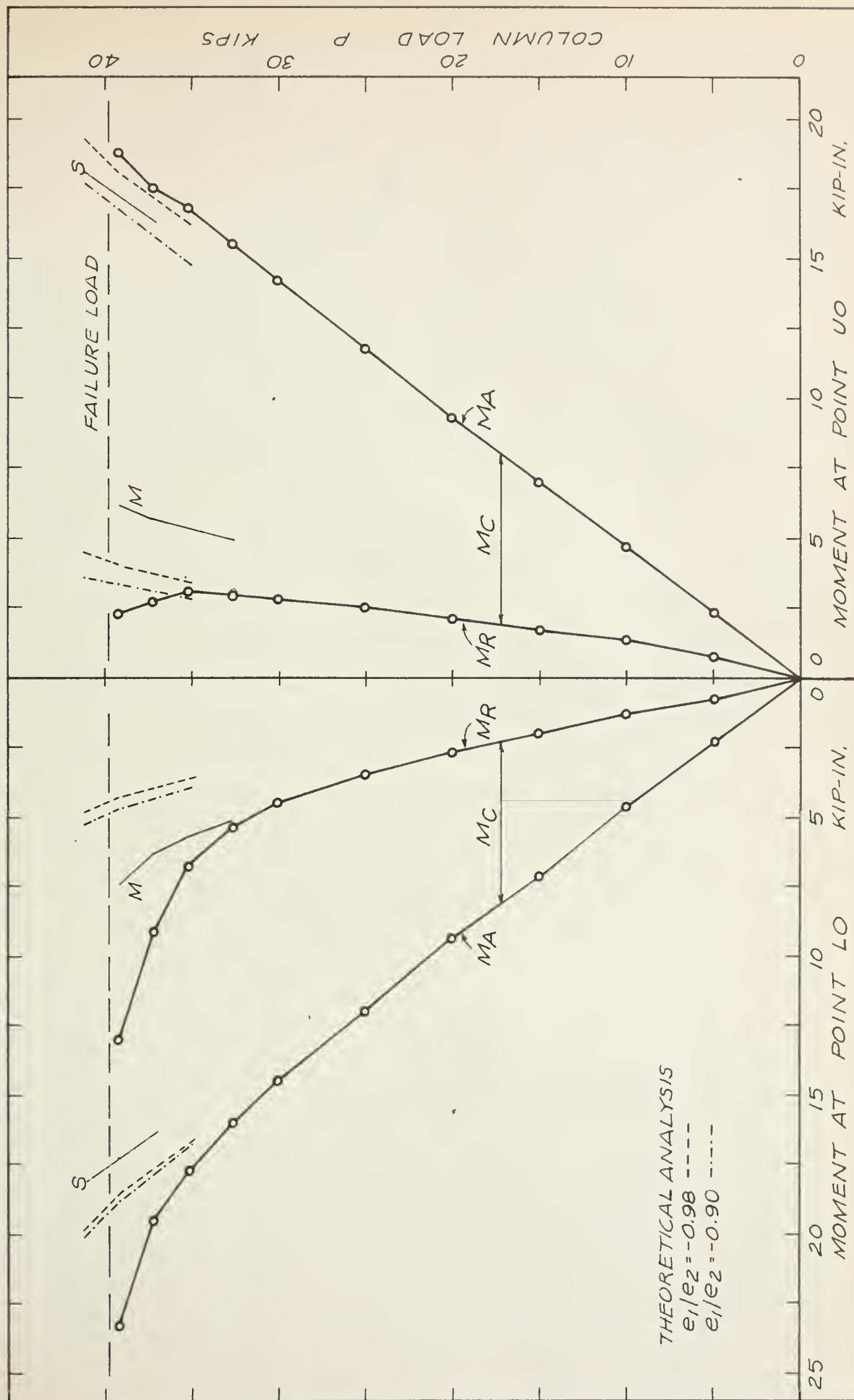


FIGURE 5-16 MOMENT DISTRIBUTION DIAGRAM, SPECIMEN C 2

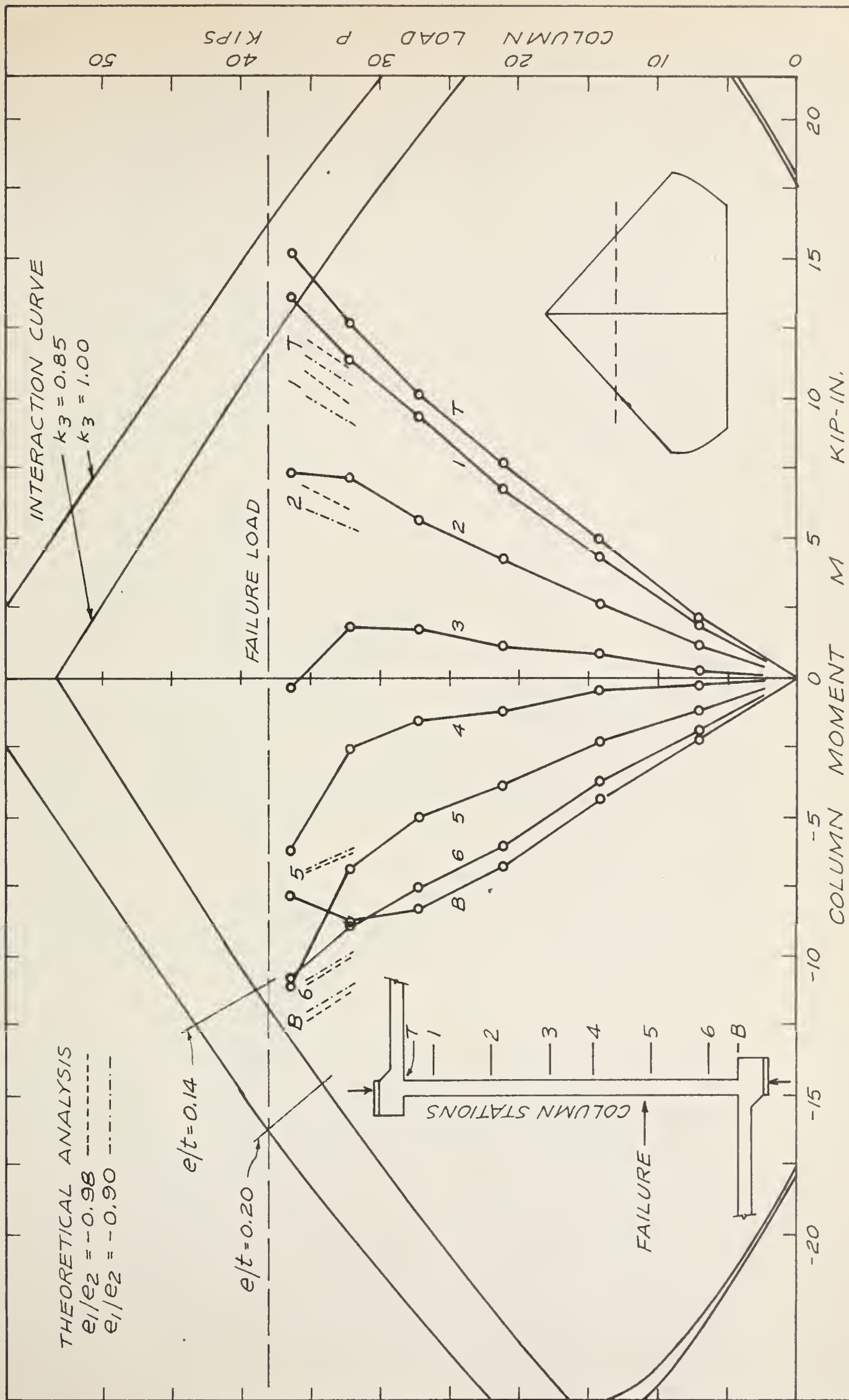


FIGURE 5-17 LOAD-MOMENT DIAGRAM, SPECIMEN C1

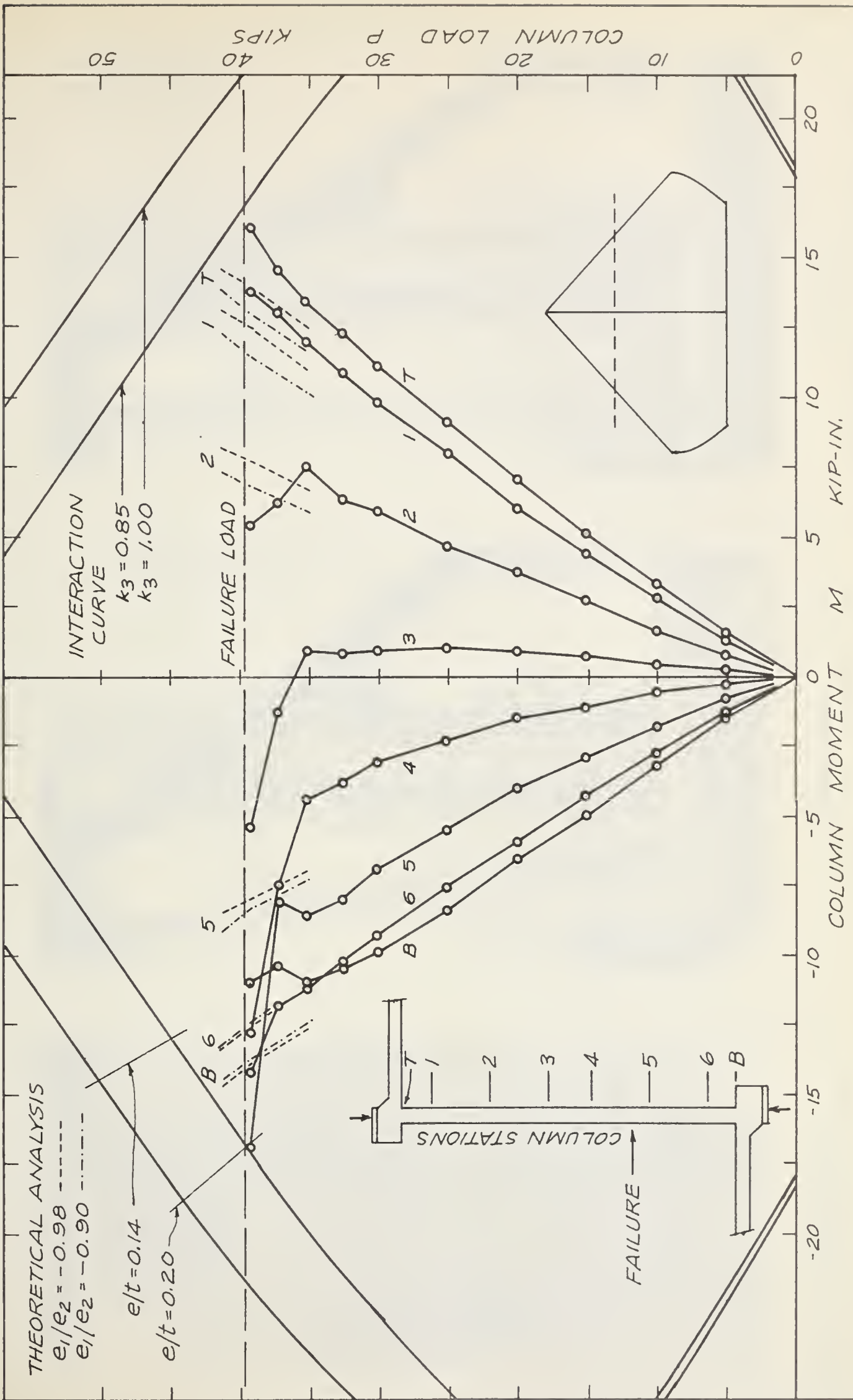


FIGURE 5-18 LOAD-MOMENT DIAGRAM, SPECIMEN C 2



FIGURE 5-19
SPECIMEN A2 FAILURE ZONE



FIGURE 5-20
SPECIMEN D2 AT 7.50 KIPS LOAD



FIGURE 5-21
SPECIMEN C2 AT 35.00 KIPS LOAD

At 32.00 kips nominal load, deflections at the lower end of the specimen continued to increase, while those at the upper end began to decrease. The point of zero deflection had risen from mid-height to about Station 2, as shown in FIGURE 5 - 9. The maximum deflection of the lower portion of the column was about six times that of the upper portion. Cracking increased in the lower portion of the column and lower beam, while there was no change in the upper end.

The last observations before failure were made 36.00 kips nominal load. The previous deflection trend had continued. The upper beam reaction, which had been slowly increasing, showed a decrease at this load (FIGURE 5 - 13). The deflections due to creep were not measured in this test.

An error is believed to have occurred in recording the strain indicator reading for the lower beam reaction, R_L , at this load ($D = 36.00$ kips). The reading shown on the original data sheet was 91.8, corresponding to $R_L = 387$ pounds. The correct reading is believed to be 71.8 which corresponds to the tabulated net reading of 69.0, and gives $R_L = 300$ pounds. The 300 pound value is given in TABLE C-5 and was used in all the computations. The adoption of the reading 71.8 was based on consideration of the lower beam reaction-deflection curves and on additional test data. A plot of the deflections at each station on the beams, against the value of the beam reaction, indicated that the use of $R_L = 387$

pounds corresponded to a significant decrease in the rate of change of deflection with load when compared with earlier deflections. This did not agree with similar plots for other restraining beams, in which a slight increase in the rate of change of deflection with load was always found. The use of $R_L = 300$ pounds fitted well with an extrapolation of earlier deflections, and indicated a slight increase in the rate of change of deflection with load. In addition, an indicator reading of 80.5 was recorded following the reading under consideration, when creep deflections were observed just before the next load increment was added. Since the indicator reading had been continually increasing throughout the test, this indicated that an earlier reading of 91.8 was improbable, while a reading of 71.8 could possibly have been obtained.

Failure occurred while the next load increment was being added. The load dial reached a maximum reading of 37.50 kips, when crushing of the concrete was observed. The load could not be maintained or exceeded. Crushing occurred on the compression face over a length of about eight inches, centered one inch above Station 5. Crushing did not penetrate the full depth of the cross-section. Short cracks were observed on the tension face at the failure zone. There was no sign of distress in the upper portion of the column or in either beam. The pattern of cracking shortly before failure was similar to that shown in FIGURE 5 - 8. The appearance of the specimen immediately after failure is shown in FIGURE 3 - 6.

The ultimate column load was reported as 37.50 kips nominal load, which corresponded to 38.01 kips corrected axial load. The column failed by initial crushing of the concrete and was a typical compression failure. The failure section was located as shown in FIGURE 5 - 8.

(ii) Specimen C2. The first observations were made at 5.00 kips nominal load. The deflected shape was approximately antisymmetrical. No tension cracks were found.

At 10.00 kips and 15.00 kips nominal load the deflected shape remained approximately antisymmetrical, as shown in FIGURE 5 - 10. Tension cracks appeared in the high moment regions of both beams, but none were found in the column.

At 20.00 kips and 25.00 kips nominal load the observations were about the same as for 15.00 kips load.

At 30.00 kips and 32.50 kips nominal load, the lower portion of the column and the lower beam had deflected considerably more than the upper end, as shown in FIGURE 5 - 10. From this trend it appeared that failure would probably occur in the lower portion of the column. There was an increase in cracking in the lower beam, while the upper beam showed little change. No tension cracks were found in the column.

At 35.00 kips nominal load several small tension cracks appeared in the lower portion of the column, while the upper portion remained uncracked. The appearance of the specimen at 35.00 kips load is shown in FIGURE 5 - 21.

At 37.00 kips nominal load, lateral deflections of the lower portion of the specimen continued to increase while those of the upper portion began to decrease. The point of zero deflection had risen from mid-height to between Stations 1 and 2 as shown in FIGURE 5 - 10. The maximum deflection of the lower portion of the column was about nine times that of the upper. Cracking increased in the lower portion of the column and lower beam, while there was no change at the upper end.

The last observations before failure were made at 39.00 kips nominal load. The previous unsymmetrical deflection trend had continued. The upper beam reaction, which had been slowly increasing, showed a decrease at this load (FIGURE 5 - 14). An increased strain rate was required to maintain the load during the observation period. The deflections due to creep were not measured in this test.

Failure occurred while the next load increment was being added. The load dial reached a maximum reading of 39.35 kips, when crushing of the concrete was observed. The load could not be maintained or exceeded.

Crushing occurred on the compression face over a length of about eight inches, centered two inches above Station 5. Crushing did not penetrate the full depth of the cross-section. Short cracks were observed on the tension face at the failure zone. There was no sign of distress in the upper end of the column or in either beam. The pattern of cracking shortly before failure was similar to that shown in FIGURE 5 - 8.

The ultimate column load was reported as 39.35 kips nominal load, which corresponded to 39.69 kips corrected axial load. The column failed by initial crushing of the concrete and was a typical compression failure. The failure section was located as shown in FIGURE 5 - 8.

(c) Discussion Of Test Series C

Load-Deflection Graphs are shown in FIGURES 5 - 11 and 5 - 12 for Specimen C1 and C2, respectively. In both cases the failure section was located near Station 5, while Station 2 was the symmetrically located point in the lower portion of the column. Up to about 50 percent of the ultimate column load, the deflections at Column Stations 2 and 5 were roughly equal to each other, as were those at Beam Stations U2 and L2. As the ultimate load was approached, the deflections at Stations 5 and L2 increased at a much greater rate than before, while the deflections at Stations 2 and U2 remained steady, then decreased. The point zero deflection moved well into the upper half of the column as the deflected

shape became very unsymmetrical. A conservative straight line projection of the load-deflection curves indicated the maximum deflection at ultimate load was from 70 to 80 percent of the nominal end eccentricity. This was of the same order as in the hinged column tests of Series A. In both tests the small value of the slope of the load-deflection curve for Station 5, near the ultimate load, indicated rapidly decreasing column stiffness, as well as the effect of P_y -moments. The deflections due to creep were not measured in these tests.

Beam Reaction Graphs are shown in FIGURES 5 - 13 and 5 - 14 for Specimens C1 and C2, respectively. In both tests the upper and lower reactions were roughly equal up to about 50 percent of ultimate load. As the ultimate load was approached, the lower beam reaction increased at a much greater rate than before, while the upper beam reaction remained steady, then decreased. At the last observations the lower beam reaction was from five to seven times as large as the upper beam reaction.

As described in Chapter III, the beam supports were adjusted during the tests to eliminate induced moments due to differential settlement of the two ends of each beam. Since the amount of the adjustment depended on the measurement of the column shortening, the adjustment could not be made until each load increment was fully applied. Therefore, until the adjustments were made the restraining moments were somewhat smaller than the tabulated values, and the column moments

were correspondingly larger. The effect of the adjustment procedure on the test results at loads less than the failure load was believed to be small, since any extra lateral deflection due to the higher column moments would be almost entirely recovered when the beam supports were adjusted.

In this test series, column failure occurred as load was being added, while the beam supports were still at the setting for the previous load reading. The ultimate column loads were therefore influenced to some extent by effect of differential settlement of the beam supports.

In the case of Specimen C2, failure occurred after a load increment of only 0.35 kips above the previous setting, so the moments induced by further shortening of the column during this increment were believed to be small.

In the case of Specimen C1, however, column failure occurred after a considerably larger load increment of 1.50 kips above the previous setting. It was not possible to measure the column shortening at failure, but it was estimated that the column shortened by about 0.1 inches during the 1.50 kips load increment. A very approximate analysis, ignoring reductions in column stiffness, suggested that at ultimate load the actual beam reactions were about 20 pounds smaller than they would have been had there been no differential settlement effect. If the

reduction in column stiffness were taken into account the difference would have been less. The estimated difference was small compared to the last observed value of the lower beam reaction, 300 pounds, but it was not small compared to the last observed value of the upper beam reaction, which was 41 pounds. The failure section was located in the lower portion of the column and the moment at that point was affected by the lower beam reaction to a greater extent than by the upper beam reaction. It was therefore concluded that the ultimate column load for Specimen C1 was relatively unaffected by the differential settlement effect.

It was calculated that the ultimate moment capacity of a restraining beam would be reached, adjacent to the column, if the beam reaction exceeded 349 pounds. A value about 15 pounds less would produce first yielding of the tension reinforcement. The theoretical maximum reaction of 349 pounds was plotted on the Beam Reaction Graphs. The magnitude of each beam reaction, at the ultimate column load, was estimated by a straight-line projection of the last segment of each load-reaction curve. For Specimen C1, it appeared that R_L was about equal to the theoretical maximum reaction at the ultimate column load, while for Specimen C2 it appeared that R_L was somewhat less than the theoretical limit. This is in agreement with the test observations, which showed that the upper and lower beams of both specimens were still intact after the columns failed. It was concluded that the restraints were in full

effect when the columns failed.

The Moment-Distribution Diagrams for Specimens C1 and C2 are shown in FIGURES 5 - 15 and 5 - 16, respectively. Up to about 50 percent of the ultimate column load, the ratio of column moment to applied moment, M_C/M_A , was nearly constant at both Point UO and Point LO. As the ultimate column load was approached, the ratio M_C/M_A decreased considerably at Point LO in both tests, as the lower restraining beam relieved the column of a portion of the moment it had originally been carrying. This was apparently due to a decrease in stiffness and large lateral deflections in the lower portion of the columns, where the failure sections were located. A considerable degree of relief was provided by the lower beams and at ultimate load the columns were subjected to smaller eccentricities than at lower load levels.

The Moment Distribution Diagrams show that the applied load eccentricity at Points UO and LO, as given by the ratio of applied moment to true column load, M_A/P , increased considerably as the ultimate column load was approached. The increase was due to the lateral displacement, Δ , of Points UO and LO, and the effects of the interaction of the beam reactions. The effect of the latter factor was small compared to the effect of the displacement, Δ . These factors are shown in the expressions for the applied moment, M_A , given in Appendix C (EQ. C - 5 and C - 8). The lines marked "S" represent

the initial applied load eccentricity at Points UO and LO (0.44 inches), and the difference in moment between the M_A -curves and Line S indicates the combined effect of these two factors.

Load-Moment Diagrams are shown in FIGURES 5 - 17 and 5 - 18 for Specimen C1 and C2, respectively. Up to 50 percent of the ultimate column load, the load-moment curves for corresponding stations in the upper and lower portions of each column are similar, as expected from the symmetry of the deflection profiles and of the distribution of moment at the upper and lower beam-column joints.

As the ultimate load was approached, the load-moment curves were affected by the increasing P_y -moments and restraining moments. Although there were some differences in details, the general trend in both tests was the same. The moments at Stations T and 1 increased since the increase in P_y -moments at these points was counteracted by an increase in restraining moment at the upper end of the columns. At Station B the moments decreased, since the affect of the increase in restraining moment at the lower beam-column joint was greater than the additional P_y -moments at this point.

The failure section was located near Station 5 in both tests. At Station 5 the effect of the decrease in the ratio of column moment to applied moment, M_C/M_A , was not as great as the additional P_y -moments,

and there was an increase in moment in both tests. The moment also increased at Station 4, where the deflections, and hence P_y -moments, were about the same as at Station 5. In both tests, at the last observation before column failure, both the moment and the rate of increase of moment were larger at Station 5 than at any other station. This was in agreement with the observed location of the failure sections.

In both tests of Series C the ultimate column load was believed determined by material failure and not instability. The behavior was similar to that in Case (b), described in Section 2.1(c), in which the failure section was located away from the column end. This conclusion was based primarily upon test observations, although the plotted test data appears in agreement. The test observations indicated that material failure occurred simultaneously with maximum column load, which is characteristic of a material failure. The slopes of the load-moment curves for Station 5, near the failure sections, were decreasing as the ultimate load was approached. However, it appears likely the slopes were positive at failure, which would also indicate a material failure, as discussed in Section 2.1(c).

It was not possible to make a direct comparison between the measured strength of the column cross-section and that predicted by the interaction curves since the load-moment curves could not be accurately

projected. For Specimen C1 the trend of the load-moment curve for Station 5, near the failure section, appeared to indicate good agreement between measured and predicted strengths. At the last observation before failure, the measured moment at Station T was 15 percent greater than that given by the interaction curve, and the section had not failed. However, the measured point fell within the interaction curve for $k_3 = 1.00$.

For Specimen C2, at the last observation before failure all the moments fell within the limits of the interaction curve. The trend of the load-moment curve for Station 5, near the failure section indicated good agreement with the interaction curve.

The columns of Test Series A and C were similar, except that the former were hinged while the latter were restrained. The effect of the end restraints may be seen in a comparison of the results of the two test series. In both test series the columns failed at points located from 16 to 23 percent of the column length away from mid-height. In both cases the column deflections were large enough to shift the point of maximum moment away from the end of the column. At the same load levels, the maximum column deflections in Test Series C were about equal to those in Test Series A, in spite of the presence of the end restraints. It is possible that the effects of creep were more pronounced in Test Series C, since the length of the tests was about twice that of

Test Series A. In order to compare the ultimate column loads, they were made non-dimensional by dividing by $f_c''bt$, giving average values of 0.84 in Test Series A and 1.03 in Test Series C. The higher load capacities in Test Series C were the result of the restraining beams relieving the columns of a portion of the applied end moments.

CHAPTER VI

THEORETICAL ANALYSIS OF LONG COLUMNS

6.1 Theoretical Analysis

(a) Introduction

The purpose of the analysis presented in this chapter was to provide a means of comparing a portion of the test results with calculated values based on a commonly used theory. A full analytical solution of the test columns would have required the use of an electronic computer. This was beyond the scope of the investigation so the computations were limited to some extent.

The analysis consisted of the calculation of theoretical lateral deflections and moments by numerical integration of unit curvatures. The analysis was limited to the range of loads for which convergence was reasonably quick. This limitation was most noticeable when higher loads were considered for the columns with small eccentricity (Test Series A and C). In this load range the column stiffness decreased considerably and a small change in moment produced a large change in deflection. It

was not possible to compute the theoretical ultimate loads in this case. Ultimate loads for the columns with large eccentricity (Test Series B and D) could be estimated fairly closely because of the more linear behavior.

The derivation of the load-moment-curvature relationship for the column cross-section is described in Section 6.1(b). The assumptions made concerning the action of the column and beams are given in Section 6.1(c). The method of computation is described in Section 6.1(d).

(b) Column Load-Moment-Curvature Relationship

(i) General. The first step in the analysis was to obtain the relationship between load, moment and curvature for the column cross-section. This information was required in the form of plots of curvature versus moment for given values of axial load. Typical moment-curvature curves are shown in FIGURE 6 - 1. The assumptions used in computing interaction curves (Section 2.2(b)) were also used for the moment-curvature curves. One additional assumption, concerning strain reversal, was required and is discussed in the following paragraphs. As mentioned previously, the maximum compressive stress, f_c'' , in the columns and beams was assumed equal to 0.85 times the cylinder strengths in these computations.

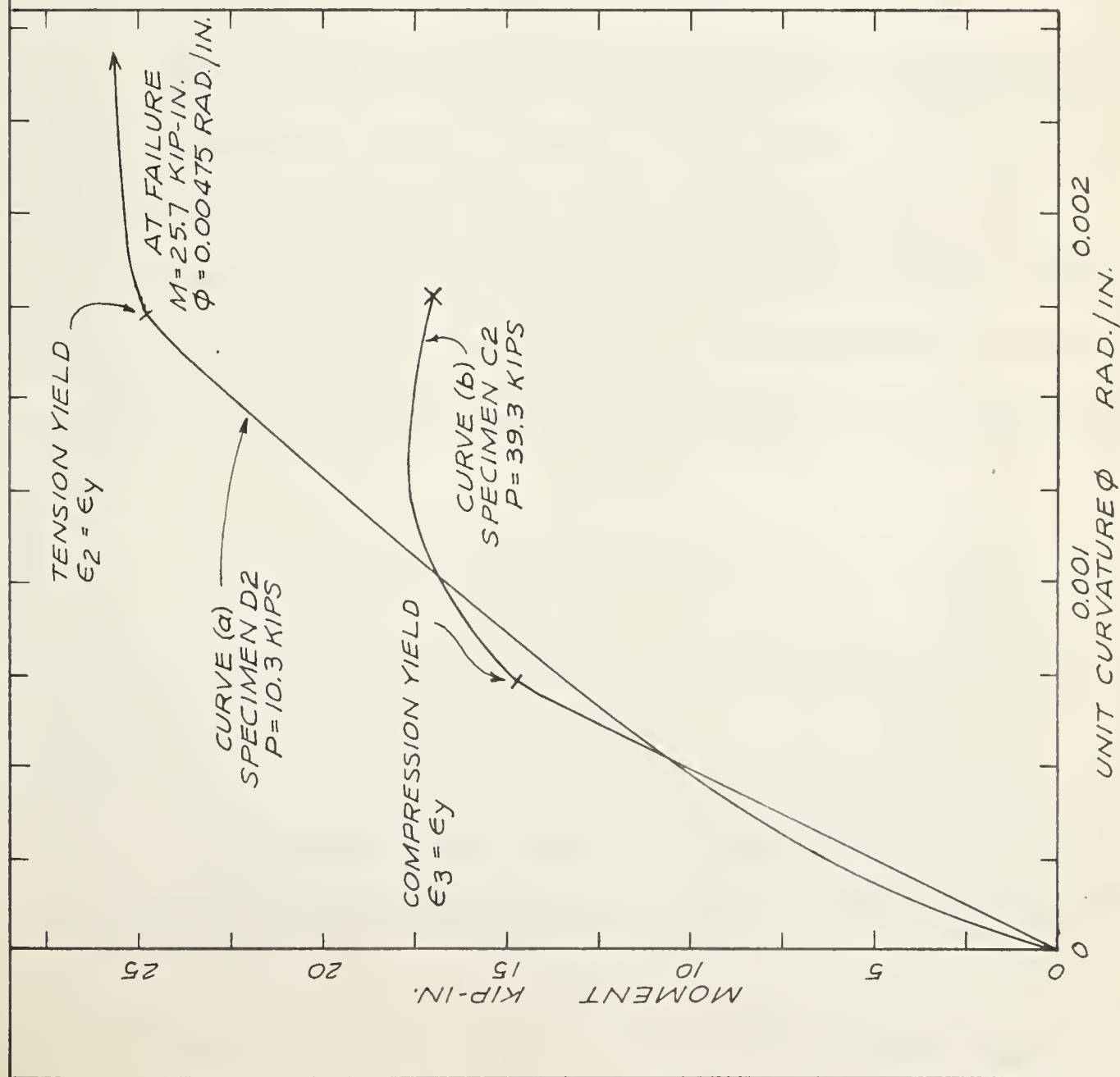


FIGURE 6-1 TYPICAL MOMENT-CURVATURE CURVES

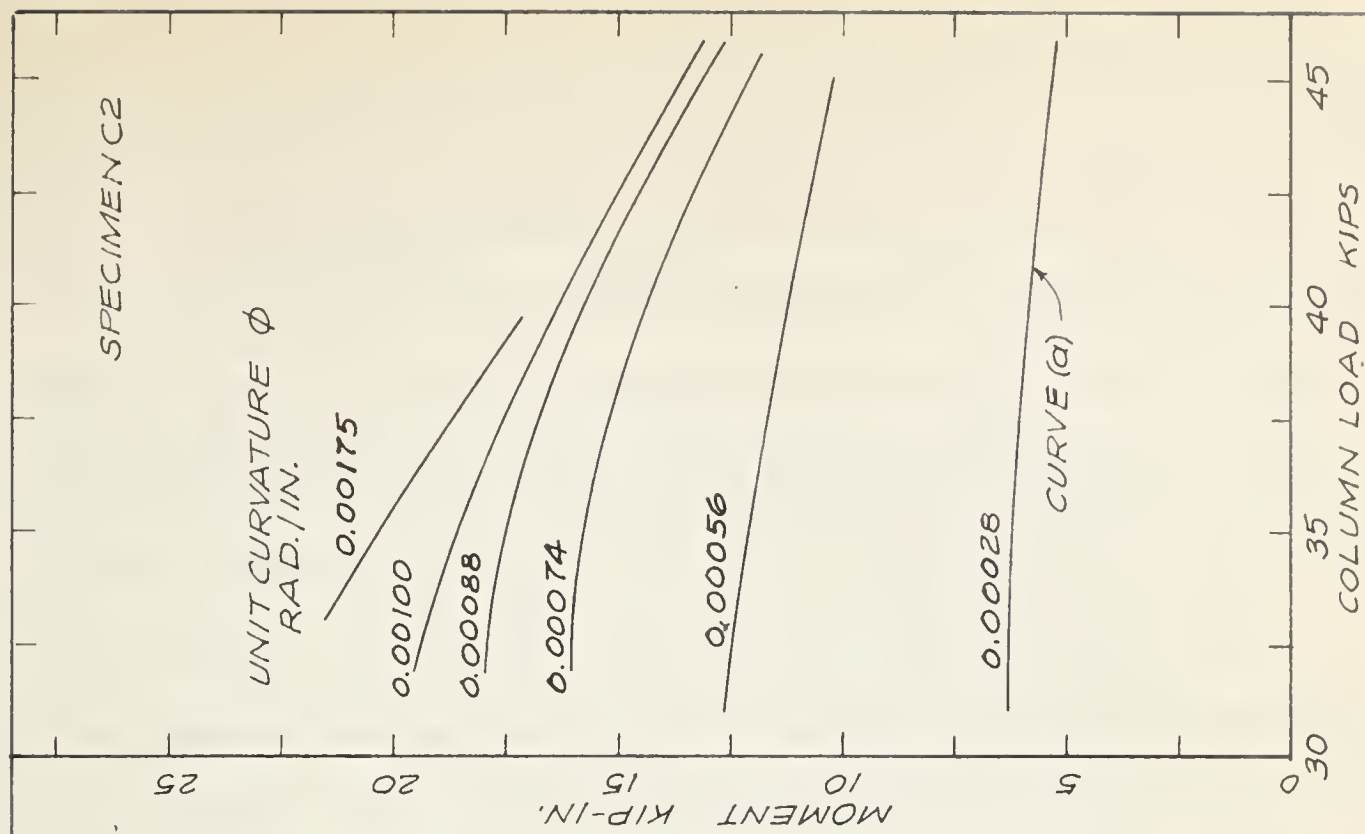


FIGURE 6-2 TYPICAL LOAD -
MOMENT - CURVATURE CURVES

(ii) Strain Reversal. The steel and concrete stress-strain curves described previously (Section 2.2(b)) were obtained from tests in which load was increased continually from zero until failure occurred. The curves do not apply to the case in which load is applied and then wholly or partially released, resulting in unloading of a portion of the cross-section. The use of moment-curvature relationships derived from these curves implies that strain reversal will not be encountered in the analysis, and if the analysis truly represents the behavior of the actual test specimen this limitation is presumed to apply there as well.

Strain reversal would not generally be found in columns loaded in single curvature, except perhaps during buckling. However, with columns bent in double curvature there is a possibility that strain reversal might occur at loads considerably less than ultimate. This is particularly true with small eccentricities, where deflections at some points may change direction as the column takes on an unsymmetrical shape.

In the theoretical analysis presented in this chapter the assumption of no strain reversal was valid for the range of loads considered in the computations for each test series.

A rough analysis of some of the measured load-moment curves indicated that the assumption of no strain reversal was generally valid

for the actual behavior of the test specimens. Since strains were not measured, the analysis was made using computed load-moment-curvature relationships which did not themselves include the effects of strain reversal. Nevertheless, it appeared likely that strain reversal did not take place in Test Series B and D, nor at loads less than about 90 percent of the ultimate load in Test Series A and C.

(iii) Computation Of Moment-Curvature Curves. The method used in obtaining a typical moment-curvature curve was as follows:

- (1) The concrete strength, f'_c , was assumed and f''_c taken as $0.85 f'_c$.
- (2) A value was assumed for $(\epsilon_4 - \epsilon_1)$ and the unit curvature, ϕ , was computed from:

$$\phi = (\epsilon_4 - \epsilon_1)/t \quad (\text{EQ. 6 - 1})$$

- (3) The axial load, P , and moment, M , were computed for the assumed value of $(\epsilon_4 - \epsilon_1)$ and various values of ϵ_4 . P and M were computed in the same manner as for the interaction curves (Section 2.2). These values of P and M were plotted giving one curve similar to Curve (a) in FIGURE 6 - 2.
- (4) The previous step was repeated for various values of $(\epsilon_4 - \epsilon_1)$ and the results were plotted giving a series of curves for constant values of ϕ , as shown in FIGURE 6 - 2.

- (5) The value of axial load, P , for which the deflection calculation was to be made was assumed. For this load the corresponding values of M and ϕ were obtained from the series of curves, as shown in FIGURE 6 - 2.
- (6) These values of M and ϕ were plotted and a smooth curve fitted through the points. This yielded a moment-curvature curve similar to the examples shown in FIGURE 6 - 1.

In the analysis of restrained columns it was necessary to obtain moment-curvature curves for the beam cross-section. These were computed in the same manner as for the columns. In this case the axial load was zero for all the curves.

(c) Additional Assumptions

In addition to the assumptions made in deriving the moment-curvature relationships, assumptions were made in the numerical integration calculations.

(i) Ratio Of End Eccentricities. If a perfectly symmetrical column is loaded with exactly equal and opposite end eccentricities it will have an antisymmetrical shape at all loads up to failure. If a

small deviation is introduced and the antisymmetry is destroyed the behavior of the column will be altered. The deflection profile will tend toward the single curvature shape and the column may fail at a lower load than determined for the ideal case. This behavior may be shown for elastic conditions using equations presented in Timoshenko (1936). Baker, et al (1956) carried out a test of a steel column with $e_1/e_2 = -1$ in which this type of behavior was observed throughout the plastic and elastic load range.

Inspection of the deflection profiles for the test specimens of the present investigation showed that all the columns exhibited a tendency toward the single curvature shape, to some extent. The effect was most pronounced in Test Series A and C. It was apparent that some modification of the nominally antisymmetrical condition was required to obtain agreement between the theoretical and observed behavior.

This problem occurred in the theoretical analysis of columns of this type by Pfrang and Siess (1961). Round-off errors in the computer solution caused the columns to slowly tend toward the single curvature shape instead of remaining antisymmetrical. To take into account the unsymmetrical behavior of real columns the ratio of end eccentricities was later taken as -0.98 rather than the nominal value of -1 . The effect of the difference of two percent in end moments was assumed to

replace the effect of imperfections possible in a real column. The ratio $e_1/e_2 = -0.98$ was chosen arbitrarily and would be expected to vary with the precision of the fabrication and loading conditions.

The approach used by Pfrang and Siess (1961) was also used in the theoretical analysis presented in this chapter. It was not possible to determine a representative value of e_1/e_2 from the test results although several methods were tried. Therefore, it was necessary to assume different values of e_1/e_2 and compare the results of the analysis with the test results. Assumed values ranged from -0.99 to -0.90 . In every case the larger eccentricity, e_2 , was taken at end of the column at which failure actually occurred in the tests. The comparison of this variable with the test results is discussed in Section 6.2.

(ii) The Column Model For Analysis. For the purpose of numerical integration, the column was divided into 13 equal segments of 5.25 inches length. The total length was 68.25 inches which was equal to the distance between load pivot axes. Zero deflection was assumed at the load pivot axes and a line joining these points formed the reference line for all computed deflections. The model column is shown in FIGURE 6 - 3. This arrangement was used for both hinged and restrained columns.

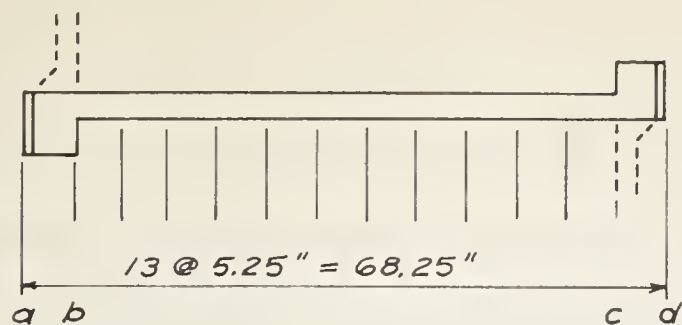


FIGURE 6-3 COLUMN MODEL FOR ANALYSIS

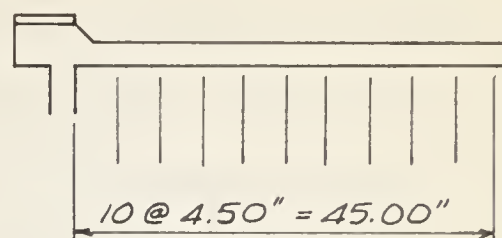


FIGURE 6-4 BEAM MODEL FOR ANALYSIS

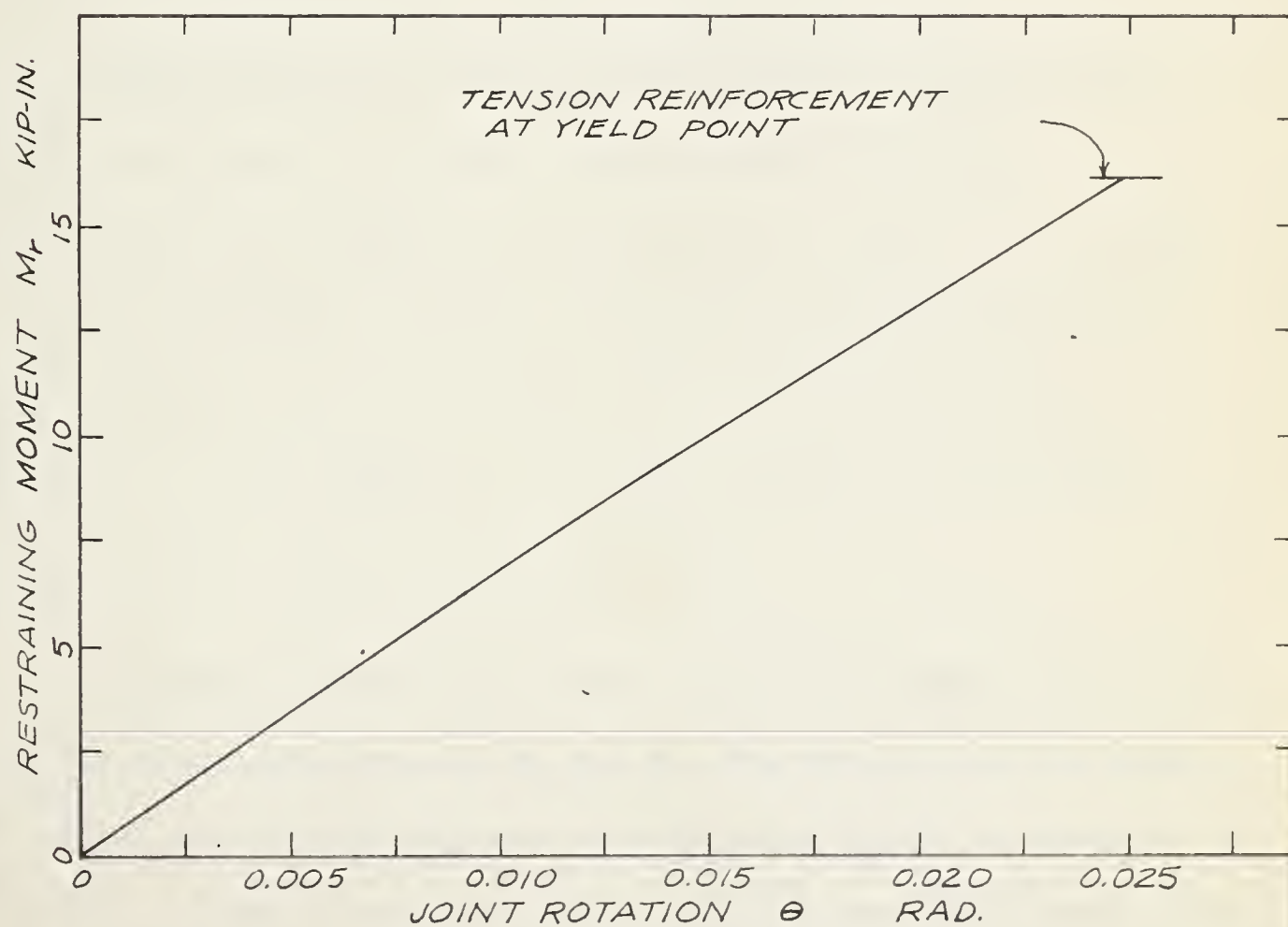


FIGURE 6-5 RESTRAINING MOMENT - JOINT ROTATION CURVE

The first segment at each end extended exactly to the section at which the column was thickened to form the end block. The gross moment of inertia of the end block cross-section was about 14 times that of the column cross-section so the end segments were assumed to have infinite stiffness.

(iii) The Beam Model For Analysis. The beam-column joints of the restrained columns were assumed rigid so that moment applied to the end blocks was resisted by both the column and the beam. The moment taken by the beam was termed "restraining moment" and denoted by the symbol M_r .

The restraining moment was assumed to be a function of the rotation of the beam-column joint. The rotation, Θ , was taken as the average slope of end segments of the column (a - b and c - d in FIGURE 6 - 3). It was therefore possible to take into account the effect of the beam by using a restraining moment-joint rotation curve as given in FIGURE 6 - 5. The magnitude of the beam reaction was obtained by dividing M_r by the moment arm, 46.25 inches.

Numerical integration of a unit curvature diagram was used to obtain the relationship between M_r and Θ . For this purpose the beam was divided into 10 equal segments of 4.50 inches length, as shown in FIGURE 6 - 4. The moment-curvature curve for the beam cross-section

was obtained in the same manner as for the column. Since the relationship varied little with concrete strength, an average value of $f_c'' = 3500$ psi was used throughout, giving one $M_r - \Theta$ curve for all the specimens. Conventional numerical integration procedure was used, with equivalent concentrated angle changes computed using Simpson's Rule. A value of Θ was determined for various values of M_r and the results plotted as shown in FIGURE 6 - 5. This curve was used in all the restrained column computations.

(d) Lateral Deflection Calculations

(i) Hinged Columns. Each deflection computation was carried out for a given specimen, load, and value of e_1/e_2 . A moment-curvature curve was plotted for the given load as described previously.

Deflections were computed by means of numerical integration of unit curvatures taking into account the resulting P_y -moments. The maximum thrust line eccentricity was taken at Point (a) in FIGURE 6 - 3 and was equal to the nominal end eccentricity of the test specimen being considered. The thrust line eccentricity at Point (d) was taken as that at Point (a) multiplied by the assumed value of e_1/e_2 . Moments at each node point were determined as described in Appendix C, and corresponding values of unit curvature were read from the moment-curvature curve. Equivalent concentrated angle changes were computed using Simpson's Rule.

The procedure was one of trial and error and was continued until trial and final deflections agreed within ± 0.004 inches. Normally four to six cycles were required.

(ii) Restrained Columns. By representing the effect of the restraining beams with a restraining moment-joint rotation curve, the restrained columns could be treated as if hinged. The lateral deflection computations were the same as for the hinged columns with the exception of the calculation of thrust line eccentricities. The calculation of thrust line eccentricities is described in Appendix C (Section C.3). The assumed ratio of end eccentricities, e_1/e_2 , was taken into account by suitably modifying the equations for the lower joint as shown in the Appendix.

The trial and error procedure was continued until trial and final deflections agreed within ± 0.004 inches and beam reactions agreed within ± 2 pounds. From five to nine cycles were generally required.

(e) Presentation Of Results

The results of the analysis described in this section are plotted on a number of the graphs of the test results in Chapters IV and V. The theoretical values are plotted as thin dashed lines, with the assumed

value of e_1/e_2 indicated. Two types of lines were used to indicate different values of e_1/e_2 .

The graph titles and numbers given below refer to the types described in Section 3.5.

(3) Load-Deflection Graph. Theoretical deflections for Column Stations 2 and 5 were actually computed at node points of the numerical integration which were $3/4$ inch nearer mid-height than the exact location of the stations. The effect of this difference appeared to be small compared to the precision of the test results.

The theoretical deflections for Beam Stations U2 and L2 were computed at the true location of these stations.

(4) Load-Moment Diagram. Theoretical moments are shown for Stations T, 1, 2, 5, 6 and B. The moments at Stations 2 and 5 were computed at the points described in (3) above.

(6) Moment Distribution Diagram. The theoretical distribution of moment was plotted in the same manner as for the test results.

6.2 Comparison of Test Results with Theoretical Analysis

(a) Restraining Beams

Rotations of the beam-column joints were not measured so it was not possible to make a direct comparison with the theoretical $M_r - \theta$ curve of FIGURE 6 - 5. However, a good indication of the agreement may be obtained from the data plotted in FIGURE 6 - 6. In this graph the measured deflections at Stations U2 and L2 have been plotted against the measured moment at the face of the column. Data from all the restrained column tests was plotted. Stations U2 and L2 were chosen because the maximum deflections generally occurred at these stations.

For comparison, the theoretical deflection at Station U2 and L2 has also been shown. These deflections were based on the same analysis used in establishing the $M_r - \theta$ curve of FIGURE 6 - 5. The moment at which the tension reinforcement would theoretically reach the yield point has been indicated and the deflection curve is valid only where the maximum amount is less than this value.

In general good agreement was found between the measured and theoretical deflections. For moments less than 7 kip-in. the theoretical curve was close to the mean of the measured points. At larger moments

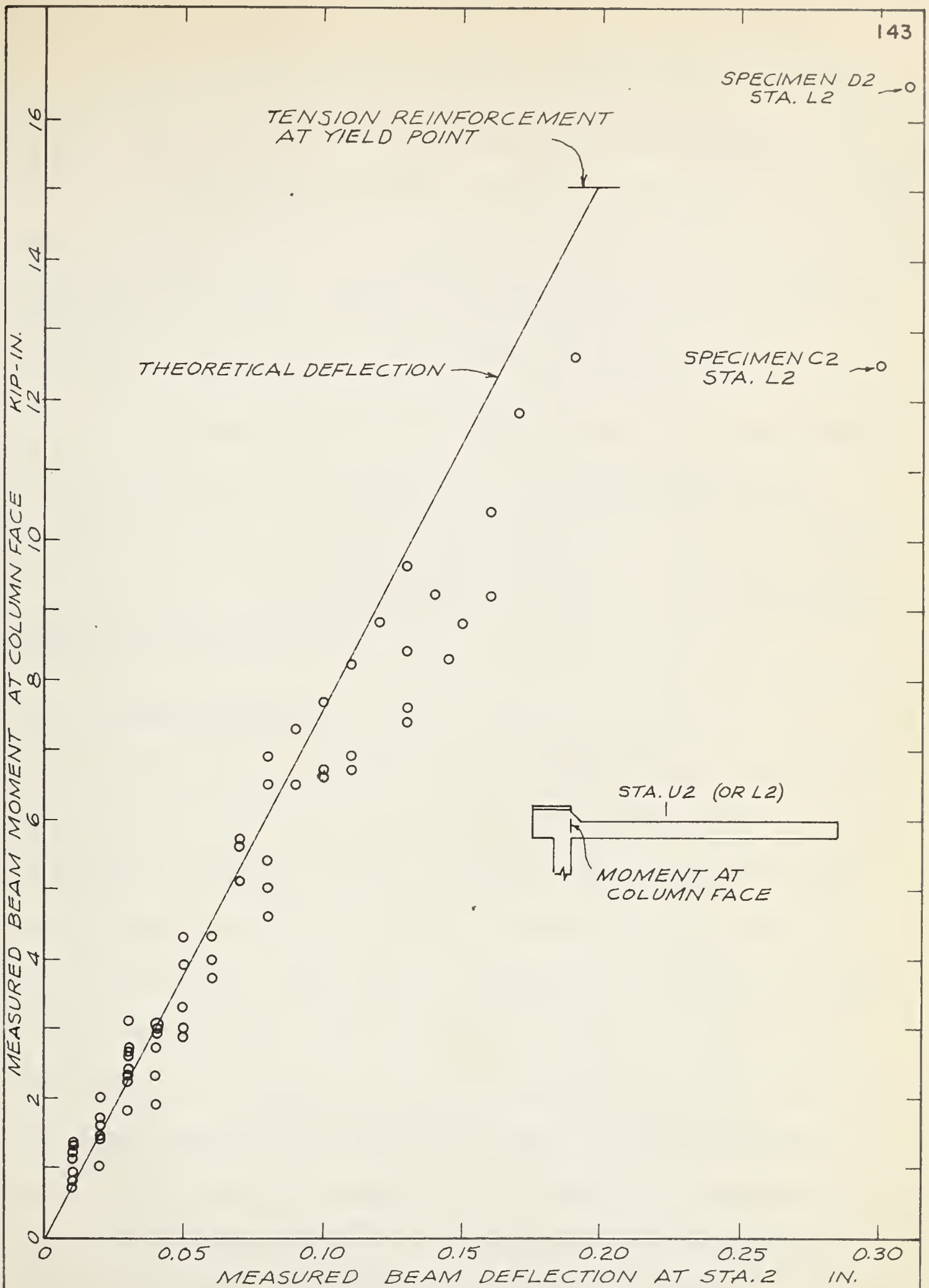


FIGURE 6 - 6 BEAM MOMENT - DEFLECTION DATA

the test results showed deflection somewhat larger than predicted, and there was considerably more scatter of results. The excessive deflections were believed to result from the effects of creep since they were more pronounced at the higher moments. The same trend was found in similar graphs for Beam Stations 1, 3 and 4, which were not included here.

The range of values of M_r found in the theoretical column analysis did not exceed 9 kip-in. In FIGURE 6 - 6 reasonable agreement was found over this range. It was concluded that the $M_r - \Theta$ curve in FIGURE 6 - 5 gave a good representation of the behavior of the actual restraining beams of the test specimens.

(b) Test Series B

The columns of Test Series B were hinged and had large end eccentricities ($e/t = 1.5$). The results of the theoretical analysis are plotted in FIGURES 4 - 4 to 4 - 7. In order to introduce a small imperfection simulating practical conditions the theoretical computations were based on the ratio $e_1/e_2 = -0.99$. This value corresponded to a difference in end eccentricities of 0.04 inches. The exact value of this ratio appeared to have little effect on the results of the computations because the deflections were small compared to the end eccentricities. Both the measured and theoretical deflected configurations were nearly antisymmetrical over the load range considered. It was not possible to determine within the precision of the test results, whether a slightly

different assumed value of e_1/e_2 would give better agreement.

The measured deflections were considerably larger than the theoretical deflections, as shown in FIGURES 4 - 4 and 4 - 5. However, since the deflections contributed little to the total eccentricity at each station there was good agreement between the measured and theoretical load-moment curves in FIGURES 4 - 6 and 4 - 7.

Although theoretical ultimate loads were not computed, a good approximation could be obtained by projecting the theoretical load-moment curve for Station B to intersect the interaction curve. Since the measured and theoretical load-moment curves were in good agreement, the measured and theoretical ultimate loads would also agree well.

(c) Test Series D

The columns of Test Series D were restrained and had large end eccentricities ($e/t = 1.5$). The results of the theoretical analysis are plotted in FIGURES 4 - 11 to 4 - 18. In order to introduce a small imperfection simulating practical conditions the theoretical computations were based on $e_1/e_2 = -0.99$. As in Test Series B, the exact value of the ratio appeared to have little effect on the results of the computations.

Close agreement was found between measured and theoretical column deflections at all loads, as shown in FIGURES 4 - 11 and 4 - 12.

The agreement was much better than in Test Series B. There was no apparent reason for this, since the actual end moments applied to the columns were in good agreement with those of the theoretical analysis for both series.

Curve (a) in FIGURE 6 - 1 is a typical moment-curvature curve for the range of loads found in the computations for Test Series D. The point on the curve marked "Tension Yield" indicates the moment at which the unit strain in the tension reinforcement becomes equal to the yield strain ($\epsilon_2 = \epsilon_y$ in FIGURE 2 - 7). The curves marked "Tension Yield" in FIGURES 4 - 17 and 4 - 18 give combinations of load and moment which produce this condition. When the Tension Yield curve is reached at a column section, the theoretical behavior at the section will be similar to that found in a steel member at the formation of a plastic hinge, as indicated by the shape of Curve (a) in FIGURE 6 - 1.

Up to about 90 percent of ultimate column load the measured and theoretical values of the ratio of column moment to applied moment, M_C/M_A , agreed closely, as shown in FIGURES 4 - 15 and 4 - 16. Apparently the actual rotations of the beam-column joints were close to the predicted values, which resulted in good agreement between measured and computed restraining moments. It appeared that the decrease in the ratio M_C/M_A at Point LO, found in the tests, would not have occurred

in the theoretical analysis until the tension reinforcement yielded at Station B, at the load indicated by the Tension Yield curve.

There was good agreement between measured and theoretical load-moment curves (FIGURES 4 - 17 and 4 - 18) except for slight differences at loads above 90 percent of ultimate as mentioned above.

Because of the difficulties introduced by a portion of the column reaching the "yield point" it was not possible to compute theoretical ultimate loads. However, it was indicated that theoretical ultimate loads would be somewhat greater than given by the intersection of the load-moment curve for Station B and the Tension Yield curve (FIGURES 4 - 17 and 4 - 18). Beyond this load the lower beam would carry most of the additional moment and failure would occur only after there was sufficient deformation at Station B to cause crushing of the concrete. The trend of the theoretical load-moment curves for Station B indicated the theoretical ultimate loads would have been somewhat larger than the measured values.

(d) Test Series A

The columns of Test Series A were hinged and had small end eccentricities ($e/t = 0.2$). The results of the theoretical analysis are plotted in FIGURES 5 - 4 to 5 - 7. In order to introduce a small

imperfection simulating practical conditions the theoretical computations were based on values of $e_1/e_2 = -0.98$ and -0.90 . These values corresponded to a difference in end eccentricities of 0.01 inches and 0.05 inches, respectively. The computations based on the ratio -0.90 agreed more closely with the test results, particularly with regard to unsymmetrical behavior. However, even the fictitious 10 percent difference in end eccentricities was not sufficient to reproduce the large increase in deflections found in the upper portion of the test columns as the ultimate load was approached. It did not appear possible to obtain closer agreement between measured and theoretical deflections merely by assuming a value of e_1/e_2 different from unity.

Up to about 75 percent of ultimate load there was reasonable agreement between measured and theoretical deflections, as shown in FIGURES 5 - 4 and 5 - 5. The value of e_1/e_2 had little effect in this range. At higher loads agreement was poor. Since deflections due to creep were significant in the test results, and the theoretical analysis did not include time effects, agreement was not expected in this range.

As a result of the differences between measured and computed deflections, at loads greater than 75 percent of the ultimate column load the measured moments were much larger than theoretical values (FIGURES 5 - 6 and 5 - 7). The computed P_y -moments were not large

enough to shift the point of maximum moment away from the column end, Station T, as was the case in the tests.

Although the theoretical ultimate loads were not computed, the trend of the computed load-moment curves for Station T indicated they would be little different from the measured ultimate loads, as seen in FIGURES 5 - 6 and 5 - 7. It appeared, however, that the theoretical failure section would be much closer to the end of the column, and the P_y -moments at failure would be much smaller than in the tests. Since the observed and theoretical behavior were very different, the apparent agreement between measured and computed ultimate loads was believed to be largely coincidental.

(e) Test Series C

The columns of Test Series C were restrained and had small end eccentricities ($e/t = 0.2$). The results of the theoretical analysis are plotted in FIGURES 5 - 11 to 5 - 18. In order to introduce a small imperfection simulating practical conditions the theoretical computations were based on values of $e_1/e_2 = -0.98$ and -0.90 . The computations based on the ratio -0.90 agreed more closely with the test results, but in neither case was close agreement found. As in Test Series A, it did not appear possible to obtain closer agreement merely by varying the assumed value of e_1/e_2 .

The measured deflected configuration was considerably more unsymmetrical than predicted by the computations, as shown in FIGURES 5 - 11 and 5 - 12. It was apparent that some modification of the assumed load-moment-curvature relationship to include time effects was required to obtain closer agreement.

Because of the differences between measured and theoretical deflections, the measured and computed ratios of column moment to applied moment, M_C/M_A , do not show agreement (FIGURES 5 - 15 and 5 - 16). The differences are most noticeable at higher loads, where the measured restraining moments at the lower beam-column joint were much greater than predicted.

The measured and theoretical load-moment curves do not agree, particularly at Stations B and 6, as seen in FIGURES 5 - 17 and 5 - 18. The computed P_y -moments were not large enough to shift the point of maximum moment away from the column end, Station B, as was the case in the tests.

Although the theoretical ultimate loads were not computed, the trend of the computed load-moment curves for Station B indicated they would be little different from the measured ultimate loads (FIGURES 5 - 17 and 5 - 18). It appeared, however, that the theoretical failure section would be much closer to the end of the column, and the P_y -moments

and restraining moments at failure would be much smaller, than in the tests. Since the observed and theoretical behavior were very different, the apparent agreement between measured and computed ultimate loads was believed to be largely coincidental, as was the case in Test Series A.

CHAPTER VII

DISCUSSION

7.1 Effect Of Slenderness On Column Strength

(a) Introduction

The slenderness of a column may have considerable effect on the ultimate load capacity. Two terms used in analyzing this effect are " P_{Long} " and " P_{Short} ", which may be defined as follows:

" P_{Long} ", or long column strength, refers to the load capacity of the actual column under consideration, including the effect of P_y -moments and any restraints present.

" P_{Short} ", or short column strength, refers to the load capacity of the column under consideration, if it were reduced to a very small length, thereby eliminating

P_y -moments. Since the short column has infinite relative stiffness the effect of restraints, if present, are neglected.

Theoretical short column strength may be determined directly from the interaction curve using the maximum initial eccentricity.

A convenient method of studying the effect of slenderness on the ultimate load capacity of columns is by means of the ratio P_{Long}/P_{Short} . If P_{Long}/P_{Short} is less than unity it indicates that the slenderness of the column has an adverse effect on the load capacity. Values of P_{Long}/P_{Short} greater than unity are possible for restrained columns since the beneficial effects of end restraints are neglected in computing P_{Short} .

The effect of the slenderness of the test columns on the ultimate load capacity was investigated using this approach. Values of P_{Long}/P_{Short} based on the test results are presented in TABLE 7 - 1, and discussed in Section 7.1(b). Theoretical values of P_{Long}/P_{Short} computed by Pfrang and Siess (1961) are also presented in TABLE 7 - 1, and are compared with the test results in Section 7.1(c). The analysis used by Pfrang and Siess has been described in Section 1.2.

The end blocks (FIGURE 3 - 2(c)) formed the ends of the columns, and were therefore located at the points of maximum initial eccentricity. This made it necessary to make certain assumptions regarding the values of h/t and e/t to be used in evaluating the ratio P_{Long}/P_{Short} , from both the test results (Section 7.1(b)) and the theoretical analysis by Pfrang and Siess (Section 7.1(c)).

TABLE 7 - 1

EFFECT OF COLUMN SLENDERNESS

$h/t = 27.3$

--

$h/r = 91$

Test Specimen	e/t	T e s t R e s u l t s			Pfrang & Siess $\frac{P_{Long}}{P_{Short}}$
		Measured P_{Long} kips	Computed P_{Short} kips	$\frac{P_{Long}}{P_{Short}}$	
A1	0.20	37.95	38.6	0.98	1.00
A2	0.20	38.00	38.0	1.00	1.00
B1	1.27	7.45	(7.45)	1.00	1.00
B2	1.27	7.06	(7.06)	1.00	1.00
C1	0.20	38.01	32.1	1.18	1.12
C2	0.20	39.69	37.1	1.07	1.12
D1	1.27	9.33	7.4	1.26	1.28
D2	1.27	10.36	7.5	1.38	1.28

It was assumed that the ratio $h/t = 27.3$ ($h/r = 91$) was applicable to both the hinged and restrained columns. This value corresponds to an unsupported length equal to the distance between load pivot axes. This assumption appears reasonable for the hinged columns, since the end blocks should have had little or no effect on the effective column length.

For the restrained columns it might be considered that the effective column length should be taken as the distance between the centers of the beam-column joints. However, the restraining beams were free to slide at the beam supports, and provided no lateral support for the column. Therefore it appeared reasonable to take the effective length as the distance between the load pivots where the lateral support was provided.

Values of e/t for each test series are given in TABLE 7 - 1. These eccentricity ratios were used in computing P_{Short} and in entering the charts of $P_{\text{Long}}/P_{\text{Short}}$ given by Pfrang and Siess. No allowance was made for the effect of restraints, in accordance with the definition of P_{Short} given previously.

The value of $e/t = 1.27$ given for Test Series B and D corresponds to the initial eccentricity at Station B and is indicated in FIGURES 4 - 6, 4 - 7, 4 - 17 and 4 - 18. This value was used, instead of the nominal end eccentricity ratio ($e/t = 1.5$), to compensate for the effect of the end blocks. The end blocks prevented failure from taking place at the larger eccentricities found above Station T and below Station B. It is possible to combine the e/t ratio determined at Station T (or B) with the h/t ratio based on lateral supports located at the load pivots because the effect of P_y -moments on the measured ultimate loads was

small. It should be noted that the actual eccentricities at Station B at ultimate load were from one to two percent greater than the initial eccentricity as a result of the small deflections which occurred in the tests. Since this additional eccentricity was small it was neglected in these calculations.

The value of $e/t = 0.2$ given for Test Series A and C in TABLE 7 - 1 corresponds to the nominal end eccentricity at the load pivots and is indicated in FIGURES 5 - 6, 5 - 7, 5 - 17 and 5 - 18. Since the failure sections were located away from the column ends in all the tests, the end blocks did not affect the measured ultimate loads. Therefore, it was not necessary to modify the nominal end eccentricity.

At the ultimate load the restrained columns were actually subjected to end eccentricities as much as four percent greater than the values given above, due to the interaction of the beam reactions. This interaction is shown in the equations given in Appendix C for the column moment, M_C . Since this additional eccentricity was small, and was not constant throughout the tests, it was neglected in these calculations.

(b) Discussion Of Test Results

The evaluation of the ratio P_{Long}/P_{Short} for each test specimen is given in TABLE 7 - 1. P_{Long} was taken as the measured ultimate

column load. P_{Short} was computed using the interaction curves plotted in the Load-Moment Diagrams, and the tabulated eccentricities. The interaction curves based on $k_3 = 0.85$ were used.

(i) Test Series B. The Deflection Profile Diagrams (FIGURES 4 - 2 and 4 - 3) show that there were small lateral deflections, and hence P_y -moments, at the failure section (Station B). However, if the specimens were idealized, with end blocks of negligible length, there would have been no deflection at the failure section. Therefore, the small P_y -moments were attributed to the construction details and not to the basic action of the columns. For this reason the value of $P_{\text{Long}}/P_{\text{Short}}$ was shown as 1.00 in TABLE 7 - 1 for both tests. It was concluded that for the basic column action of Test Series B there was no long column strength reduction.

(ii) Test Series D. In both tests of this series $P_{\text{Long}}/P_{\text{Short}}$ was greater than unity indicating there was no adverse long column effect. As in Test Series B, the small P_y -moments at the failure sections, shown in the Deflection Profile Diagrams (Station B, FIGURES 4 - 9 and 4 - 10), were attributed to the construction details and not to the basic column action.

The combined effect of slenderness and restraints resulted in values of P_{Long} that were 26 and 38 percent greater than P_{Short} for

Specimen D1 and D2, respectively. The flexibility of the columns allowed the restraining beams to take a portion of the applied moment, thereby decreasing the effective column eccentricity and increasing the ultimate loads. The tabulated values of P_{Long}/P_{Short} would have been somewhat larger if the test columns had developed the full strength given by the interaction curves, as discussed in Section 4.3(c).

(iii) Test Series A. In the test of Specimen A1 the value of P_{Long}/P_{Short} was less than unity indicating there was an adverse long column effect. For Specimen A2 the value of P_{Long}/P_{Short} was equal to unity. The Deflection Profile Diagrams (FIGURES 5 - 2 and 5 - 3) showed there were large deflections at the failure section in both tests. Unsymmetrical behavior and the effects of creep added to the deflections and resulting Py-moments.

The effect of slenderness resulted in values of P_{Long} two percent less than P_{Short} for Specimen A1, and equal to P_{Short} for Specimen A2. Although the Py-moments at both failure sections, at ultimate load, were considerably larger than the moments due to the initial eccentricity, there was only an average of one percent reduction in load capacity. This illustrates the inherent strength of the double curvature loading condition.

(iv) Test Series C. In both tests of this series the value of P_{Long}/P_{Short} was greater than unity indicating there was no adverse long column effect. The Deflection Profile Diagrams (FIGURES 5 - 9 and 5 - 10) showed there were large deflections at the failure section in both tests. Unsymmetrical behavior added to the deflections and resulting P_y -moments.

The combined effect of slenderness and restraints resulted in values of P_{Long} 18 percent and 7 percent greater than P_{Short} for Specimen C1 and C2, respectively. The flexibility of the columns, particularly near the failure zone at high loads, allowed the restraining beams to take a large proportion of the applied moment. This decreased the effective column eccentricities sufficiently to raise the load capacity in spite of the large P_y -moments.

(c) Analysis By Pfrang and Siess (1961)

Data given in Pfrang and Siess (1961) was used to provide a comparison between measured and theoretical values of P_{Long}/P_{Short} . From the results of their analytical investigation, Pfrang and Siess obtained curves of P_{Long}/P_{Short} for various slenderness ratios, end eccentricities and restraint coefficients. Values are given in TABLE 7 - 1 for comparison with the test results.

The analysis used by Pfrang and Siess was mentioned briefly in Section 1.2. There were some differences between the cross-sectional properties of the analytical columns and those of the test specimens. However, there were enough similarities that the comparison is believed valid. The main assumptions used in the analysis are compared with the properties of the test specimens in the following tabulation:

<u>ITEM</u>	<u>PFRANG AND SIESS</u>	<u>TEST SPECIMENS</u>
f'_c	3000 psi	3630 to 4880 psi
f_y	45000 psi	46400 psi
steel ratio	0.04	0.04
d/t	0.90	0.82
e_1/e_2	-0.98	-1
restraints	elastic	apparently nearly elastic, see FIGURE 6 - 6.

In addition to the above items, further assumptions were used in evaluating P_{Short} for the test specimens. These are compared with the assumption made by Pfrang and Siess in the following tabulation:

ITEM	PFRANG and SIESS	TESTS
f_c''	$0.85 f_c'$	$0.85 f_c'$
concrete stress block	Hognestad	Hognestad
ϵ_o	0.0020	varies
ϵ_u	0.0040	0.0038
concrete tension	neglected	neglected

As mentioned previously h/t was taken as equal to 27.3 for all the test specimens. The values of e/t given in TABLE 7 - 1 were used.

The degree of end restraint was given by Pfrang and Siess in terms of the restraint coefficient $\alpha / f_c'' bt^2$. For the test specimens this coefficient varied from 6.4 to 8.0. The average value of 7.0 was used in interpolating between charts for $\alpha / f_c'' bt^2 = 0$ and 10. The average slope of the theoretical $M_R - \theta$ curve of FIGURE 6 - 5 was used to determine the value of α for the test specimens.

As shown in TABLE 7 - 1 remarkably good agreement was found between the test results and the analysis by Pfrang and Siess for the columns with large eccentricity, Test Series B and D. For hinged columns with e/t as large as in Test Series B the analysis indicated that there would be a long column strength reduction only for much more slender columns. For Test Series D, the average value of P_{Long}/P_{Short} from the test results was 1.32, which was close to the value of 1.28

predicted by the analysis and indicated good agreement between actual and assumed relative stiffnesses. The major difference between the test and analytical columns was the concrete strength. Since variations in concrete strength have relatively little effect on stiffness at low stresses good agreement was expected.

As shown in TABLE 7 - 1 relatively good agreement was found between the test results and the analysis by Pfrang and Siess for the columns with small eccentricity, Test Series A and C. The values of P_{Long}/P_{Short} from the test results ranged from 5 percent smaller to 6 percent larger than computed by Pfrang and Siess.

It was mentioned in Chapter VI that the apparent agreement between measured and computed ultimate loads in Test Series A and C was largely coincidental since there was a considerable difference between the observed and theoretical behavior (6.2(d) and 6.2(e)). The analysis used by Pfrang and Siess was very similar to that presented in Chapter VI, and it is believed the good agreement between measured and computed values of P_{Long}/P_{Short} in TABLE 7 - 1 is also largely coincidental.

7.2 American Concrete Institute Building Code (ACI 318-63)

(a) Moment-Distribution Analysis

For restrained columns, the short column strength referred to in the American Concrete Institute Building Code (ACI 318-63) is not the same as that defined as P_{Short} in Section 7.1(a). The Code specifies that the short column strength is to be determined using a reduced eccentricity obtained from a moment-distribution analysis.

A moment-distribution analysis was carried out for the restrained columns of Test Series C and D. The recommendations given in the Code were followed, where applicable. Relative stiffnesses were based on the moment of inertia of the uncracked sections, with the reinforcement neglected. The column length was taken as 60.00 inches which was equal to the distance between the centers of the upper and lower beam-column joints. The beam length was taken as 46.25 inches and the far end was assumed hinged. The effects of axial load were neglected. Column end moments were applied in the same manner as in the tests. The results of the moment-distribution computation indicated that at each beam-column joint the column would take 68 percent of the applied moment and the beam would take 32 percent. Since the relative stiffnesses, as computed above, were the same for all the restrained columns, the computations apply equally to Test Series C and D.

The results of the moment-distribution analysis were compared with the measured distributions of moment in the tests, which were plotted in FIGURES 4 - 15, 4 - 16, 5 - 15 and 5 - 16. In these figures the thin solid lines marked "M" correspond to a ratio of column moment to applied moment, M_C/M_A equal to 0.68. At any load level the difference in moment between Line M and the M_A -curve is equal to the computed column moment. As explained previously the difference in moment between the M_R -curve and the M_A -curve is equal to the measured column moment, M_C .

Reasonably good agreement was found between measured and computed column moments in both tests of Series D, as shown in FIGURES 4 - 15 and 4 - 16. Up to about 90 percent of ultimate column load the measured column moment was about 10 percent greater than given by the moment-distribution analysis. This indicated the columns were slightly stiffer in relation to the beams than assumed in the analysis.

At the ultimate column load there was better agreement between the test results and the computations, at the lower end of the columns, where the failure sections were located. At this load level the measured column moments were about four percent larger than the computed moments. It appears that the effective column eccentricities given by the moment-distribution analysis would be sufficiently accurate for use in the design of the columns of Test Series D.

In Test Series C, the measured distributions of moment involved both the action of the restraints and the effect of P_y -moments. However, up to about 60 percent of ultimate load the effect of P_y -moments was relatively small and a comparison of measured and computed column moments was possible. Over this load range reasonably good agreement was found between measured and computed column moments in both tests, as shown in FIGURES 5 - 15 and 5 - 16. At the upper beam-column joints the measured column moments were about 20 percent greater than the computed values, while at the lower joint they agreed within plus or minus 5 percent. In the tests the conditions at the lower joint had the greatest effect on the ultimate load capacity since the failure sections were located in the lower portion of the columns. From this comparison it appeared that the moment distribution analysis would give a reasonable estimate of the initial distribution of applied moment for the columns of Test Series C.

(b) Long Column Strength Reduction

The provisions governing long column strength reductions in the American Concrete Institute Building Code (ACI 318-63) are found in ACI Section 916. The Code specifies that applied loads and moments are to be divided by a reduction factor, R , and the required section selected on the basis of short column strength.

It was mentioned in Section 7.2(a) that the short column strength referred to in the Code is not the same as that defined as P_{Short} in Section 7.1(a).

In order to distinguish between the two types of short column strengths, the one based on the reduced eccentricity after moment-distribution, as defined in ACI 318-63, is designated P'_{Short} . For restrained columns P'_{Short} will be greater than, or equal to P_{Short} . For hinged columns P'_{Short} is identical to P_{Short} .

The reduction factor R may be considered as a factor by which the short column strength must be multiplied to give the long column strength. Used in this manner R is the allowable value of $P_{\text{Long}}/P'_{\text{Short}}$. The values of R given in the Code are applicable to both working stress and ultimate strength design. In this discussion only ultimate strength design has been considered.

All the test specimens fall into classification given for ACI Equation 9 - 2 in the Code, since lateral displacement of the ends was prevented and there was a point of contraflexure between the ends under the initial loading conditions. This equation is given in the Code as:

$$R = (1.32 - 0.006h/r) \leq 1.0 \quad (\text{ACI EQ. 9 - 2})$$

As explained previously h/r was taken as 91 for all the test specimens.

For Test Series A and C the design ultimate loads were greater than the balanced load, so the value of R was taken directly from ACI Equation 9 - 2. For Test Series B and D the design ultimate load was less than the balanced load, so the value of R was modified in accordance with ACI Section 916(b), which allows the designer to increase R as the pure bending condition is approached. The resulting values of R are given in TABLE 7 - 2.

TABLE 7 - 2						
ULTIMATE STRENGTH DESIGN						
Test Specimen	e/t	Test Results		ACI 318 - 63		$\frac{P_{Long}}{P_{Design}}$
		$\frac{P_{Long}}{P_{Short}}$	P_{Long} kips	Factor R	P_{Long} kips	
A1	0.20	0.98	37.95	0.77	28.7	1.32
A2	0.20	1.00	38.00	0.77	28.0	1.36
B1	1.27	1.00	7.45	0.92	5.9	1.26
B2	1.27	1.00	7.06	0.93	6.0	1.18
C1	0.14	1.03	38.01	0.77	27.7	1.37
C2	0.14	0.93	39.69	0.77	31.7	1.25
D1	0.86	0.77	9.33	0.87	9.2	1.01
D2	0.86	0.84	10.36	0.88	9.6	1.08

The measured values of $P_{Long}/P_{Short}^{\dagger}$ given in TABLE 7 - 2 were obtained from the test results and interaction curves in the same manner as the ratios P_{Long}/P_{Short} described in Section 7.1(a). The eccentricity ratios, e/t , used on computing P_{Short}^{\dagger} are given in TABLE 7 - 2. For the hinged columns these values of e/t were the same as those discussed in Section 7.1(a) and used in determining P_{Long}/P_{Short} . For the restrained columns the eccentricity ratios in TABLE 7 - 2 are equal to those discussed in Section 7.1(a), multiplied by 0.68 in accordance with the moment-distribution analysis. The discussion of the accuracy of the assumed eccentricities in Section 7.1(a) also applies to the eccentricity ratios in TABLE 7 - 2.

The columns of Test Series A and C were similar except that the former were hinged while the latter were restrained. In each test the measured value of $P_{Long}/P_{Short}^{\dagger}$ was larger than the value of R specified by the Code. The Code values were based on a long-time load analysis which assumed that concrete strains doubled while stresses remained constant (Broms and Viest, 1958-(3)). It would be expected that long column strength reductions given by this analysis would be greater than indicated by the short-time tests of this investigation.

Since the Code expression for R does not take end restraints into account, the same value of R was given for both Test Series A and C. In Test Series A, the average measured value of P_{Long}/P'_{Short} was 29 percent greater than R , while in Test Series C the average was 27 percent greater. The similarity indicates that for these particular columns the effect of the restraints was adequately taken into account by simply reducing the design eccentricity in accordance with the moment-distribution analysis.

The columns of Test Series B and D were similar, except that the former were hinged while the latter were restrained. In both tests of Series B, the measured value of P_{Long}/P'_{Short} was greater than the value of R given by the Code. The provisions of the Code required long column strength reductions of 8 percent and 7 percent for Specimens B1 and B2, respectively, while the test results indicated that no long column strength reduction was necessary.

In both tests of the restrained columns of Series D, the measured value of P_{Long}/P'_{Short} was smaller than the values of R specified by the Code. The provisions of the Code required an average long column strength reduction of 12 percent, while the test results indicated an average reduction of 20 percent. However, if the strength of the test columns had been accurately given by the interaction curves, and if the value of e/t given in TABLE 7 - 2 had been the same as that

found in the tests, the test results would have shown no long column strength reduction, since the measured ultimate load was relatively unaffected by P_y -moments. The greater part of the indicated 20 percent average reduction was due to the fact that the test columns did not develop the full strength given by the interaction curves, as discussed in Section 4.3(c). A smaller part was the result of the fact that the measured eccentricities at the failure sections (Station B) were slightly larger than the assumed values, as indicated by the line representing $e/t = 0.86$ in FIGURES 4 - 17 and 4 - 18.

(b) Ultimate Load Capacity

The provisions in the American Concrete Institute Building Code (ACI 318-63) governing ultimate strength design of members subjected to combined axial load and bending are found in ACI Chapter 19. A summary of the comparison of the measured ultimate load capacities of the test columns with the design ultimate load capacities is given in TABLE 7 - 2. The measured ultimate loads were taken as the corrected axial column loads from the test results, and are tabulated with the designation P_{Long} under the heading "Test Results".

The design ultimate loads were tabulated with the designation P_{Long} under the heading "ACI 318-63". These loads were equal to the short column loads, based on ACI Section 1902, multiplied by the

reduction factor R . The eccentricity ratios given in TABLE 7 - 2 were used in computing the short column loads. Since the capacity reduction factor, ϕ , given in the Code is essentially a load factor it was neglected in these calculations. The measured values of P_{Long} were divided by the Code values and the ratio given in TABLE 7 - 2 as P_{Test}/P_{Design} .

The columns of Test Series A and C were similar, except that the former were hinged while the latter were restrained. For Test Series A, the average value of P_{Test}/P_{Design} given in TABLE 7 - 2 was 1.34 while for Test Series C the average value was 1.31. The closeness of these values indicates that the effect of the restraints in Test Series C was accurately taken into account by the moment-distribution analysis (Section 7.2(a)) used to compute the design eccentricity.

The columns of Test Series B and D were similar, except that the former were hinged while the latter were restrained. For Test Series B the average value of P_{Test}/P_{Design} from TABLE 7 - 2 was 1.22, while for Test Series D the average value was 1.04. As discussed in Section 7.2(a) the design eccentricity for Test Series D was somewhat smaller than the eccentricities found in the tests, and this contributed to the low values of P_{Test}/P_{Design} . It was mentioned

in Section 4.3(c) that the columns of Test Series D did not develop the full theoretical strength indicated by the interaction curves, and this apparent understrength also contributed to the low value of $P_{\text{Test}}/P_{\text{Design}}$. In Section 7.2(a) it was shown that these factors resulted in an indicated long column strength reduction of 20 percent where theoretically there should have been no reduction.

The columns of Test Series A and C had small end eccentricities and failed in compression, and the average value of $P_{\text{Test}}/P_{\text{Design}}$ was 1.32. The columns of Test Series B and D had large end eccentricities and failed in tension, and the average value of $P_{\text{Test}}/P_{\text{Design}}$ was 1.13. The difference between the two averages shows that there was a small additional factor of safety for the brittle failures of Test Series A and C as compared to the ductile failures of Test Series B and D.

CHAPTER VIII

SUMMARY AND CONCLUSIONS

8.1 Summary

Eight eccentrically loaded reinforced concrete columns were tested under short-time loading conditions. Four of the columns were hinged and four were restrained. The restraints were provided by reinforced concrete beams cast integrally with the columns. The column loads were applied to end blocks cast integrally with the ends of the columns. The columns were bent in double curvature, with equal and opposite end eccentricities. All the deflections were in the plane of the applied eccentricities, and sidesway was prevented.

All the columns had the same dimensions and reinforcement. The thickness of the column cross-section, measured perpendicular to the axis of bending, was 2.50 inches, and the width was 4.40 inches. The overall length of the columns was 68.25 inches, giving a slenderness ratio $h/t = 27.3$. The concrete strengths ranged from 3630 psi to 4880 psi. The longitudinal reinforcement consisted of four #3 deformed bars, giving a steel ratio of four percent. The yield point of the reinforcement

was 46,400 psi and it was positioned such that $d/t = 0.82$.

All the restraining beams of the restrained column specimens had the same dimensions and reinforcement. The thickness of the beam cross-section, measured perpendicular to the axis of bending, was 2.25 inches, and the width was 4.40 inches. The effective length of the beams was 46.25 inches and the far ends were freely hinged. The longitudinal reinforcement consisted of two #3 deformed bars top and bottom, with the same yield point as in the columns.

The two columns of Test Series B were hinged, and had nominal end eccentricity ratios $e/t = 1.5$, which would produce a tension failure in a short column. The column deflections were small, and contributed little to the total eccentricity at the failure section. The deflected configuration remained approximately antisymmetrical throughout the tests. Both columns failed in tension at the end of the column section adjacent to the end block. There was no long column strength reduction.

The two columns of Test Series D were restrained and had nominal end eccentricity ratios $e/t = 1.5$. The deflected configuration remained approximately antisymmetrical throughout the tests. The column deflections were small, and contributed little to the total eccentricity at the failure section. Both columns failed in tension at the end of the column section adjacent to the end block. The ultimate

column loads in Test Series D were considerably larger than in Test Series B, primarily because the end restraints reduced the column moments by taking a portion of the applied end moments. The average long column strength was 32 percent greater than the unrestrained short column strength.

The two columns of Test Series A were hinged and had nominal end eccentricity ratios $e/t = 0.2$, which would produce a compression failure in a short column. Large column deflections developed, and the deflected configuration was very unsymmetrical at higher loads. Deflections resulting from creep were very significant. In both tests the deflections were large enough to shift the location of the failure section away from the end of the column. Both columns failed in compression, and the deflections added considerably to the total eccentricity at the failure section. The average long column strength reduction was one percent.

The two columns of Test Series C were restrained and had nominal end eccentricity ratios $e/t = 0.2$. Large column deflections developed, and the deflected configuration was very unsymmetrical at higher loads. In both tests the deflections were large enough to shift the location of the failure section away from the end of the column. Both columns failed in compression, and the deflections added considerably to the total eccentricity at the failure section. The columns of

Test Series C developed a greater proportion of their short column strength than did those of Test Series A, primarily because the end restraints reduced the column moments by taking a portion of the applied end moments. The average long column strength was 12 percent greater than the unrestrained short column strength.

8.2 Conclusions

For the columns of this investigation, the following conclusions were drawn from the results of the tests:

- (1) The magnitude of the end eccentricities had a considerable effect on the location of the failure section and the amount of the long column strength reduction.
- (2) Although the columns were loaded in a nominally antisymmetrical manner, unsymmetrical behavior patterns developed and in some cases the ultimate load capacity was adversely affected.
- (3) Time-dependent deflections had a considerable effect on the behavior and ultimate load capacity of the hinged columns with small end eccentricities (Test Series A).
- (4) For the restrained columns, the end restraints reduced the effective column eccentricities by taking a portion of the applied end moments.
- (5) In general, the theoretical long column analysis underestimated the column deflections.

V O I D

LIST OF REFERENCES

1910

VonKármán, T., "Untersuchungen über Knickfestigkeit",
Mitteilungen über Forschungsarbeiten auf dem Gebiete des
Ingenieurwesens, No. 81, Berlin, 1910. (See Bleich (1952),
pp. 27 - 30)).

1928

Westergaard, H.M., and W.R. Osgood, "Strength of Steel Columns",
Transactions, A.S.M.E., Vol. 50, 1928. (See Bleich (1952),
pp. 33 - 34)).

1934

Baumann, O., "Die Knickung der Eisenbeton - Säulen", Eidg.
Materialprüfungsanstalt an der E.T.H. in Zurich, Bericht
No. 89, Zurich, 1934. (See Broms and Viest (1958-(1)),
p. 316).

1936

Timoshenko, S., "Theory of Elastic Stability", McGraw-Hill Book
Company, Inc., New York, 1936.

1947

Richart, F.E., J.O. Draffin, T.A. Olson, and R.H. Heitman,
"The Effect of Eccentric Loading, Protective Shells, Slenderness
Ratios, And Other Variables In Reinforced Concrete Columns",
University of Illinois Bulletin No. 368, Urbana, Illinois, Nov.,
1947.

1951

Hognestad, E., "A Study of Combined Bending and Axial Load in
Reinforced Concrete Members", University of Illinois Bulletin
No. 399, Urbana, Illinois, Nov., 1951.

1952

Bleich, F., "Buckling Strength of Metal Structures", McGraw-Hill
Book Company, Inc., New York, 1952.

1953

Ernst, G.C., J.J. Hromadik, and A.R. Riveland, "Inelastic
Buckling of Plain and Reinforced Concrete Columns", University
of Nebraska Engineering Experiment Station Bulletin No. 3,
Lincoln, Nebraska, 1953. (See Broms and Viest (1958-(1))).
National Building Code of Canada, National Research Council, Ottawa,
Ontario, 1953.

1955

Hognestad, E., N.W. Hanson, and D. McHenry, "Concrete Stress Distribution in Ultimate Strength Design", Journal of the American Concrete Institute, Proceedings Vol. 52, No. 4, Dec., 1955, pp 455-479.

1956

Baker, J.F., M.R. Horne, and J. Heyman, "The Steel Skeleton, Volume 2, Plastic Behavior and Design", Cambridge University Press, 1956.

Building Code Requirements for Reinforced Concrete (ACI 318-56), American Concrete Institute, 1956.

1958

- (1) Broms, B. and I.M. Viest, "Ultimate Strength of Hinged Columns" Transactions, American Society of Civil Engineers, Volume 126, Part II, 1961., pp. 309 - 338.
- (2) Broms, B. and I.M. Viest, "Ultimate Strength Analysis of Restrained Columns", Transactions, American Society of Civil Engineers, Volume 126, Part II, 1961, pp. 348 - 366.
- (3) Broms, B. and I.M. Viest, "Design", Transactions, American Society of Civil Engineers, Volume 126, Part II, 1961, pp 367-384.

1960

National Building Code of Canada, National Research Council,
Ottawa, Ontario, 1960.

1961

Pfrang, E.O. and C.P. Siess, "Analytical Study of the Behavior
of Long Restrained Reinforced Concrete Columns Subjected
to Eccentric Loads", Civil Engineering Studies, Structural
Research Series No. 214, University of Illinois, Urbana,
Illinois, June, 1961.

1962

Breen, J.E., "The Restrained Long Column as a Part of a
Rectangular Frame", Ph.D. Thesis, University of Texas,
Austin, Texas, June, 1962.

1963

Chang, W.F. and P.M. Ferguson, "Long Hinged Reinforced Concrete
Columns", Journal of the American Concrete Institute, Proceed-
ings Volume 60, No. 1, Jan., 1963, pp. 1 - 25.

Building Code Requirements for Reinforced Concrete (ACI 318-63),
American Concrete Institute, 1963.

APPENDIX A

DETAILS OF TESTING FRAME

The testing frame shown in FIGURE A - 1(a) was used in the tests of the restrained columns to provide structural support for the restraining beam reactions. The testing frame was not connected to the testing machine but was held in position by friction between the load pivots and the testing machine head and platten.

FIGURE A - 1(b) shows the position of the load pivots relative to end blocks of the test specimen. The desired end eccentricity was obtained by using the appropriate groove in the end bearing plate. The flange angles were bolted to the struts and were welded to the load pivots originally used in the hinged column tests.

FIGURE A - 1(c) shows the free end of a restraining beam with a load cell attached to the beam and bearing against the adjusting bolt of the beam support housing. The housings were fabricated from steel plate and were of welded construction. The adjusting bolts were fitted with two nuts and washers, and the heads were ground to provide a smooth bearing surface.

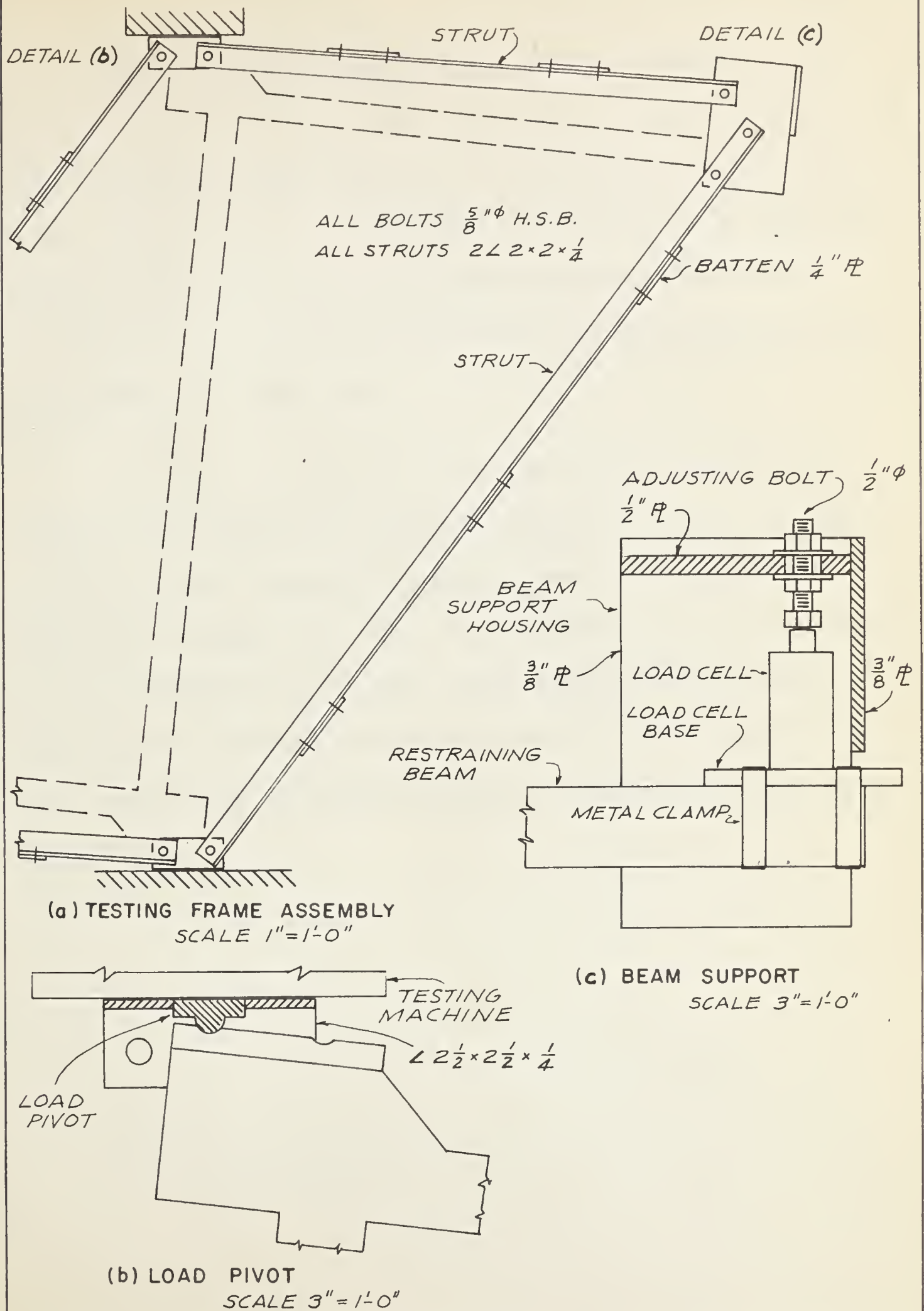


FIGURE A-1 DETAILS OF TESTING FRAME

The inclined and horizontal struts shown in FIGURE A - 1(a) were fabricated from 2" x 2" x 1/4" steel angles and had 1/4" batten plates attached with high strength bolts. In order that the same testing frame could be used in both Test Series C and Test Series D, which had different end eccentricities, a set of holes was provided in the ends of the struts to fit each eccentricity and maintain the beam bearing surfaces perpendicular to the beam axes.

The frame components were fastened together with 5/8 inch diameter high strength bolts complete with hardened washers. During assembly all slack was removed from the connections to remove the possibility of slippage under load. The bolts were tightened with a torque wrench to structural specification. Although the frame joints were not freely hinged it was assumed that resistance to the small displacements found in the tests would be small compared to the magnitude of the applied column loads.

APPENDIX B

OBSERVED TEST DATA

Observed test data is presented in TABLES B - 1 to B - 8 of this Appendix. Initial zero load readings have been subtracted from all test readings and the net values are tabulated. The locations of measuring stations and other points are given in FIGURE 3 - 8 for Test Series A and B and in FIGURE 3 - 9 for Test Series C and D.

Standard 6" x 12" cylinders were tested at the same time as each specimen. The cylinder strengths are given in TABLE 3 - 3.

For Test Series C and D, the strain indicator readings for the beam reaction load cells are tabulated. The indicator readings were multiplied by the conversion factor for each load cell to convert them to pounds and these values are also tabulated. The upper beam reaction, R_U , was measured with LOAD CELL #LC 2 - 2 which had a conversion factor 4.50 pounds per dial division. The lower beam reaction, R_L , was measured with LOAD CELL #LC 2 - 1 which had a conversion factor 4.35 pounds per dial division.

For Test Series C, estimated beam reactions at ultimate load are shown in brackets in the tables. Values were required in order to compute the corrected axial loads as described in Appendix C. Any estimating error would be very small in comparison with the magnitude of the ultimate column loads.

TABLE B - 1												OBSERVED TEST DATA				SPECIMEN A1			
Load, D	Kips	7.05	14.00	21.00	28.00	32.00	36.00	36.00	36.00	37.95									
Time	Hr:Min	0:02	0:14	0:18	0:26	0:35	0:53	0:58											
Column Deflection y in.	Station 1	0.01	0.02	0.03	0.04	0.06	0.17	0.17	0.17										
	Station 2	0.01	0.02	0.03	0.05	0.07	0.22	0.24	0.24										
	Station 3	0.01	0.01	0.02	0.03	0.05	0.18	0.20	0.20										
	Station 4	0.00	0.00	0.00	0.00	0.01	0.12	0.13	0.13										
	Station 5	-0.01	-0.02	-0.02	-0.03	-0.02	0.04	0.04	0.04										
	Station 6	-0.01	-0.02	-0.03	-0.03	-0.03	-0.02	-0.02	-0.02										

TABLE B - 2												OBSERVED TEST DATA										SPECIMEN A2			
Load, D	Kips	7.00	14.00	21.00	21.00	21.00	29.00	29.00	29.00	32.00	32.00	32.00	34.00	34.00	34.00	36.00	36.00	36.00	38.00						
Time -	Hr:Min	0:02	0:06	0:10	0:15	0:19	-	-	-	0:26	0:33	0:35	0:42	0:45	0:52	1:00									
Column Deflection y in.	Station 1	0.01	0.02	0.04	0.04	0.07	0.07	0.07	0.07	0.08	0.08	0.09	0.09	0.11	0.13	0.16	0.16	0.20	0.15	0.09					
	Station 2	0.01	0.02	0.04	0.04	0.06	0.07	0.07	0.08	0.09	0.09	0.11	0.12	0.16	0.20	0.15	0.09	0.00	0.00	0.04					
	Station 3	0.00	0.02	0.02	0.02	0.03	0.04	0.04	0.05	0.05	0.05	0.07	0.08	0.11	0.15	0.09	0.00	0.00	0.00	0.04					
	Station 4	0.00	0.01	0.00	0.00	0.01	0.01	0.01	0.01	0.02	0.02	0.03	0.04	0.06	0.09	0.00	0.00	0.00	0.00	0.04					
	Station 5	-0.01	-0.02	-0.03	-0.03	-0.04	-0.04	-0.04	-0.04	-0.03	-0.03	-0.04	-0.03	-0.02	0.00	0.00	0.00	0.00	0.00	0.04					
	Station 6	-0.01	-0.02	-0.03	-0.03	-0.04	-0.04	-0.04	-0.04	-0.04	-0.04	-0.04	-0.04	-0.04	-0.04	-0.04	-0.04	-0.04	-0.04	-0.04	0.04				
B3																									

TABLE B - 3									
OBSERVED TEST DATA							SPECIMEN B1		
Load, D	Kips	2.00	2.00	4.00	4.00	4.00	6.00	7.50	
Time	Hr:Min	0:03	--	0:26	--	--	0:41	--	0:58
Column Deflection y in.	Station 1	0.04	0.04	0.08	0.08	0.12	0.12	0.12	
	Station 2	0.04	0.04	0.08	0.08	0.12	0.12	0.12	
	Station 3	0.01	0.01	0.03	0.03	0.04	0.04	0.04	
	Station 4	-0.01	-0.01	-0.02	-0.02	-0.02	-0.02	-0.02	
	Station 5	-0.03	-0.03	-0.06	-0.06	-0.11	-0.11	-0.11	-
	Station 6	-0.03	-0.03	-0.06	-0.06	-0.11	-0.11	-0.11	

TABLE B - 4									
OBSERVED TEST DATA							SPECIMEN B2		
Load, D	Kips	2.00	2.00	4.00	4.00	4.00	6.00	7.00	7.10
Time	Hr:Min	0:02	--	0:13	--	--	0:33	0:50	--
Column Deflection y in.	Station 1	0.04	0.04	0.08	0.08	0.13	0.13	0.15	
	Station 2	0.04	0.04	0.08	0.08	0.11	0.11	0.13	
	Station 3	0.01	0.01	0.02	0.02	0.03	0.03	0.02	
	Station 4	-0.01	-0.01	-0.03	-0.03	-0.04	-0.04	-0.07	
	Station 5	-0.04	-0.04	-0.08	-0.08	-0.13	-0.13	-0.18	
	Station 6	-0.02	-0.02	-0.06	-0.06	-0.12	-0.12	-0.18	B4

TABLE B - 5			OBSERVED TEST DATA										SPECIMEN C1	
Load, D	Column	dh	Kips	7.00	14.00	21.00	27.00	32.00	36.00	37.50				
Time			Hr:Min	0.016	0.032	0.050	0.068	0.092	0.160					
				0:03	0:20	0:40	1:00	1:20	1:40					
Column Deflection y in.			Station 1	0.01	0.02	0.02	0.03	0.02	0.01					
			Station 2	0.02	0.01	0.02	0.01	0.00	-0.06					
			Station 3	0.00	0.00	-0.01	0.02	-0.05	-0.17					
			Station 4	0.00	-0.01	-0.03	-0.05	-0.10	-0.25					
			Station 5	-0.01	-0.02	-0.04	-0.06	-0.12	-0.28					
			Station 6	-0.01	-0.01	-0.03	-0.04	-0.07	-0.17					
Beam Deflection in.	Beam U		Station U1	0.00	0.01	0.01	0.01	0.02	0.02					
			Station U2	0.02	0.02	0.03	0.03	0.04	0.03					
			Station U3	0.01	0.01	0.02	0.02	0.02	0.02					
			Station U4	0.01	0.01	0.01	0.01	0.02	0.01					
	Beam L		Station L1	0.01	0.01	0.03	0.05	0.10	0.18					
			Station L2	0.01	0.04	0.05	0.08	0.13	0.25					
			Station L3	0.01	0.02	0.04	0.05	0.09	0.20					
			Station L4	0.01	0.01	0.01	0.02	0.04	0.10					
Beam Reaction	U		Indicator R _U lb..	4.8 22	7.0 31	9.5 43	10.8 49	11.2 50	9.2 41	(33)				
	L		Indicator R _L lb..	4.5 20	9.7 42	14.9 65	23.8 103	37.9 165	69.0 300	(349)				B5

APPENDIX C

REDUCED TEST DATA

C.1 Hinged Column Tests

Reduced test data for the hinged columns, Test Series A and B, is given in TABLES C - 1 to C - 4. The reduced test data consisted of corrected axial column loads and column moments. The methods and assumptions used in reducing observed test data are given in this section.

(a) Corrected Axial Column Load

The corrected axial column load, P , was found by multiplying the applied load, D , by the cosine of the angle between the thrust line and the column axis. Effects of vertical deflections on the geometry were neglected. The resulting equations were:

$$\text{Test Series A} \quad P = 0.999 \ D \quad (\text{EQ. C - 1})$$

$$\text{Test Series B} \quad P = 0.994 \ D \quad (\text{EQ. C - 2})$$

TABLE C - 1		REDUCED TEST DATA						SPECIMEN A1			
Load, D	Kips	7.05	14.00	21.00	28.00	32.00	36.00	36.00	36.00	37.95	
Column Load, P	Kips	7.05	14.00	21.00	28.00	32.00	36.00	36.00	36.00	37.95	
Column Moment M Kip-in.	Station 1	2.5	5.2	8.0	10.9	13.1	18.7	18.7	18.7		
	Station 2	1.5	3.1	4.8	7.0	8.6	15.1	15.1	15.8		
	Station 3	0.5	1.0	1.7	2.5	3.5	8.6	8.6	9.4		
	Station 4	-0.4	-0.8	-1.3	-1.7	-1.6	2.2	2.2	2.5		
	Station 5	-1.5	-3.1	-4.6	-6.4	-7.0	-5.8	-5.8	-5.8		
	Station 6	-2.5	-5.2	-8.0	-10.6	-12.2	-13.3	-13.3	-13.3		

TABLE C - 2		REDUCED TEST DATA										SPECIMEN A2	
Load, D	Kips	7.00	14.00	21.00	21.00	29.00	29.00	32.00	32.00	34.00	34.00	36.00	38.00
Col. Load, P	Kips	7.00	14.00	21.00	21.00	29.00	29.00	32.00	32.00	34.00	34.00	36.00	38.00
Column Moment M Kip-in.	Station 1	2.5	5.2	8.2	8.2	12.2	12.2	13.4	13.8	15.0	15.6	17.3	18.4
	Station 2	1.5	3.1	5.2	5.0	7.8	7.8	9.0	9.3	10.5	10.9	13.0	14.4
	Station 3	0.4	1.1	1.7	1.7	2.6	2.9	3.5	3.5	4.4	4.8	6.1	7.6
	Station 4	-0.4	-0.7	-1.3	-1.3	-1.5	-1.5	-1.6	-1.3	-1.0	-0.7	0.0	1.1
	Station 5	-1.5	-3.1	-4.8	-4.8	-7.0	-7.0	-7.7	-7.4	-7.8	-7.8	-7.9	-7.2
	Station 6	-2.5	-5.2	-8.0	-8.0	-11.3	-11.3	-12.5	-12.5	-13.2	-13.2	-14.0	-14.0

TABLE C - 3		REDUCED TEST DATA						SPECIMEN B1	
Load, D	Kips	2.00	2.00	4.00	4.00	6.00	6.00	7.50	
Col. Load, P	Kips	1.99	1.99	3.97	3.97	5.96	5.96	7.45	
Column Moment M Kip-in.	Station 1	5.3	5.3	10.7	10.7	16.3	16.3	16.3	
	Station 2	3.1	3.1	6.4	6.4	9.8	9.8	9.8	
	Station 3	0.9	0.9	1.8	1.8	2.8	2.8	2.8	
	Station 4	-0.9	-0.9	-1.8	-1.8	-2.7	-2.7	-2.7	
	Station 5	-3.1	-3.1	-6.3	-6.3	-9.8	-9.8	-9.8	
	Station 6	-5.3	-5.3	-10.6	-10.6	-16.3	-16.3	-16.3	

TABLE C - 4		REDUCED TEST DATA						SPECIMEN B2	
Load, D	Kips	2.00	2.00	4.00	4.00	6.00	6.00	7.00	7.10
Col. Load, P	Kips	1.99	1.99	3.97	3.97	5.96	5.96	6.96	7.06
Column Moment M Kip-in.	Station 1	5.3	5.3	10.7	10.7	16.4	16.4	19.3	
	Station 2	3.1	3.1	6.4	6.4	9.8	9.8	11.5	
	Station 3	0.9	0.9	1.8	1.8	2.8	2.8	3.2	
	Station 4	-0.9	-0.9	-1.8	-1.8	-2.8	-2.8	-3.5	
	Station 5	-3.1	-3.1	-6.4	-6.4	-9.9	-9.9	-11.9	
	Station 6	-5.3	-5.3	-10.6	-10.6	-16.3	-16.3	-19.5	

(b) Column Moments

The columns were assumed freely hinged at each end and therefore statically determinate. The moment at each station was computed from the relationship:

$$M = P(e_i + y) \quad (\text{EQ. C - 3})$$

Where: M = bending moment referred to the column centroid.

e_i = initial eccentricity at the station, measured between the column centroid and the thrust line.

y = lateral deflection from the initial position, as tabulated in Appendix B.

C.2 Restrained Column Tests

Reduced test data for the restrained columns, Test Series C and D, is given in TABLES C - 5 to C - 8. The reduced test data consisted of corrected axial column loads, moments at the beam-column joints, and column moments. The methods and assumptions used in reducing observed test data are given in this section.

TABLE C - 5			REDUCED TEST DATA						SPECIMEN C1	
Load, D	Column Load, P	Kips	7.00	14.00	21.00	27.00	32.00	36.00	37.50	
		Kips	7.04	14.07	21.10	27.15	32.21	36.41	(38.01)	
Upper Joint UO	Δ	In.	0.00	0.01	0.01	0.01	0.01	0.01		
	M _A	Kip-In.	3.2	6.4	9.8	12.6	15.2	17.7		
	M _R	Kip-In.	1.0	1.4	2.0	2.3	2.3	1.9		
	M _C	Kip-In.	2.2	5.0	7.8	10.3	12.9	15.8		
Lower Joint LO	Δ	In.	0.01	0.01	0.02	0.03	0.06	0.11		
	M _A	Kip-In.	-3.2	-6.5	-10.0	-13.2	-16.4	-21.0		
	M _R	Kip-In.	-0.9	-1.9	-3.0	-4.8	-7.6	-17.9		
	M _C	Kip-In.	-2.3	-4.6	-7.0	-8.4	-8.8	-3.1		
Column Moment M Kip-In.	Station 1		1.8	4.3	6.7	9.3	11.3	14.2		
	Station 2		1.1	2.6	4.2	5.6	7.1	8.5		
	Station 3		0.2	0.8	1.1	1.7	1.8	1.3		
	Station 4		-0.3	-0.5	-1.2	-1.6	-2.6	-4.0		
	Station 5		-1.2	-2.3	-3.9	-5.0	-6.9	-8.3		
	Station 6		-1.9	-3.7	-6.1	-7.6	-8.9	-7.4		

C5

TABLE C - 6														REDUCED TEST DATA										SPECIMEN C2			
Load, D		Kips		5.00	10.00	15.00	20.00	25.00	30.00	32.50	35.00	37.00	39.00	39.35													
Column Load, P		Kips		5.03	10.06	15.07	20.10	25.12	30.16	32.67	35.20	37.26	39.33	(39.69)													
Upper Joint	Δ	In.	0.00	0.01	0.01	0.01	0.02	0.02	0.02	0.02	0.02	0.02	0.02														
	M _A	Kip-In.	2.3	4.7	7.0	9.3	11.8	14.2	15.5	16.8	17.9	19.2															
	M _R	Kip-In.	0.7	1.3	1.7	2.1	2.5	2.8	3.0	3.1	3.1	2.7															
	M _C	Kip-In.	1.6	3.4	5.3	7.2	9.3	11.4	12.5	13.7	14.8	16.5															
Lower Joint	Δ	In.	0.01	0.01	0.02	0.02	0.02	0.03	0.03	0.03	0.05	0.07	0.13														
	M _A	Kip-In.	-2.3	-4.6	-7.1	-9.4	-12.0	-14.5	-16.0	-17.7	-19.5	-23.3															
	M _R	Kip-In.	-0.8	-1.3	-2.0	-2.7	-3.5	-4.5	-5.4	-6.8	-9.2	-13.0															
	M _C	Kip-In.	-1.5	-3.3	-5.1	-6.7	-8.5	-10.0	-10.6	-10.9	-10.3	-10.3															
Column Moment M Kip-In.	Station 1		1.3	2.8	4.4	6.0	8.0	9.8	10.8	11.9	13.0	13.8															
	Station 2		0.7	1.6	2.7	3.7	4.7	5.9	6.3	7.5	6.2	5.4															
	Station 3		0.2	0.4	0.7	0.9	1.0	0.9	0.8	0.9	-1.3	-5.4															
	Station 4		-0.3	-0.6	-1.1	-1.5	-2.3	-3.1	-3.8	-4.4	-7.5	-12.8															
	Station 5		-0.8	-1.8	-2.9	-4.0	-5.5	-6.9	-8.0	-8.6	-8.1	-16.9															
	Station 6		-1.3	-2.8	-4.3	-5.9	-7.6	-9.3	-10.2	-11.2	-11.8	-14.2															

C6

TABLE C -- 7									
REDUCED TEST DATA					SPECIMEN D1				
Load, D	Kips								
Column Load, P	Kips								
		1.50	3.00	4.50	6.00	7.50	9.00		
		1.54	3.09	4.65	6.20	7.76	9.33		
Upper Joint									
	Δ	In.	0.02	0.03	0.04	0.05	0.06		
	M _A	Kip-In.	10.3	15.7	21.0	26.2	31.6		
	M _R	Kip-In.	3.0	4.2	5.6	6.9	8.6		
	M _C	Kip-In.	7.3	11.5	15.4	19.3	23.0		
Lower Joint									
	Δ	In.	0.02	0.03	0.04	0.05	0.07		
	M _A	Kip-In.	-10.4	-15.6	-21.0	-26.3	-31.9		
	M _R	Kip-In.	-2.4	-3.8	-5.2	-6.9	-9.5		
	M _C	Kip-In.	-8.0	-11.8	-15.8	-19.4	-22.4		
Column Moment									
	M Kip-In.	Station 1	2.9	9.3	12.5	15.8	19.2		
		Station 2	1.6	5.4	7.4	9.5	11.9		
		Station 3	0.3	1.4	1.9	2.7	3.7		
		Station 4	-0.7	-1.7	-2.4	-2.8	-2.8		
		Station 5	-2.0	-5.8	-7.9	-9.6	-11.0		
		Station 6	-3.3	-9.7	-13.0	-16.0	-18.6		

TABLE C - 8

REDUCED TEST DATA

SPECIMEN D2

Load, D		1.50	3.00	4.50	6.50	7.50	8.00	8.50	9.00	9.50	10.00	10.50	11.50
Column Load, P		1.56	3.11	4.66	6.70	7.74	8.26	8.77	9.30	9.83	10.36	10.93	12.05
Upper Joint UO	Δ In.	0.01	0.02	0.02	0.03	0.04	0.04	0.04	0.05	0.05	0.05	0.06	0.08
	Kip-In.	5.2	10.4	15.7	22.7	26.2	27.9	29.7	31.5	33.4	35.3	37.4	41.6
	MA	1.7	3.2	4.4	5.8	6.7	7.1	7.5	8.0	8.4	9.1	9.9	12.1
Lower Joint LO	Kip-In.	3.5	7.2	11.3	16.9	19.5	20.8	22.2	23.5	25.0	26.2	27.5	29.5
	Kip-In.	0.01	0.02	0.02	0.03	0.04	0.05	0.06	0.06	0.07	0.07	0.09	0.19
	MA	-5.3	-10.5	-15.7	-22.7	-26.2	-27.9	-29.9	-31.6	-33.4	-35.4	-37.5	-42.6
Column Moment M Kip-In.	Kip-In.	-1.4	-2.8	-4.0	-5.9	-6.7	-7.1	-7.8	-8.6	-9.5	-10.7	-13.0	-17.0
	Kip-In.	-3.9	-7.7	-11.7	-16.8	-19.5	-20.8	-22.1	-23.0	-23.9	-24.7	-24.5	-25.6
	Station 1	2.8	5.8	9.1	13.9	16.0	17.1	18.3	19.5	20.7	22.1	23.3	25.3
	Station 2	1.6	3.3	5.3	8.2	9.6	10.2	11.0	11.8	12.8	13.6	14.9	16.4
	Station 3	0.3	0.7	1.4	2.3	2.6	2.9	3.1	3.4	3.9	4.4	5.4	6.3
	Station 4	-0.7	-1.2	-1.7	-2.3	-2.7	-2.9	-3.1	-3.0	-2.9	-2.8	-2.1	-1.7
	Station 5	-1.9	-3.8	-5.7	-8.1	-9.7	-10.3	-11.0	-11.4	-11.7	-12.0	-11.7	-12.1
	Station 6	-3.1	-6.2	-9.4	-13.6	-15.9	-17.0	-18.1	-18.9	-19.7	-20.3	-20.2	-21.5

(a) Correction For Lateral Displacement Of Beam-Column Joints

The lateral column deflections tabulated in Appendix B were measured with reference to a line joining the centers of the beam-column joints, Points UO and LO, as shown in FIGURE 3 - 9. As each column deflected laterally, Points UO and LO were displaced laterally with respect to the load pivots, thereby adding to the applied eccentricity at these points. Measurements of the displacements were not included in the instrumentation, so it was necessary to estimate the displacements from the test data. The estimated values of the lateral displacements of Points UO and LO with respect to the load pivots was denoted by the symbol Δ , and is included in the tables of reduced test data.

Since the restraining beams were rigidly connected to the end blocks, expressions were derived relating Δ to the measured deflection of each beam station. These expressions were based on the same assumptions used in computing the theoretical restraining moment-joint rotation curve of Chapter VI. The average of the values of Δ determined from each beam station reading are tabulated.

(b) Method Of Reducing Test Data

Although the interaction of the internal and external forces was complex, the test specimens were statically determinate because the beam reactions were measured. The external forces acting on a restrained

column test specimen are shown in FIGURE C - 1.

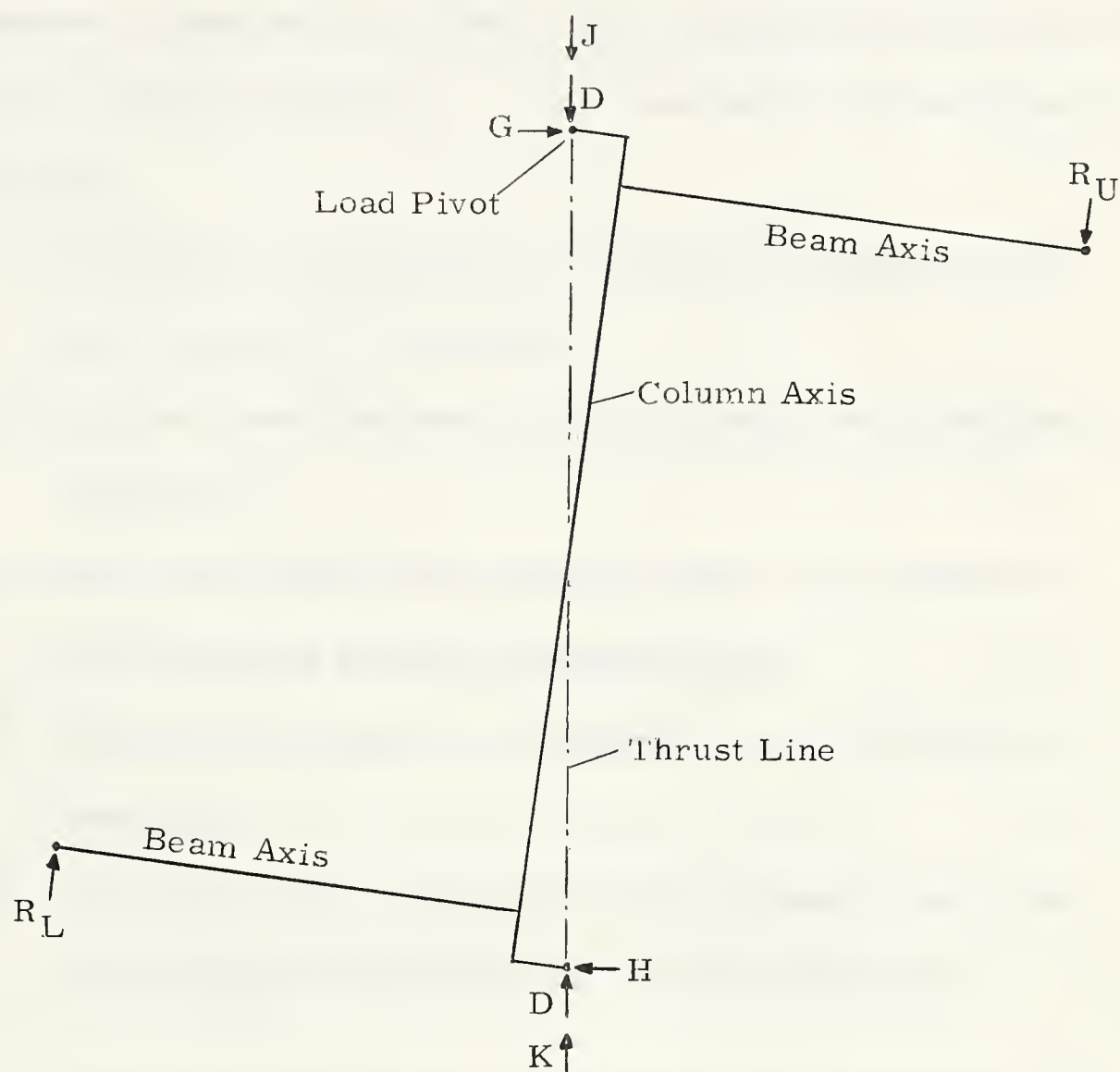


FIGURE C - 1 EXTERNAL FORCES ON RESTRAINED COLUMN SPECIMEN

The load applied by the testing machine, D , and the beam reactions, R_U and R_L , were measured in the tests. The reactive shears, G and H , resulted from the unbalanced moment on the test specimen caused by the beam reactions, and were a function of R_U and R_L . The forces imposed on the testing frame by the beam reactions were transferred

to the load pivots through the inclined and horizontal struts. The vertical components of these forces, J and K, were resisted by the test specimen. The forces shown in FIGURE C - 1 were resolved using the following assumptions:

- (1) The effects of deflections on the geometry of the external force system were neglected.
- (2) The load pivots and beam reaction bearings were considered frictionless.
- (3) The loads applied by the testing machine were assumed to act along a line joining the load pivot axes.
- (4) The beam reactions were assumed to act normally to the beam axes.
- (5) The forces in the testing frame were assumed to act along lines joining the load pivots and the beam reactions.

The results of the analysis were expressed by the following equations. All dimensions are in inches, and all forces in kips. The symbols are defined in Section 1.5.

Test Series C

The corrected axial column load, P, was given by:

$$P = D + 0.95 R_U + 0.95 R_L \text{ kips} \quad (\text{EQ. C - 4})$$

The moments at Point UO were given by:

$$M_A = (0.44 + \Delta) D + 3.25 R_L + 2.69 R_U \text{ kip-in.} \quad (\text{EQ. C - 5})$$

$$M_R = 46.25 R_U \text{ kip-in.} \quad (\text{EQ. C - 6})$$

$$M_C = M_A - M_R = (0.44 + \Delta) D + 3.25 R_L - 43.56 R_U \text{ kip-in.} \quad (\text{EQ. C - 7})$$

The moments at Point LO were given by:

$$M_A = (0.44 + \Delta) D + 3.25 R_U + 2.69 R_L \text{ kip-in.} \quad (\text{EQ. C - 8})$$

$$M_R = 46.25 R_L \text{ kip-in.} \quad (\text{EQ. C - 9})$$

$$M_C = M_A - M_R = (0.44 + \Delta) D + 3.25 R_U - 43.56 R_L \quad (\text{EQ. C - 10})$$

In order to calculate the corrected axial loads at failure it was necessary to estimate values of R_U and R_L for use in EQ. C - 4. Straight line projections of the last measured values were used, and the estimated values are given in TABLES B - 5 and B - 6, enclosed in brackets.

Test Series D

The corrected axial load, P, was given by:

$$P = 0.995 D + 0.97 R_U + 0.97 R_L \text{ kips} \quad (\text{EQ. C - 11})$$

The moments at Point UO were given by:

$$M_A = (3.28 + \Delta) D + 6.20 R_L + 2.46 R_U \text{ kip-in} \quad (\text{EQ. C - 12})$$

$$M_R = 46.25 R_U \text{ kip-in.} \quad (\text{EQ. C - 6})$$

$$M_C = M_A - M_R = (3.28 + \Delta) D + 6.20 R_L - 43.79 R_U \text{ kip-in.} \quad (\text{EQ. C - 13})$$

The moments at Point LO were given by:

$$M_A = (3.28 + \Delta) D + 6.20 R_U + 2.46 R_L \text{ kip-in.} \quad (\text{EQ. C - 14})$$

$$M_R = 46.25 R_L \text{ kip-in.} \quad (\text{EQ. C - 9})$$

$$M_C = M_A - M_R = (3.28 + \Delta) D + 6.20 R_U - 43.79 R_L \text{ kip-in.} \quad (\text{EQ. C - 15})$$

(c) Column Moments

The moments at each column station were computed in the same manner as for the hinged columns, using EQUATION C - 3. The thrust line eccentricity at Points UO and LO was taken as M_C/P . The value of e_i used in the equation was taken as the distance from the thrust line to initial position of the column axis.

6.3 Thrust Line Computations For Analysis Of Restrained Columns in Chapter VI

Thrust line eccentricities were computed for the restrained column analysis of Section 6.1(d)(ii) using the following equations. The equations were derived from those previously given for reducing test data. The assumed ratio of end eccentricities, e_1/e_2 , was taken into account by suitably modifying the equations. All dimensions are in

inches and all forces are in kips. The symbols have the same meaning as before.

Test Series C

The corrected axial column load, P , was taken as given by EQ.

C - 4. The column moment, M_C , at Point UO, was taken as given by

EQ. C - 7. The column moment M_C , at Point LO, was taken as:

$$M_C = ((0.44 e_1/e_2) + \Delta) D + 3.25 R_U - 43.56 R_L \text{ kip-in.} \quad (\text{EQ. C - 16})$$

Test Series D

The corrected axial column load, P , was taken as given by EQ.

C - 11. The column moment, M_C , at Point UO, was taken as given by

EQ. C - 13. The column moment, M_C , at Point LO, was taken as:

$$M_C = ((3.28 e_1/e_2) + \Delta) D + 6.20 R_U - 43.79 R_L \text{ kip-in.} \quad (\text{EQ. C - 17})$$

B29815